

Diss. ETH Nr. 13794

**OPTICAL WAVEGUIDE LIGHTMODE  
SPECTROSCOPY AS A BIOSENSOR TO MONITOR  
ADHESION AND METABOLIC STATE OF  
ANCHORAGE-DEPENDENT CELLS**

A dissertation submitted to the  
SWISS FEDERAL INSTITUTE OF TECHNOLOGY ZURICH (ETHZ)  
for the degree of  
Doctor of Technical Sciences

Presented by

Thomas Silvan Hug

dipl. chem. ETH

born June 12, 1973

Citizen of Switzerland

accepted on the recommendation of

Prof. Dr. M. Morbidelli, examiner

Dr. J.E. Prenosil, co-examiner

Prof. Dr. P. Maier, co-examiner

Zurich 2000

## Danksagung

Die vorliegende Arbeit wurde in der Zeit vom Mai 1997 bis Juli 2000 am Laboratorium für technische Chemie durchgeführt. Zahlreichen Personen, die mich bei der Durchführung dieser Arbeit unterstützt haben, möchte ich an dieser Stelle meinen Dank aussprechen.

- Prof. Massimo Morbidelli möchte ich dafür danken, dass ich meine Dissertation bei ihm durchführen konnte. Weiter möchte ich ihm sowohl für die gewährte Freizügigkeit als auch die grosszügige finanzielle Unterstützung bei der Durchführung dieser Arbeit danken.
- Dr. Jiri Prenosil möchte ich für den Vorschlag dieses Projektes und die grosszügig gewährte Freiheit bei den Experimenten danken.
- Prof. Peter Maier, der nachträglich zu diesem Projekt gestossen ist, möchte ich meinen tiefen Dank für die zahlreichen und lehrreichen Diskussionen sowie die kritische, biologische Betrachtungsweise des Versuchsaufbaus danken. Weiter möchte ich ihm meinen Dank dafür aussprechen, dass ich die *viability* Versuche in seinem Labor durchführen durfte.
- Dem Erfinder von OWLS, Dr. Kurt Tiefenthaler, möchte ich für die zahlreichen technischen Auskünfte zu OWLS danken.
- Dr. Masahiro Kino-oka möchte ich für die Hilfe beim Start dieses Projekts danken.
- Sabina Mazza möchte ich für Einführung in die Geheimnisse von Zellkulturen danken.
- Dr. Carmen Nievergelt danke ich sowohl für die zahlreichen biologischen Tips als auch die anregenden Gespräche.

- Franz Mayer möchte ich für seine tägliche Hilfe bei der Lösung von Laborproblemen danken.
- Max Wohltwend danke ich für die raffinierten, elektronischen Installationen bei der Erstellung dieser Apparatur.
- Der Werkstatt, insbesondere Markus Küpfer und Roland Mäder möchte ich meinen Dank für die wundervolle Hülle für meine Apparatur und die ausgeklügelten Vorschläge bei der Entwicklung meiner Messzelle danken.
- Meinen Mitdoktoranden Diane Carine, Alexander Hipp und Franscesa Quattrini möchte ich für das witzige und geistreiche Klima in unserem Büro danken.
- Für die moralische Unterstützung in guten und schlechten Zeiten möchte ich Philippe Pointet, Lukas Lüchinger und Judit Solt danken.
- Zuletzt möchte ich meinen Eltern und meinem Bruder für ihr stetiges Verständnis und ihre moralischen Beistand danken.

Zürich, den 1. Juli 2000

Thomas Hug

## Abstract

Optical Waveguide Lightmode Spectroscopy (OWLS) measures the refractive index within a 100 nm thin layer above a SiO<sub>2</sub>/TiO<sub>2</sub> surface. It has been used to monitor the adsorption kinetics of globular proteins such as albumin. Only in 1995 OWLS was shown to measure cell adhesion and spreading of Baby Hamster Kidney cells. Driven by the pharmaceutical research for drugs and the search for new high-throughput assays screening, the goal of this work was to develop a cell-based biosensor to monitor cell adhesion as an indicator of metabolic state.

Anchorage-dependent cells such as fibroblasts and hepatoma cells need a surface in order to adhere and spread. Cell adhesion is a complex biological process. On the extracellular side extracellular matrix proteins induce integrin-clustering and sites of focal contact are formed. On the intracellular side, the cytoskeleton mainly consisting of filamentous actin and microtubuli is responsible for cell morphology. Cytoskeletal activity is guided through transmembrane receptors and integrin clustering. A rac-mediated pathway has a direct effect on cytoskeletal activity within minutes, whereas rho-mediated activation is dependent on DNA transcription and a response is only observed 30 min later.

Due to the different size of proteins and cells, the sensor selectivity towards protein and cell detection is different: Since serum proteins lie fully within the 100 nm penetration depth of the OWLS sensor, they are completely detected. In contrast, the size of a cell is in the range of several  $\mu\text{m}$  and thus only the parts close to the surface contribute to the sensor signal. Consequently, OWLS monitors the cell contact area which is an indicator of cell adhesion.

Since OWLS is nonselective and both serum proteins and cells adsorb and adhere, a reproducible procedure for measuring cell adhesion and spreading had to be found. The time-dependent selectivity of the sensor consisted in the fundamentally different rates of protein adsorption and cell adhesion: When serum adsorption and cell settling were finished within 10 min, cell adhesion and spreading was monitored with OWLS. After 4 – 6 h when cell spreading was completed the sensor signal reached a steady state.



The sensor response was verified by varying several experimental input parameters such as cell density and cell-line: For their firm adhesion on the biocompatible SiO<sub>2</sub>/TiO<sub>2</sub> surface a fibroblast and a hepatoma cell-line were chosen for further experiments. Due to the different proliferation rate of the selected fibroblasts and hepatoma cells, the OWLS-signal of long-term cultures (48 h) was different: In the situation of fibroblasts, the OWLS signal remained almost constant over 48 h, whereas in the case of the fastly proliferating hepatoma cells cell growth was followed with the OWSL signal for up to 48 h. The reproducible long-term behavior of the OWLS signal was a prerequisite for the experiments with drugs.

In a number of biological situations with varying effects on cell adhesion, the OWLS biosensor was validated. In addition, cell morphology within the sensing region was observed at different time points through a viewing window of the OWLS measuring cuvette. In parallel, the cell viability was determined with three biochemical assays namely the neutral red-, the tetrazolium- and a total protein content assay.

Addition of serum medium was found to induce cell spreading of purely adhering cells in serum-free medium. Using OWLS cell spreading became visible within minutes. In contrast, serum-deprivation of fibroblasts reduced the contact area considerably, which was followed with OWLS as well. This result was in close correlation with the viability measurements and the cell morphology observed by microscopy. After exposure to the microtubuli disrupting agent colchicine (2.5 mM) an immediate reduction of the cell contact area was monitored for both cell-lines. This finding was confirmed by microscopy, whereas the effect of colchicine on cell viability became only visible after more than 2 h. On the search for possible applications benzalkonium chloride (BAC) - a strong skin irritant – was selected as a test compound for fibroblasts. After administration of BAC (3-5 µg/ml) to fully spread fibroblasts a dose-dependent cell shrinking over 12 h was observed. After administration of the protein-inhibitor cycloheximide (4 µg/ml) to the fastly proliferating hepatoma cells, the usually steadily increasing OWLS-signal started to decrease 5 h later. Similarly, the cytotoxic and alkylating anti-tumor drug cyclophosphamide, which needs metabolical activation, reduced cell proliferation (5-10 mM), which became visible with OWLS after 4 h. In the situation of hepatoma cells, OWLS-monitored cell proliferation was found to be a fast indicator of toxicity.

In summary, the sensor selectivity and sensitivity were studied and accordingly a procedure was found, where reproducible measurements were possible. With two different cell-lines of human and rodent origin several biological scenarios were studied. The OWLS measurements were in close correlation to the microscopic observations and the result of the viability assays. In conclusion, OWLS was found to monitor cell adhesion quantitatively and in real-time.

## Zusammenfassung

Optische Wellenleiterspektroskopie (OWLS) misst den Brechungsindex innerhalb einer 100 nm dicken Schicht über einer  $\text{SiO}_2/\text{TiO}_2$  Oberfläche. Anfangs wurde mittels OWLS die Adsorptionskinetik von globulären Proteinen wie Albumin gemessen. Erst 1995 wurde die Adhäsion und die Ausbreitung von *Baby-Hamster* Nierenzellen mit OWLS verfolgt. Im Zuge der pharmazeutischen Forschung nach neuen Medikamenten und der Suche nach neuen *high-throughput* Tests für *screening*, wurde später ein Biosensor zur quantitativen *on-line* Messung von Zelladhäsion als Indikator des metabolischen Zustandes entwickelt.

Oberflächenabhängige Zellen wie Fibroblasten- und Hepatomazellen brauchen eine Oberfläche um haften und sich auszubreiten zu können. Zelladhäsion ist ein komplizierter Vorgang: Auf der extrazellulären Seite lösen extrazelluläre Matrixproteine die Clusterbildung von Integrinen aus, worauf sich dort fokale Kontaktpunkte ausprägen. Auf der intrazellulären Seite ist das Zytoskelett aus Actinfilamenten und Microtubuli für die Zellform verantwortlich. Einerseits regulieren transmembrane Rezeptoren die Zytoskelettaktivität, und andererseits spielt die Clusterbildung von Integrinen dabei eine Rolle. Der rha-abhängige Signalweg wirkt sich innerhalb von Minuten auf die Zytoskelettaktivität aus, während eine Antwort des rho-abhängigen Signalweges, welcher über eine DNA-Transkription führt, erst nach 30 Minuten beobachtet wird.

Wegen der verschiedenen Grösse von Proteinen und Zellen ist die Sensorselektivität für Proteine und Zellen unterschiedlich: Serumproteine liegen vollständig innerhalb der 100 nm dicken Eindringtiefe des OWLS-Sensors und werden darum vollständig detektiert. Die Grösse eine Zelle hingegen ist im Bereich von mehreren Mikrometern, und deshalb tragen nur Teile der Zelle in der Nähe der  $\text{SiO}_2/\text{TiO}_2$  Oberfläche zum Signal bei. Folglich misst OWLS die Zellkontaktfläche, welche ein Mass für Zelladhäsion darstellt.

Weil OWLS nicht selektiv ist, tragen sowohl Serumproteine und Zellen, welche auf der Sensorfläche adsorbieren und adhären, zum Signal bei. Deshalb musste ein selektives Verfahren zur reproduzierbaren Messung von Zelladhäsion und Zellausbreitung gefunden werden: Nachdem die Serumproteine nach 10 Minuten adsorbiert waren und sich gleichzeitig die Zellen gesetzt hatten, konnte die Adhäsion und die Ausbreitung der

Zellen mit OWLS verfolgt werden. Nach 4 bis 6 Stunden war der Ausbreitungsprozess abgeschlossen und das Sensorsignal erreichte einen stabilen Wert.

Mit unterschiedlichen experimentellen Eingangsvariablen wie Zelldichte und Zelllinie wurde das Sensorsignal überprüft: Wegen der ausgeprägten Adhäsionseigenschaften der beiden Zelllinien auf der biokompatiblen  $\text{SiO}_2/\text{TiO}_2$ -Sensoroberfläche wurde eine Fibroblasten- und eine Hepatomazelllinie ausgewählt. Durch die verschiedenen Wachstumsraten der ausgewählten Fibroblasten- und Hepatomazelllinie war das Langzeitverhalten des OWLS Signals unterschiedlich: Mit Fibroblasten blieb das OWLS Signal beinahe konstant, während im Falle der schnellwachsenden Hepatomazelllinie das Zellwachstum bis zu 48 Stunden lang verfolgt werden konnte. Das reproduzierbare Langzeitverhalten des OWLS Signals war der Schlüssel zu den Experimenten mit chemischen Testsubstanzen.

In einer Anzahl von verschiedenen biologischen Fällen mit unterschiedlicher Auswirkung auf die Zelladhäsion wurde der OWLS Biosensor überprüft. Durch ein Beobachtungsfenster der OWLS-Messküvette konnte die Zellform innerhalb der empfindlichen Sensorfläche zu unterschiedlichen Zeitpunkten beobachtet werden. Parallel dazu wurde die Vitalität mit drei klassischen biochemischen Testverfahren bestimmt.

Die Zugabe von Serum löste die Zellausbreitung von nur adhärierenden Zellen in serumfreiem Medium aus. Mit OWLS wurde die Ausbreitung innerhalb von wenigen Minuten sichtbar. Wurde hingegen den Fibroblasten das Serum entzogen, reduzierte sich die Kontaktfläche beträchtlich, was auch mit OWLS verfolgt werden konnte. Dieses Resultat steht in engem Zusammenhang mit den Vitalitätsmessungen und der Zellform, welche mit Phasenkontrastmikroskopie beobachtet werden konnte. Nach der Zugabe der mikrotubuli-verändernden Substanz Colchicine (2.5 mM) konnte eine sofortige Abnahme der Zellkontaktfläche verfolgt werden. Diese Tatsache wurde unter dem Mikroskop durch die andersartige Zellform bestätigt, während die Auswirkungen von Colchicine auf die Zellvitalität erst nach mehr als zwei Stunden sichtbar wurden. Auf der Suche nach möglichen Anwendungen wurde Benzalkoniumchlorid, ein starke Hautreizungen verursachender Stoff, als Testsubstanz für die Fibroblasten ausgewählt. Nach der Anwendung von BAC (3-5  $\mu\text{g}/\text{ml}$ ) zu vollständig ausgebreiteten Fibroblasten wurde ein

dosisabhängiges Zellschrumpfen innerhalb eines Zeitraumes von 12 h beobachtet. Nach der Zugabe des Proteinsyntheseblockers Cycloheximide (4 µg/ml) begann das gewöhnlich leicht steigende OWLS Signal der schnellwachsenden Hepatomazellen nach 5 Stunden abzunehmen. Das zytotoxische und alkylierende Antikrebsmedikament Cylophosphamid, welches einer metabolische Aktivierung durch das P450 Enzymsystem bedarf, bremste das Zellwachstum (5-10 mM), was mit OWLS nach 4 Stunden sichtbar wurde. Im Falle von Hepatomazellen kann das mittels OWLS verfolgte Zellwachstum als ein schneller Indikator für akute Toxizität betrachtet werden.

Durch die Untersuchung der Sensorsensitivität und Selektivität konnte ein Verfahren für reproduzierbare Messungen gefunden werden. Mit zwei verschiedenen Zelllinien von Mensch und Maus wurden verschiedene biologische Testszenarien untersucht. Die OWLS-Messungen sind in guter Übereinstimmung mit den mikroskopischen Beobachtungen und den Vitalitätstests. Abschliessend lässt sich sagen, dass sich die Zelladhäsion, welche ein Indikator des metabolischen Zustandes sein kann, mittels OWLS quantitativ und in Echtzeit erfassen lässt.

---

<b>1. INTRODUCTION</b>	<b>4</b>
1.1. Aim	4
1.2. Motivation	4
1.3. Objectives and procedures	6
1.4. Validation	8
1.5. Biochemical Assays	8
1.6. Cell-based biosensors	9
1.6.1. Optical Waveguide Lightmode Spectroscopy	11
1.6.2. Quartz Crystal Microbalance	11
1.6.3. Reflexion Interference Contrast Microscopy	13
<b>2. PROTEIN ADSORPTION AND CELL ADHESION</b>	<b>16</b>
2.1. Protein Adsorption	16
2.2. Extracellular matrix (ECM)	19
2.3. Cytoskeleton	20
2.4. Fibroblasts	23
2.5. Skin irritants	25
2.6. Human hepatoma cells	27
2.7. Cycloheximide	29
2.8. Cyclophosphamide	29
2.9. Cell-spreading and cell-death	31
<b>3. OPTICAL WAVEGUIDE LIGHTMODE SPECTROSCOPY</b>	<b>33</b>
3.1. Basic principles	33
3.2. Sensitivity	36
3.3. Time-dependent selectivity	38
<b>4. MATERIALS AND METHODS</b>	<b>41</b>
4.1. Materials	41
4.2. Cell culture	41
4.3. Viability measurements	42
4.4. The OWLS-Setup and the measuring cuvette	42

---

<b>4.5.</b>	<b>Experiments</b>	<b>45</b>
<b>4.6.</b>	<b>Cell visualization by microscopy</b>	<b>47</b>
<b>5.</b>	<b>RESULTS</b>	<b>50</b>
<b>5.1.</b>	<b>Protein adsorption</b>	<b>50</b>
5.1.1.	Adsorption of serum bovine albumin and serum proteins	50
5.1.2.	Dynamics of serum adsorption at high bulk concentrations	54
5.1.3.	Protein adsorption and desorption	57
<b>5.2.</b>	<b>Cell Adhesion and Spreading</b>	<b>61</b>
5.2.1.	Adhesion and spreading of different cell-lines	61
5.2.2.	OWLS sensitivity and cell density	64
5.2.3.	OWLS measurements of long-term cultures	67
5.2.4.	Effect of serum on cell adhesion spreading and the contact area	72
5.2.5.	Effect of serum deprivation on cell adhesion	73
5.2.6.	Effect of colchicine	78
5.2.7.	Effect of benzalkonium chloride	83
5.2.8.	Effect of cycloheximide	86
5.2.9.	Effect of cyclophosphamide	90
<b>6.</b>	<b>DISCUSSION</b>	<b>94</b>
<b>6.1.</b>	<b>Sensitivity</b>	<b>96</b>
<b>6.2.</b>	<b>Time-dependent selectivity</b>	<b>96</b>
<b>6.3.</b>	<b>Protein adsorption</b>	<b>97</b>
<b>6.4.</b>	<b>Extracellular matrix</b>	<b>98</b>
<b>6.5.</b>	<b>Cell adhesion</b>	<b>98</b>
<b>6.6.</b>	<b>Reproducibility</b>	<b>99</b>
<b>6.7.</b>	<b>Applications</b>	<b>101</b>
<b>6.8.</b>	<b>Cytoskeletal activity and its relation to the metabolic state</b>	<b>101</b>
<b>6.9.</b>	<b>Validation</b>	<b>102</b>
<b>6.10.</b>	<b>Biokinetic modelling</b>	<b>103</b>
<b>6.11.</b>	<b>Outlook</b>	<b>104</b>
	<b>ABBREVIATIONS, SYMBOLS AND INDICES</b>	<b>105</b>
	Abbreviations	105
	Symbols	106
	Indices	106
	<b>REFERENCES</b>	<b>107</b>

---

<b>APPENDIX</b>	<b>115</b>
<b>BSA Model</b>	<b>115</b>
<b>Solutions for MTT, NR and BCA assays</b>	<b>116</b>
<b>Assays-procedures</b>	<b>116</b>



## **1. Introduction**

There has been growing evidence in cell biology that the morphology and shape of anchorage-dependent cells is governed by a defined biological program. Characteristic morphological changes of the cells were observed after exposure to cytoskeleton-modifying compounds such as colchicine. This indicates that cell adhesion may be an indicator of the metabolic state.

Since 1993 Optical Waveguide Lightmode Spectroscopy (OWLS) has been used to measure in real-time protein adsorption quantitatively. Only in 1995 OWLS was used for the first time to monitor the adhesion and spreading of anchorage-dependent cells.

### **1.1. Aim**

The aim of this work was to develop a cell-based biosensor based on the OWLS, which is capable to detect changes of cell adhesion at the cell-surface interface. The development of the biosensor must include a biological interpretation of the sensor response as well as the search for its applications according to the hallmark of the sensor technique. Since this is the first time that cell adhesion could be measured quantitatively and in real-time, this project represented an new application of OWLS, where the main uncertainty was in the rather vague biological meaning of cell adhesion.

### **1.2. Motivation**

The main goal of toxicology is to manage and minimize the risk of hazardous chemicals. A thorough understanding of the adverse effects may help to assess this risk. This includes the dose-response relationship, the mechanism of action, the influence of exposure conditions, species, age and sex.

#### Legislation

Today, some 100,000 chemicals are in commercial use and some 2000 new chemicals are launched on the world market each year (Koeter 1994). Before placing a new chemical on the market, the manufacturer or importer must notify it in the appropriate EC country and perform a safety assessment. Tests for acute and subacute toxicity, skin and eye irritation and genotoxicity are required (Evans 1994).

By legislation and for ethical reasons the use of animals to perform the required safety assessment has been restricted. As a consequence a growing interest in alternative tests to reduce animal testing was observed. These alternative test systems have to be developed and accepted by the regulating authorities.

The skin and eye irritation assays are an excellent example, where alternative tests had a tremendous success. Considerable efforts were made to replace the famous Draize eye

tests with rabbits by alternative tests (Draize et al. 1944). Today the most severely irritating compounds *e.g.* benzalkonium chloride (BAC) can be identified by *in vitro* screening without the need to undertake any animal testing. Alternatives to the Draize eye irritation test are at the final stage of validation. Methods for predicting effects such as contact allergenicity, where the underlying mechanism is still not clearly understood, are an object of research.

#### *In vitro* and *in vivo* assays

The research and development for new test systems is also motivated by other advantages: Compared to *in vivo* investigations *in vitro* tests are more mechanistic and present new means for basic and academic research on the mechanism of toxicity. The extrapolation from animals to humans is not necessary, because they offer the possibility of using human materials by the use of human cell-lines (Fentem and Balls 1994). In most cases a battery of complementary assays increases the probability to identify a hazardous chemical (Koeter 1995). However, a cellular *in vitro* test system is not expected to fully compensate animal test systems *e.g.* systemic toxicity can only be studied using whole organisms. Generally speaking, *in vitro* test systems are less time consuming and less expensive than *in vivo* tests.

Risk assessment of new substances is not the only reason for these tests. When a method proves to be relevant to a defined set of applications, it may be used as a screening tool. The use of *in vitro* methods permits the elimination of 90% of new chemicals, which means that few compounds will have to be assessed *in vivo* (Loprieno, Bruner et al. 1995).

#### High-throughput screening

There is still a list of illnesses which can not be treated effectively. To increase the chance to find a new substance huge libraries of chemical compounds, which have been synthesized by methods of combinatorial chemistry are screened. For the screening all kinds of assays have emerged. Accordingly, there is a growing interest for new assays, which can fulfill the requirements for high-throughput screening. An effective assay should have a testing capacity in the range of 100'000 compounds per week otherwise the screening assay would represent a bottleneck in the search for new compounds. In order to be fast and attractive, the assay must be simple and must provide precise information.

Major shortcomings of most classical biochemical assays is that the chemicals needed for immuno- and fluorescence assays interfere with cellular functions: Assays such as neutral red (NR) and tetrazolium salt (MTT) are based on artificial substances interfering with the cell-metabolism (Borenfreund and Puerner 1984), (Ishiyama, Shiga et al.

1995). Despite a defined interference of the additional substance with the cell, a prolonged exposure of the cells to these additional substances may also modify and therefore falsify the activity of the cell. Finally, the endpoint of the assays can only be measured by killing (and fixing/lysing) the cells. As a consequence traditional biochemical assays are labour-intensive as well.

## OWLS

In contrast, monitoring cell adhesion with the OWLS is based on a purely optical effect and thus no labelling is necessary. Thus OWLS displays one characteristic strength. The method is *non-invasive* and *on-line* measurements over many hours are possible. However, cell adhesion is a complex process and it is involved in many cellular processes. Accordingly, cell adhesion as an endpoint may not have a sufficiently defined mechanism.

Driven by the pharmaceutical research for new drugs and assays and knowing advantages of non-invasive purely optical methods, there was a clear motivation to see whether or not OWLS could serve as a new screening-method or as a cell-based biosensor for acute toxicity-measurements.

### 1.3. Objectives and procedures

An experimental procedure had to be established exhibiting a sufficiently high reproducibility. A constraint was that the procedure needed to be simple and fast in order to fulfill the requirements for screening. The selectivity and sensitivity of the biosensor needed to be assessed. The next step was to find relevant biological scenarios and possible applications. Finally, it was necessary to develop a coherent theory for the interpretation of the OWLS measurements.

#### Procedure for reproducible measurements

The first objective was to prove the reproducibility of the method. The earlier OWLS experiments with single proteins were relatively straightforward because they dealt with simple and well defined systems. In contrast, experiments with cells introduced many unknown parameters. First of all, the critical parameters had to be recognized and subsequently the experimental procedure was optimized. The most important technical parameters of the measuring procedure included:

- To develop an appropriate cell culture medium with respect to pH and air-bubbles
- To design an appropriate measuring cuvette for cell experiments with respect to the cell-number, air-bubbles and fluid-handling

- To develop a reproducible cleaning procedure including in- and outlet tubes and waveguide chips

### Applications

Preliminary experiments showed that cell-lines with different morphology displayed a different adhesion behavior which resulted in different OWLS-signals. A firm cell adhesion was found to be a prerequisite for a high sensor sensitivity. After having chosen the cell-lines with the strongest adhesion, several possible applications were tested. Basically, cell adhesion, spreading, shrinking<sup>1</sup> and growth were monitored with OWLS. For each application the experimental conditions were adapted. For instance, the best strategy for testing toxic substances was to monitor cell shrinking.

### Validation of the OWLS measurements with respect to other assays

The last step was the biological interpretation of the OWLS-signal. First, the sensitivity of the OWLS-signal due to cell adhesion was investigated. The OWLS-signal could be correlated to the contact area between the cell and the substrate. This was quantitatively shown by varying the cell density. Second, in several basic biological scenarios the contact area can be alternatively reduced or increased. To test the biological significance the key experiments were performed with two very different types of cells, namely fibroblasts and hepatoma cells. An overview of the performed OWLS experiments is given in Table 1.3.

*Table 1.3: Most important experiments performed with OWLS:*

Experiments	Input parameter	Cell-lines
Cell-contact area	cell number	fibroblasts / hepatoma cells
Cell-morphology	cell-line	fibroblasts
Cell-spreading	growth factors (serum)	fibroblasts / hepatoma cells
Cell-growth	cell number	hepatoma cells
Cell-shrinking	colchicine	fibroblasts / hepatoma cells
	serum-removal	fibroblasts / hepatoma cells
	benzalkoniumchloride (BAC)	fibroblasts
	cycloheximide (CY)	hepatoma cells
	cyclophosphamide (CP)	hepatoma cells

<sup>1</sup> Cell shrinking means the reduction of cell adhesion and the contact area with the underlying surface due to alterations of the ECM and cytoskeletal activity.

In order to observe cell adhesion, cell morphology was qualitatively controlled by phase-contrast microscopy. In addition, the metabolic state of the cells was determined by accepted biochemical viability assays. Finally the OWLS results were compared to either the cell morphology observed by microscopy or the results of the viability assays.

#### **1.4. Validation**

Validation has been defined as a process by which the reliability and relevance of a procedure are established for a specific purpose (Fentem, Prinsen et al. 1995). In order to be accepted by the authorities a test must fulfill certain criteria:

##### Requirements for new tests to pass a validation process

(Koeter 1994), (Koeter 1995), (Fentem, Prinsen et al. 1995)

- Sensitivity
- Selectivity
- Reproducibility
- Simple endpoints  
(includes the elucidation of the mechanism and the relation to specific toxicological effects *in vivo*)
- Critical appraisal/evaluation  
(includes its scientific justification, its sensitivity, its reproducibility)
- Comparative study  
(includes other *in vitro* tests, animals test, reliable *in vivo* toxicity data)
- Standardization of the methodology / establishing standard operating procedure (SOPs)
- Defined purpose and known applicability
- Selection of chemicals
- Publication in a high quality peer-review journal

Due to a poor selection of any required points listed above the validation may fail. A high number of *in vivo-in vitro* correlations may be a critical parameter to increase the attraction of a new test. Another problem may be a lack of interpretation of the endpoints (Fentem, Prinsen et al. 1995).

#### **1.5. Biochemical Assays**

Because of mostly unknown mechanisms *in vivo*-toxicity data are difficult to obtain and they often show a high variability (Loprieno, Bruner et al. 1995). Obviously, it may then be

difficult to establish a good correlation between *in vivo* and *in vitro* data. Instead, other validated assays can be used for correlation with the new test system. This was also true for this study and three classical viability assays were chosen for comparison. In the following section a brief introduction into the basic concept of *in vitro* assays will be given.

### Mechanism

Biochemical assays are often based on a defined process in the cell. Typically, this process has a very precise endpoint which can be measured as a physical unit such as optical transmission. The basic idea of a biochemical assay assumes a direct correlation between a defined process in the cell and the metabolic state of the cell. To refer to the metabolic state of the cells the terms viability and vitality are used. However, it needs to be stressed that this metabolic state of the cell is related to the assay.

### Sensitivity

Depending on the hazard, one test is more sensitive to a certain group of toxic substances than another one, *e.g.* a membrane-permeability test is more sensitive to membrane-perturbing substances such as surfactants than a test based on cell-growth. Obviously, at certain concentration the toxicity of the membrane-perturbing agent is so high, that cell proliferation is inhibited as well. The result of the assay must thus be considered with respect to the class of chemicals and the type of assay.

Selected list of accepted biochemical assays for measuring acute toxicity:

- Membrane-permeability (incorporation of neutral red (NR))
- Membrane-integrity (lactate dehydrogenase-(LDH)-release, trypan blue exclusion)
- Metabolic-activity (reduction of tetrazolium salt (MTT))
- Proliferation (total protein-measurement, [<sup>3</sup>H]-thymidine-incorporation )

## 1.6. Cell-based biosensors

In the canonical way the principle of a biosensor is based upon a specific interaction between an analyte and a receptor, which is transmitted by a transducer into an electrical signal. The measuring principle should be fast and reversible such that on-line measurements are possible. Moreover, miniaturization can make the use of biosensors attractive for mass production and in other words attractive for applications such as parallel measurements or implantation (Kunz 1997).

For a cell-based biosensor living organisms are immobilized and their metabolic status is interrogated by the sensor. The concept of cell-based biosensor is similar to that of biochemical assays which measure a defined process representative for the metabolic

activity; *e.g.* a cell metabolite such as lactat is specifically detected (Bains 1994). The specificity may be located even within the cell by a fluorescent light emitting enzyme system (Wood and Gruber 1996). Moreover, less specific tests such as conductivity measurements belong to cell-based biosensors as well (Ehret, Baumann et al. 1997), (Wolf, Brischwein et al. 1998).

### New technologies

Recently, several techniques measuring the adsorption of mass emerged. Through these techniques it became possible to monitor cell adhesion and shape quantitatively. The measuring principle of these techniques is not based upon a very specific interaction though. Two of them are based on microscopy, namely reflexion interference contrast microscopy (RICM) and confocal laser scanning microscopy (CLSM). In this study OWLS, which measures the refractive index within a 100 nm thin layer above a surface, was used. Although the measuring principle of OWLS is nonspecific, it was shown that the sensor may measure the cell-surface contact area under defined conditions. Finally, the quartz crystal microbalance (QCM) is based upon mass detection by oscillations.

Phase-contrast microscopy should also be mentioned, by which cell morphology and shape can be observed as well. However, the quantification requires extensive and complex software and results only in so called shape-factors<sup>2</sup>, which have no real biological meaning. The quantification of cell adhesion by CLSM becomes only possible using additional fluorescent markers.

### Potential of new technologies

Despite the well-known potential of these techniques to measure cell adhesion they were hardly exploited because in contrast to the defined processes measured in biochemical assays, the biological meaning of cell adhesion and cell shape was not sufficiently elucidated yet.

Since it was the first time that cell adhesion and shape could be followed on-line, one part of this work included the search for basic biological scenarios in order to show the relation of cell adhesion and metabolism. In fact, cell adhesion and morphology were followed by inverted phase-contrast microscopy and metabolic activity was observed by three biochemical assays.

A deeper insight in the role of cell adhesion and shape can be illustrated by the comparison of recent research results. The sensing principle of OWLS, QCM, RICM and a brief overview of the research regarding cell adhesion and spreading will be

---

<sup>2</sup> The relation of the surface and circumvention of a certain shape represents a typical example of a shape factor. However, the shape factor contains no biological information such as the strength of cell adhesion.

presented in the following section and summarized in Table 1.6. The similarity between OWLS and QCM is especially striking; both techniques have to solve similar problems such as concomitant protein adsorption.

### 1.6.1. Optical Waveguide Lightmode Spectroscopy

Sensing principle

See section 3.1. *Basic principles*

Research results

Ramsden showed for the first time that the OWLS can be used to monitor the adhesion and spreading of cells (Ramsden, Li et al. 1994), (Ramsden 1995). Baby hamster kidney (BHK) cell attachment and spreading was monitored up to three hours. In addition, fibronectin (Fn) coating and serum containing medium were found to considerably accelerate the spreading process (Li, Ramsden et al. 1994). If the divalent ions necessary for integrin binding were chelated with EDTA, spreading was retarded. In the case of hybridoma cells serum did not contribute to the spreading process (Ramsden, Li et al. 1994), (Li, Ramsden et al. 1994). In all experiments, the spreading process was not monitored to the end, where the adhesion of the cell becomes stable.

### 1.6.2. Quartz Crystal Microbalance

Sensing principle

The QCM-D sensor technology can be used to determine the mass and viscoelastic properties of ultra-thin films (Rodahl, Hook et al. 1997). The system consists of the sensor crystal in a measurement chamber. The active sensor component in the system is a thin disc made from a piezoelectric quartz crystal. The resonance frequency of the sensor crystal depends on the total oscillating mass as illustrated in Fig. 1.1. The adsorption of very small masses on the electrode (less than 5 ng/cm<sup>3</sup> in water) can be detected by measuring the change in the resonance frequency according to the Sauerbrey equation (Eq. 1)

$$\Delta f = -k \cdot \Delta m \quad \text{Equation 1}$$

where  $\Delta f$  is the change in the resonant frequency,  $\Delta m$  is the change in the deposited mass and  $k$  is the mass sensitivity constant. The crystal oscillation is damped by the viscoelastic properties of the adsorbed film. By measuring the damping factor  $D$  a measure of the viscoelastic properties is obtained.

Thus the QCM-D technique, similar to the OWLS, allows real-time, non-invasive adsorbed-mass-measurements. The sensor can be coated with almost any thin film



biomolecules, proteins or living cells. The sensitivity decreases exponentially with the distance from the surface. The detection range for cells is estimated to be a few micrometers. The time resolution is about one measurement per second.

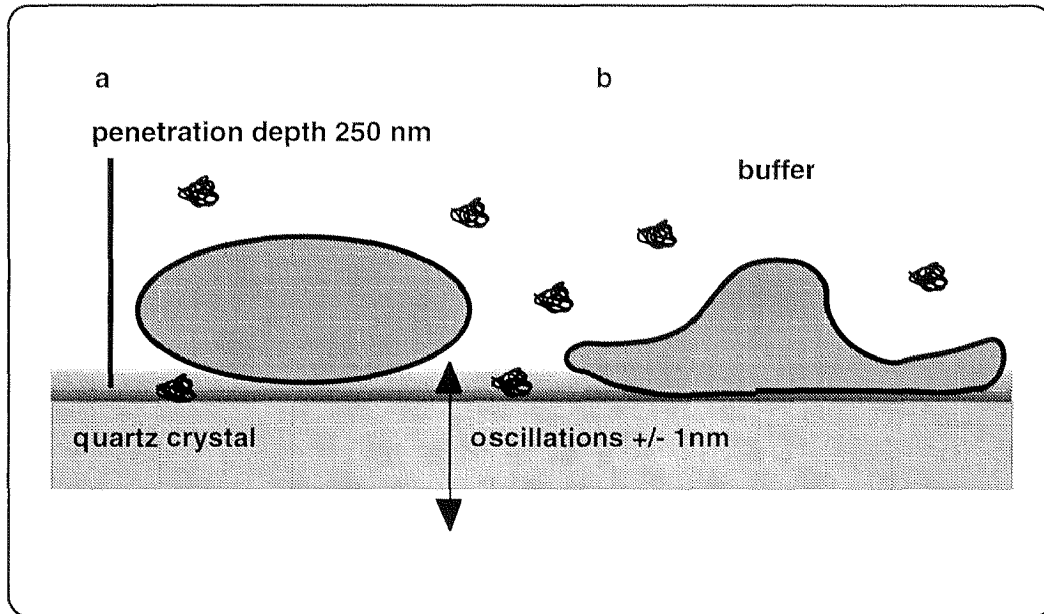


**Fig. 1.1:** *Principle of QCM* (Rodahl, Hook et al. 1997). The shear wave induced in the liquid by the QCM oscillation decays perpendicularly to the crystal surface. The sensor crystal has a resonance frequency, which depends on the total oscillating mass. The adsorption of proteins as well as the adhesion of cells affects the resonance frequency. a) Round cells having a weak adhesion to the QCM damp the oscillations weakly. b) In contrast, strongly adherent cells reduce the resonance frequency.

#### Research results

The attachment and spreading of several cell strains such as Monkey Kidney Epithelial (MKE) and Chinese Hamster Ovary (CHO) was monitored (Fredriksson, Kihlmann et al. 1998). The attachment and spreading of neutrophils on different coatings (polystyrene (PS), immunoglobulin G (IgG), human serum albumin (HSA) and fibrinogen (Fg)) showed a different sensor response depending on cell spreading. After spreading a decrease of the sensor signal was assigned to the enzymatic digestion of already adhered proteins. Using African Green Monkey Cells (VERO) the influence of a lethal dose of NaOH and cell lysis after virus infection is investigated (Gryte, Ward et al. 1993), (Nimeri, Fredriksson et al. 1998). Regarding the sensitivity, the results of several studies are inconsistent. Especially the contact area as a measure of cell density has never been investigated in detail.

### 1.6.3. Reflexion Interference Contrast Microscopy

#### Sensing principle

The reflexion interference contrast microscopy (RICM) is based upon the reflectance of light at several distances from the substratum as shown in Fig. 1.2 (Goldmann, Schindl et al. 1995). RICM is a form of incident light interferometry in which radiance of an image of an adherent cell is a derivative of the width of the gap separating the cell's undersurface from the substratum. The beam of polarized light (546 nm) is sent from below of the substrate and is reflected by the substrate and the lower part of the membrane of the cell. At regions of close contact of the cell with the substratum more light is reflected due to the interference of the reflected light at the substratum and the cell membrane. The reflected light can be detected up to some 100 nm above the substrate and depends strongly on  $\alpha$ , the value of illumination aperture (INA). Thus if the cell is very flat the light is also reflected at the upper part of the membrane. Depending of the amount of light reflected by the cell, lighter and darker areas are observed by RICM. Focal contacts<sup>3</sup> appear as black streaks in interference reflection images. Another form of cell attachment is a close contact<sup>4</sup> appearing gray by interference reflection.

The window size for RICM observations is 65\*45  $\mu\text{m}$  corresponding to the area of about four cells. The strength of the RICM is the three dimensional resolution. Quantification of the data is obtained by image analysis (IA). Together with time lapse video microscopy and digital image processing the RICM can be used to measure the time course of pseudopod or filapodia extension in contact with the substratum. In addition regions of focal contacts can be recognized.

---

<sup>3</sup> Focal contacts (focal contact) are points of very tight cell adhesion, see 2.3.2 Cytoskeletal pathway

<sup>4</sup> Close contact are areas of close cell adhesion. It is assumed that receptor-binding does not play a role.

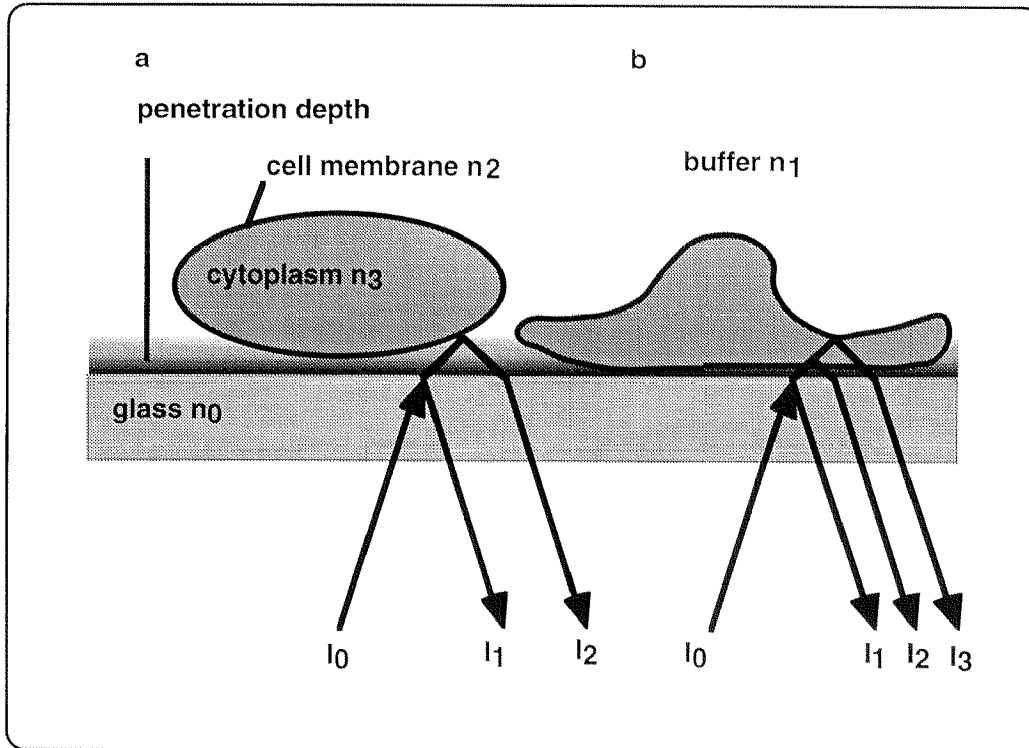


**Fig. 1.2:** Principle of RICM image formation (Schindl, Wallraff et al. 1995):

a) The image is formed by the interference of light reflected from the surface of the glass with light reflected from cellular surfaces that are in short distance from the surface. Reflective surfaces correspond to steps in the refractive index  $n$  ( $n_0 = 1.51$ ;  $n_1 = 1.33$ ;  $n_2 \cong 1.36$ ;  $n_3 \cong 1.33$ ), and their reflectivity is proportional to the size of these steps. b) Small distance of ventral and dorsal membrane from the substrate leads to triple appearance, which causes very dark appearance at portions of thin lamellipodal lobes in RICM.

### Research results

The cytoskeletal protein vinculin was showed to have a strong influence on the adhesion (Goldmann, Schindl et al. 1995). Vinculin-deficient cells could not form regions of close contact. Consequently these cells showed a more spherical morphology and a different extension behavior of filapodia due to a weaker adhesion. Moreover, in a different study the temporal changes of contact area with respect to different surfaces and absence of various cytoskeletal proteins were investigated (Schindl, Wallraff et al. 1995). Last but not least, it was found that after the exposure to the metabolic inhibitor  $\text{NaN}_3$ , the contact area diminished immediately (Schindl, Wallraff et al. 1995).

**Table 1.6:** Summary of the most important features of OWLS, QCM and RICM (Tiefenthaler 1989), (Fredriksson, Kihlmann et al. 1998), (Schindl, Wallraff et al. 1995)

Method	OWLS	QCM	RICM
<b>Sensing principle</b>	refractive index	resonant frequency	interference
<b>Protein-cell selectivity</b>	partly selective	partly selective	selective
<b>Sensing depth</b>	100 nm	250 nm	100 nm
<b>Sensing area</b>	0.5 mm <sup>2</sup>	20 mm <sup>2</sup>	65*45 μm
<b>Observed cell number</b>	100-300 cells	> 1000 cells	3-4 cells
<b>Input parameters:</b> substrate coating cell strains toxins	Fn, Serum Hybridoma, BHK EDTA	PS, IgG, HSA, Fg CHO, neutrophils, VERO NaOH, Virus	glass, albumin, cleaved mica Dictostelium, F9, 5.51 NaN <sub>3</sub>

## 2. Protein adsorption and cell adhesion

Culturing animal cells mostly implies the use of serum. Since the OWLS biosensor is sensitive to any protein originating from either serum or cells a short introduction into the most common phenomena of protein adsorption will be given in the first section.

The core of the OWLS experiments focuses on cell adhesion and morphology. Cell shape was shown to be essential for cell survival and other cellular processes. Moreover, extracellular matrix (ECM), growth factors and cytoskeleton play a key role in cell shape and adhesion and are introduced in the second section of this chapter.

### 2.1. Protein Adsorption

Protein adsorption plays a role, when artificial materials come in contact with body fluids such as blood. The research interest of protein adsorption is partly motivated by the deleterious effects such as thrombogenesis and inflammation after exposure of artificial materials in the body. Protein adsorption was mainly investigated with serum and the main plasma proteins including bovine serum albumin (BSA), immunoglobulin G (IgG) and fibrinogen (Fn). These proteins have different biological functions, *e.g.*, BSA regulates the colloid osmotic blood pressure and transports many ligands such as fatty acids, amino acids, steroids, metals by binding. An overview of the most important data concerning these proteins is given in Table 2.1.

*Table 2.1: Some data of the most important serum proteins, (Gaigalas, Hubbard et al. 1992), (He 1992), (Lu and Chittur 1994), (Brusatori, Van Tassel, 1999)*

Proteins:	BSA	IgG	Fn
Serum-concentration	61 %	30.9 %	0 %
Plasma-concentration	76.9 %	19.1 %	3.84 %
$M_w$ [g/mol]	70'000	156'000	340'000
Dimension [nm]	14.1*4.2	23.5*4.4	45*9
Diffusion-const [cm <sup>2</sup> /s]	6.32*10 <sup>-7</sup>	3.84*10 <sup>-7</sup>	2*10 <sup>-7</sup>
Maximum surface concentration [μg/cm <sup>2</sup> ]	0.17	0.63-0.79	0.42-0.44
Adsorption constant $K_A$ [1/cm*s]	2.2*10 <sup>-6</sup>	1.5*10 <sup>-5</sup>	1*10 <sup>-5</sup>
Desorption constant $K_D$ [1/s]	4.4*10 <sup>-4</sup>	3.1*10 <sup>-4</sup>	0

Most of the methods to study protein adsorption can also be used to study cell adhesion as well. Among all, OWLS is the most sensitive and can detect up to 10 molecules per  $1 \mu\text{m}^2$  for an albumin sized protein (Ramsden 1995), which corresponds to  $1 \text{ ng/cm}^2$  (Tiefenthaler 1992). However, none of the techniques provides quantitative data for the thermodynamic parameters characterizing the protein adsorption and concomitant protein denaturation, which may be the reason why a comprehensive theory for protein adsorption is still lacking. The theoretical concept of the subsequent rearrangements of proteins upon adsorption is well known though. Many of these effects have been studied indirectly and are reviewed in the following paragraph.

#### Thermodynamics of protein adsorption

Protein adsorption is based on the hydrophobic effect, which chiefly states that the solubilities of nonpolar polymers in water is extremely low. Protein binding forces include electrostatic interactions, Van-der-Waals forces and Lewis acid-base interactions. The conformational stability of most globular proteins such as albumin is very low ( $2 - 8 \text{ kJ}$ ) and corresponds to several hydrogen bondings (Steadman, Thompson et al. 1992). The adsorption of proteins strongly favors conformational changes on the surface (Haynes and Norde 1994). Since the core of most proteins is more hydrophobic than the surface, the relaxation of the proteins is strongly dependent on the hydrophobicity of the surface and the nature of the protein itself. In addition the pH affects the surface charge density of the surface and the protein as well (Ramsden and Roush 1995). Consequently the highest amount of adsorbed proteins is usually measured at the pH between the pI of the protein and the surface. Last but not least, the binding site due to different orientation as well as the buffer system site may also play a role in the relaxation from the native to a more denatured form.

The different degrees of relaxation and unfolding from one type of protein structure to the next result in several thermodynamic consequences: First, protein adsorption is either an equilibrium or a non-equilibrium process meaning that protein adsorption is either reversible or irreversible. Second, the protein adsorption isotherm may reach a flat plateau at considerably low bulk concentration indicating that protein unfolding does not depend on the bulk concentration. Alternatively the adsorption isotherm may tend towards higher values indicating that protein unfolding or surface diffusion induce a closer packing of the proteins at increasing bulk concentrations (Haynes and Norde, 1995).

#### Kinetic models for protein adsorption

Globular proteins are ellipsoidal and adsorb mostly in monolayers. Thus the simplest model for proteins is that of hard spheres or discs, which stick to a surface at randomly selected positions (Talbot et al). This random sequential adsorption (RSA) model was developed and experimentally verified for BSA, which is the main protein component

of serum (Kurrat, Ramsden et al. 1994). In this model the proteins adsorb at randomly selected positions and thus the probability to form a complete monolayer is infinitely small. There is always free surface patches left, however, too small to accept further protein molecules. In the RSA model the amount of adsorbed proteins at infinite times does not depend on the bulk concentration. Thus the model of simple balls landing on a surface may become too simple as soon as the temporal conformational rearrangement affects the available surface still free for other proteins to adsorb.

To include the effect of protein unfolding upon adsorption an additional model called the scaled particle theory (SPT) was presented (Talbot, 1997). After adsorption the proteins undergo a transformation leading to a larger contact region and at the same time decreasing the probability that incoming proteins land on unoccupied surface. The transition takes only place if enough space around the protein is available. The SPT-model predicts that the extent of conformational change decreases with increasing bulk concentration. Experimental data for fibrinogen adsorption confirmed the model nicely (Brusatori and Van Tassel, 1999).

Although single protein adsorption can be easily studied with OWLS and ellipsometry, competitive protein adsorption from a mixture represents an *in vivo* situation. Especially, multiple protein adsorption plays an important role in the application of a cell-based biosensor. In addition to multiple protein adsorption, competitive settling of cells will be considered later. Since there is no technique which can measure the adsorption of individual proteins, either radioactive labelling or subsequent exposure to antibodies may help to overcome this problem (Huetz, Ball et al. 1995), (Brash and Horbett 1995). However, radioactive labelling is only possible with one protein component and can only be performed in specialized equipped laboratories. Similarly, a detection with antibodies is limited to the proteins presenting an active antibody-binding-site. In conclusion, only limited experimental methods to study competitive protein adsorption do exist, and no one is suitable for routine work.

The initial adsorption of proteins in a multi component system is controlled by several factors such as serum composition, individual diffusion rates and individual adsorption constants. A rapid turnover of the reversibly adsorbed proteins due to the same factors is observed. This replacement of reversible adsorbed proteins is named after its discoverer the Vroman effect. Huetz et al. showed that protein replacement and removal follows a double-composed first order kinetic with respect to the adsorbed protein and the protein in solution (Huetz, Ball et al. 1995). In another model it was shown that due to the Vroman effect adsorbed albumin and IgG pass an optimum and are gradually replaced by fibrinogen having the highest adsorption constant (Lu and Chittur 1994).

## 2.2. Extracellular matrix (ECM)

Tissues such as the skin and muscles are composed of cells and ECM, which serves to organize cells in space, to provide them with environmental signals to direct site-specific cellular regulation and to separate one tissue space from another.

### OWLS

The OWLS biosensor consists of a bare  $\text{SiO}_2/\text{TiO}_2$  surface, which does not represent a natural biological environment. Since cells cultured *in vitro* maintain their ability to synthesize their own ECM, certain ECM proteins are deposited on the ASI waveguide. Since the ASI waveguide is sensitive to any protein adsorption the secretion of ECM proteins may contribute to the OWLS-signal and should thus be considered. However it is difficult to quantify them.

### ECM proteins

ECM plays an important role in many cellular functions such as cell adhesion, spreading, morphology, growth, differentiation and motility (Hubbell 1999). Extracellular matrix is a complex chemically and physically cross-linked network of proteins and glycosaminoglycans. Ubiquitous components include type VI collagen, heparan sulfate proteoglycan, laminin, entactin, fibronectin and vitronectin. The ECM proteins have a molecular mass between 50,000 g/mol for the more globular proteins, and several 100,000 g/mol for the structural proteins such as collagen and laminin. In addition, many growth-factors are bound to heparin with high affinity.

### Receptors

Cell adhesion to the ECM is mediated by cell-surface receptors and nonspecific heparin binding (Dejana, Colella et al. 1988). Endothelial cells expose on their surface several receptor molecules, that on the outer side of the membrane specifically recognize and bind different components of the ECM and on the cytoplasmic side, link a chain of proteins of the membrane-microfilament interaction complex involved in the mechanism of adhesion and cytoskeletal organization.

Receptors include several members of the integrin family. Integrins are transmembrane glycoproteins consisting of an  $\alpha$ - and  $\beta$ -chain. Many extracellular matrix proteins such as collagen, fibronectin, vitronectin and laminin bind to integrin receptors by the same RGD peptide motif. Additionally, integrin binding is dependent upon  $\text{Ca}^{2+}$  and/or  $\text{Mg}^{2+}$  and physiologic temperature. Ligand binding to integrins induces clustering of several receptors and a site of focal adhesion is formed. On the intracellular side a number of cytoskeletal proteins are assembled to the cytoplasmic tails of  $\alpha$ - and  $\beta$ -integrins including vinculin, talin, tensin and  $\alpha$ -actinin. It was found that integrin clustering



preceded stress fiber formation (F-actin) emanating from focal adhesion plaques and that preventing integrin-binding by specific receptors induced apoptosis. The focal contact serves not only as an anchor of the cytoskeleton but also plays a key mechanism in cell spreading, survival and differentiation: Individual matrix ligands induce the clustering of their respective membrane receptors. The clustering of only one receptor is capable of supporting the subsequent formation of focal contacts and the local assembly of related cytoskeletal proteins. In addition, covalent grafting of RGD-containing peptide at a minimal concentration is capable of recapitulating most of the adhesive interactions of the ECM (Massia and Hubbell 1991).

#### Unspecific binding

In addition to the highly sequence-specific binding of adhesion peptides to cell surface receptors, most of the adhesion proteins also bind to cell-surface components by less specific mechanisms (Hubbell 1999). The proteins contain a heparin-binding domain that binds to cell-surface proteoglycans that contain heparin sulfate or chondroitin sulfate glycosaminoglycans. The peptide sequences that bind to cell-surface proteoglycans are rich in anionic and cationic amino acids such as arginine (R) and aspartic acid (D). Consequently, the interactions with cell-surface proteoglycans are much less specific than those with integrins. The effect can be mimicked simply by R or K residues immobilized upon a surface, albeit certainly with a great loss in specificity. Covalent grafting of amino acids on protein-repulsive surfaces and photolithographic methods allow the patterning of cell adhesion (Weber, Vasella et al, 1998), (Xiao, Textor et al. 1998), (Vaidya, Tender et al. 1998).

Overall, the interaction between cells and ECM is bidirectional: On one side cells are secreting extracellular matrix proteins and enzymes which modify and degrade the extracellular matrix proteins. On the other side cells are accepting information from ECM and they adapt their shape according to the ECM.

### 2.3. Cytoskeleton

Cytoskeleton is an integrated network of microfilaments and microtubules (MT) and plays an important role in cell locomotion, morphology and cytokinesis. The cytoskeleton serves to orient the cell in the tissue. Lack of cytoskeletal functions may induce cancer (Danowski, Harris, 1988).

#### OWLS

OWLS measures the refractive index within an 100 nm layer above the SiO<sub>2</sub>/TiO<sub>2</sub> surface. As mentioned in 2.1. *Protein adsorption* proteins are in the range of 10 – 40 nm, whereas cells are in the range of μm. The membrane of a fibroblasts is only about

8 nm thick and thus the OWLS sensor signal depends also on cellular components on the intracellular side such as the cytoskeleton.

Since the cytoskeleton is mainly responsible for cell shape and the cell contact area, the hallmarks of the cytoskeleton with respect to cell adhesion and morphology are illustrated. This includes cytoskeletal architecture, growth factors and cytoskeletal poisons. Growth factors and cytoskeleton-modifying compounds are small molecules and already minor concentration have an immediate effect on cell spreading and morphology. Therefore their effect on cell adhesion was studied by OWLS.

#### Cytoskeletal architecture

The cytoskeleton is linked to the membrane at the focal plaques, where vinculin and talin are associated with the intracellular side of integrins (Ridley and Hall 1992). The cytoskeleton basically consists of two types of fibres, filamentous actin (F-actin) and tubulin. There are structural and functional proteins such as vimentin and matrix associated proteins (MAPs) between MT and F-actin. Actin can be grouped into the cortical actin network, actin stress fibers and actin found in cell surface protrusions.

#### Cytoskeletal pathway

The regulation of the cytoskeletal activity is still not completely understood. One important pathway includes the activation through membrane receptors by mitogenes such as lysophospholipid acid (LPA) and growth factors as shown in Fig. 2.3. LPA was found to stimulate stress fibers within five minutes, whereas other growth factors only showed membrane ruffling after 10 min and some stress fiber formation after thirty min (Ridley and Hall, 1992). Accordingly two different membrane associated Ras-proteins were identified to be responsible for this different behavior: Rho was found to induce stress fiber formation and focal adhesion, whereas the Rac-protein only induced membrane ruffling within minutes. The fast response of both the Ras-proteins follows similar pathway including several kinases. Since it takes much longer for Ras to induce stress fiber formation than for Rho, growth-factor induced stress fiber formation appears to be dependent on DNA-transcription (Takai, Sasaki et al. 1995).

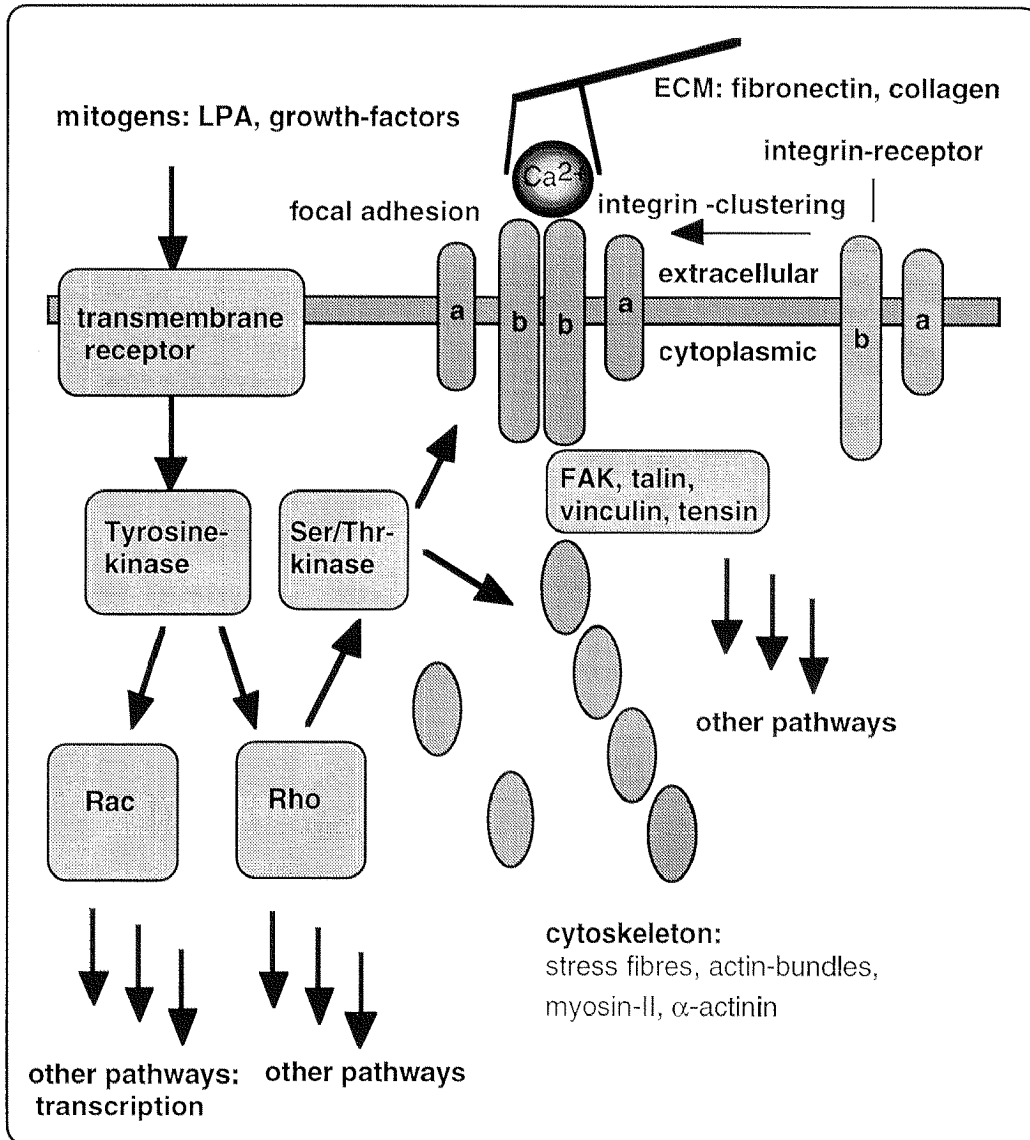


**Fig. 2.3:** *The most important cytoskeletal pathways regarding cell adhesion and spreading (Takai, Sasaki et al. 1995):* External mitogenic stimuli are transmitted through the membrane by specific receptors. On the intracellular side several kinase are responsible for signal transduction. The rac-mediated pathway includes DNA-transcription and a cytoskeletal response after external stimuli is thus only observed after more than 30 min. In contrast, the rho-mediated pathway has a direct effect on cytoskeletal activity and stress fiber formation is observed within minutes. In addition to mitogenic stimuli, focal clustering induces stress fiber formation as well.

#### Growth factors

The effect of growth factors on microtubuli formation is mostly reversible. 3T3 fibroblasts growing in the presence of FCS show abundant stress fibers, whereas serum starved cells retain very few fibers. The addition of 0.2 % FCS induced actin reorganisation in serum-starved cells within one minute. New stress fibers were

discernible after 2 min and 16 h after addition of 0.2 % FCS, the actin cytoskeleton was indistinguishable from that of control serum cells (Ridley and Hall 1992).

#### Serum removal

Serum removal was observed to have a serious impact on cell viability of fibroblasts. Moreover, it was found to induce a process between apoptosis<sup>5</sup> (DNA-degradation) and necrosis (membrane-leakage). Despite the observed membrane blebbing, which is typically for apoptosis, conductivity measurements as well as propidium iodid staining indicated membrane leakage corresponding more to necrotic events. Viability measurements showed that after 6 –18 h more than 25 – 50 % of the cells died, whereas the rest became quiescent and could be rescued by addition of serum. Cell death could be inhibited by specific proteases and protein-inhibitors such as cycloheximide (Herbert, Pandey et al. 1994), (Simm, Bretsch et al. 1997).

#### Growth factors and their effect on DNA-production

Growth factors stimulate not only the formation of microtubuli and the formation of filamentous actin, but also stimulate cell proliferation and the DNA synthesis (Shipley and Ham 1983), (Shipley and Ham 1983). The concentration of FCS (10%) inducing maximal DNA synthesis is 100-fold higher than that stimulating maximal stress fiber formation (0.1%) (Ridley and Hall 1992). Interestingly, the DNA production is dependent upon the arrangement of microtubuli. A microtubuli disrupting-agent had a promoting, whereas microtubuli stabilizing taxol had an inhibitory effect on DNA synthesis (Tsuji, Ueno et al. 1992).

## 2.4. Fibroblasts

Freshly-plated fibroblasts spread initially along all parts of their periphery through filapodia and lamellipodia attaining a typical fibroblast morphology (Harris 1998). Fibroblasts spreading occurs through a dynamic transition of several morphological types of protrusions named filapodia and lamelipodia. Lamellipodia are filled with an actin meshwork. Filapodia are spike-like protrusions. Actin filaments are the major component of the cytoskeleton involved in generating protrusions (Safiejko-Mroccka and Bell 1998), (Rosania and Swanson 1996), and display the highest amount of focal contacts (Harris 1998).

---

<sup>5</sup> Programmed cell death, better known as apoptosis has gained growing interest during the last few years. Apoptosis is regulated by a specific cellular program. Apoptotic cells undergo among other changes cytoplasmic fragmentation, blebbing of the plasma membranes, microbodies, cell shrinking and structural changes in the nucleus and DNA-fragmentation. Most importantly, the cytoplasmic membrane remains intact in the canonical pathway of apoptosis. In contrast, necrosis induces degeneration of the cells by swelling of the whole cell and organelles, vacuolisation, condensation of the chromatin, and loss of membrane integrity.

The polarized shape of fully spread fibroblasts is primarily a matter of directional protrusion (Harris 1998). The polarity is most often multipolar and only transiently monopodial. Typically fibroblast locomotion is visible by a leading lamella on the protrusive side and retraction fibers on the rear side. It is specially mentioned that retraction fibers do not show points of focal adhesion.

#### Contact guidance

Contact guidance<sup>6</sup> of fibroblasts was investigated with OWLS. It is a phenomena which is observed in confluent cell cultures. When a fibroblast comes into contact by its lamella to another fibroblast, the cell as a whole becomes temporarily immobile but then usually reverses the direction. Contact-inhibited cells do therefore not overlap and the cell growth is stopped with increasing confluency. Molecular details of contact inhibition induced by cell-cell contacts are still unknown.

#### Colchicine

Growing evidence exists that MTs are governing the cell polarity. Fibroblasts exposed to microtubuli-disrupting agent loose polarity and revert to the fried egg morphology. Morphological sensitivity to microtubuli-disrupting agents varies widely among fibroblasts. BHK cells are particularly sensitive. Moreover, fibroblasts of primary cultures do not undergo morphological depolarization, while fibroblasts from primary cultures might depend on MT to maintain polarity in contrast to the fibroblasts from cell-lines.

#### Cytoskeletal forces measured with the culture force monitor

By a special technique called the culture force monitor it was shown that spreading cells exert a pulling force on the substratum (Brown, Talas et al. 1996). These forces are increasing over several hours until they reach an equilibrium between the cellular contraction and the pushing microtubuli (*balancing of forces*). This behavior was described by a model called *residual internal tension* (RIT), where the microfilament exert tensile forces (*compressive loading*), whereas the MT counteract the actin tension through pushing forces (Table 2.4).

For different strains a different behavior was monitored. According to this model, colchicine<sup>7</sup> and taxol<sup>8</sup> showed opposite effects on the contraction forces. Colchicine showed an increase in the contraction forces due to the tensigrity model, where the

---

<sup>6</sup> The terms contact guidance, contact inhibition and contact paralysis have a similar meaning.

<sup>7</sup> Colchicine binds tightly and with high affinity to tubulin molecules, forming tubulin-colchicine complexes, and prevents tubulin polymerization. MT disappear and intermediate filament network collapse forming a perinuclear cap (Safiejko-Mroczka and Bell 1998). Cytochalasin B, colcemid, nocodazole and vinblastine have a similar effect.

<sup>8</sup> Taxol is a microtubuli stabilizing drug and causes neither a decrease nor an increase in cell contractility, but does block the increase in cell contractility that is otherwise caused by microtubuli-disrupting-agent (Dansowski, Harris, 1989).

resting cell tension (*compressive loading*) is displaced onto the matrix. In contrast, after the incubation in the MT-stabilizing agent taxol an immediate decrease of the contraction force was monitored. Using the *silicone rubber substratum technique*, the phorbol ester (TPA)<sup>9</sup> was found to disrupt F-actin and stress fibers as well (Danowski, Harris 1988), (Danowski 1989). The effects of a number of cytoskeleton-affecting agents can be observed within minutes by the silicone rubber substratum technique and the culture force monitor and were detected with OWLS as well.

**Table 2.4:** *Summary of the forces exerted by MT and F-actin and their correspondent disrupting agent*, (Brown, Talas et al. 1996), (Harris 1998), (Jung, Shin et al. 1997), (Tsuji, Ueno et al. 1992)

	RIT-Model	Colchicine	Taxol	Phorbolester
<b>Microtubuli (MT)</b>	pushing force	disrupts MT	stabilizes MT in the center of the cell	
<b>F-actin, stress fiber</b>	pulling force	promotes F-actin promotes stress fibers		disrupts F-actin disrupts stress fibers

## 2.5. Skin irritants

In earlier times ocular irritancy was assessed by a well known Draize test (Draize et al., 1944), which became questionable due to ethical reasons. Recently, a number of skin irritation assays were developed to study the ocular and skin irritation potential of surfactants such as benzalkonium chloride (BAC, ®Zephirol), (Lewis, McCall et al. 1993).

### Surfactants

Since cationic detergents are not repelled by the ordinarily negative net charge of the bacterial surface, they act as bactericide. The most effective detergents are the quaternary compounds, containing three short-chain alkyl groups as well as a long-chain alkyl group. These compounds are widely used for skin antiseptics and for neutralizing food utensils. Among them BAC is used as a preservative in topical ophthalmic preparations (Durand-Cavagna, Delort et al. 1989). Besides, BAC is used in cosmetic products as a foaming cleansing and bactericidal agent. It becomes a skin and

<sup>9</sup>12-O-tetradecanoyl-phorbol-13-acetate(TPA)

ocular irritant at concentrations greater than 0.1 % (Final report on the safety assessment of benzalkonium chloride 1989).

The toxicity of surfactants is based upon the perturbation of the cell membrane. The primary event or response of the perturbed or damaged cells is the release of one or both of the two groups of mediators:

- enzymes of respiration or metabolism, *e.g.* LDH, AP
- cytokines of the inflammation cascade, *e.g.* IL-6

After a membrane damage the intracellular ions are additionally released into the environment. Necrosis might be initiated by chemical or physical insults including the osmotic imbalance or energy deprivation. It has been proposed that due to loss of ATP a breakdown of the cytoskeleton occurs that lead to bleb like structures which are prone to shear stress. Further morphological changes include swelling of cells and disintegration of organelles.

#### Skin-irritation assays

Since it is very unlikely that any single model will provide an adequate overall indication of skin irritation potential, several *in vitro* tests systems to measure membrane permeability were established (Sandt and Rutten 1995):

- Conductivity test: transepithelial electrical resistance (TEER)
- Membrane-integrity / release: neutral red (NR) incorporation, fluorescein release
- Metabolic activity: lactate-dehydrogenase (LDH) release,
- Lysosomal and plasma membrane activity: acid-phosphatase (AP) release
- Mitochondrial activity: formazan salt (MTT)
- Morphology (vacuolisation), (Sandt and Rutten 1995)

All systems were sensitive and can distinguish between the variable toxicological potential of membrane-toxic substances *e.g.* for several detergents a dose-effect relationship behavior was observed. However, the different test systems displayed variable temporal sensitivities.

#### Assay sensitivity

The conductivity test indicated complete disruption of the membrane at high concentrations. TEER measurements were more sensitive than LDH and fluorescein release (Narai, Narai et al. 1997), (Ward, Walker et al. 1997). They detected the cytotoxic effect earlier and at lower concentrations.

Fluorescein measurements indicated a dysfunction of the tight junctions after the exposure to BAC. Subtle changes in the cytoskeletal structure observed by fluorescence microscopy confirmed the disruption of the tight junctions. The recovery profile after removal of BAC demonstrated that the change in the reduction capacity of the cells was directly related to the change in cell-junction integrity (R. Clothier et al, 1990).

AP was found to be an early indicator of membrane leakage. Only after 3 h exposure, lysosomal and plasma membrane permeability reached a peak value for toxic concentrations. However, neutral red uptake and the MTT test were more sensitive by an order of magnitude after an 24 h exposure time (Dickson, Lawrence et al. 1994), (Lawrence, Starkey et al, 1996), (Ward, Agarwala et al. 1994).

Since skin irritation is also associated with an immune response, several test systems were developed to measure the release of proinflammatory mediators and cytokines (Sandt, Maas et al. 1995), (Gueniche and Ponc 1993), (Parish 1990), (Pape, Degwert et al. 1993), (Lewis, McCall et al. 1993). However, these test systems are not successful yet.

#### Sensitivity of cell types

Since many *in vivo* data had been collected by the Draize test, it was also interesting to compare the differences between several species such as man, rabbit and rat. In fact, cells from several species were used to study the irritation potential of BAC and the results displayed only small differences in the dose-effect relationship for different species (Lawrence, Starkey et al. 1996), (Sandt and Rutten 1995).

Since the skin is constituted of several cell types such as keratinocytes and fibroblasts, the effect of BAC on keratinocytes and fibroblasts was investigated. The use of two cell types in combination could be helpful in distinguishing surfactant sensitivities depending on the cell origin, epithelial for keratinocytes and mesodermic for fibroblasts. They both showed comparable toxic concentration levels (Gueniche and Ponc 1993), (Cornelis, Dupont et al. 1992). Similarly, BAC toxicity was found to be in a comparable range for both primary cells and cell-lines (Ward, Agarwala et al. 1994).

In summary, the choice of the cell type does not greatly alter the surfactant toxicity. The deleterious effect of surfactant has a relatively non-specific effect on a variety of biological systems and due to this common mechanism of membrane-perturbation a similar dose-response relationship is observed (Durholt, Steger-Hartmann et al, 1995).

## 2.6. Human hepatoma cells

Hepatoma cells display a wide-xenobiotic metabolism and are often used to study the toxicity and degradation of xenobiotic compounds. They show a different morphology and locomotion, when compared to fibroblasts. However, the principle of the



cytoskeleton and the effects of the microtubuli-disrupting agents are similar. The culture of primary hepatoma cells requires specific know-how concerning liver-perfusion, isolation of hepatocytes and culture conditions. For this study a well established and rapidly proliferating cell line Hep G2 was used. This cell lines originates from a human tumor. Accordingly the cells are not sensitive to contact-inhibition. Although serum was essential for strong cell adhesion and spreading, this cell line was able to proliferate in serum-free medium. Finally, the exposure to drugs such as 2.7. *Cycloheximide* and 2.8. *Cyclophosphamide* displayed that the proliferation rate can indicate of toxicity. Therefore this cell-line represents an alternative to the slowly proliferating fibroblasts.

### OWLS

The measuring principle of OWLS should be universal for anchorage-dependent cells. As illustrated schematically in Table 2.6 two cell strains with completely different properties were used for the OWLS experiments. Despite the biological differences of these two cell-lines, a similar sensor response was expected. In order to better compare, the experiments with fibroblasts and hepatoma cells with serum and the cytoskeleton-modifying colchicine were run at equal experimental conditions (Table 2.6). Moreover long-term experiments showed a different proliferation rate of the two cell strains.

*Table 2.6: Comparison of the biological properties of 3T3-fibroblasts and hepatoma cells*

<b>Cell-line</b>	<b>Origin</b>	<b>Proliferation</b>	<b>Contact-Inhibition</b>	<b>Xenobiotic activation</b>
<b>Fibroblasts: Swiss-3T3</b>	Endothelial, mouse	slow, depends on growth-factors	positive	no
<b>Hepatoma cells:Hep G2</b>	Epithelial, human tumor	fast partly independent of growth factors	negative	yes

## 2.7. Cycloheximide

Cycloheximide (CY) belongs to the class of glutarimide antibiotics that inhibit protein synthesis. It specifically inhibits protein synthesis in eukaryotes (80S) having larger ribosomes than bacteria (70S). The inhibition involves mainly peptide-initiation where amino acids are transferred from aminoacyl-transfer RNA to reticulocyte ribosomes. Aminoacyl t-RNA may be enzymatically bound to the acceptor ribosomal site, but not the donor site. Translocation from the acceptor to the donor site occurs during a reaction requiring a reticulocyte-binding-enzyme-transfer-factor and the hydrolysis of GTP. The class of glutarimide antibiotics specifically inhibits the translocation from the acceptor to the donor site.

The range of CY-inhibition of t-RNA<sup>Phe</sup> binding is between  $2.8 \times 10^{-2}$  to 281  $\mu\text{g/ml}$  in cell free system ( $I_{50\%} = 2.81 \mu\text{g/ml}$ ) and the concentration range of cellular toxicity is within a very similar range (Obrig, Culp et al, 1971). Almost 90% inhibition of [<sup>3</sup>H]-leucine incorporation was observed with rat thymocytes at 4  $\mu\text{g/ml}$  CY. The exposure to CY (1  $\mu\text{g/ml}$ ) for 6 h had an immeasurable effect on the viability (MTT), whereas the protein synthesis was reduced by up to 80% (Chow, Peters et al. 1995).

## 2.8. Cyclophosphamide

Cyclophosphamide (CP, ®Endoxan) is used in tumor therapy and for immunosuppression, where both humoral and cell-mediated immunity are known to be suppressed (Kawabata, Chapman et al. 1990). Cyclophosphamide is applied in over 200'000 patients each year in the U.S. for cancer treatment. It is toxic to various tissues including the lung and bladder.

Under the influence of the cytochrome P450 monooxygenase system, CP is metabolized to 4-hydroxy-CP (Fig. 2.8). The hydroxylated metabolite nonenzymatically rearranges to aldophosphamide mustard (APM), which breaks down to phosphoramidate mustard (PAM) and acrolein. The alkylating property of PAM is thought to mediate the anti-proliferative and cytotoxic actions of CP by binding to DNA and inhibiting cell proliferation.

Acrolein is highly electrophilic and reacts with the free thiol group of the tripeptide glutathione (GSH) to form the acrolein-glutathione conjugates and other sulfhydryl groups of cellular molecules. These compounds can be further metabolized to mercapturic acids (MCA). Due to the toxicity of acrolein in lungs and bladder the transported species is unlikely to be acrolein. However the release of acrolein from various thio-conjugates via  $\beta$ -elimination reaction is possible that then affects factors

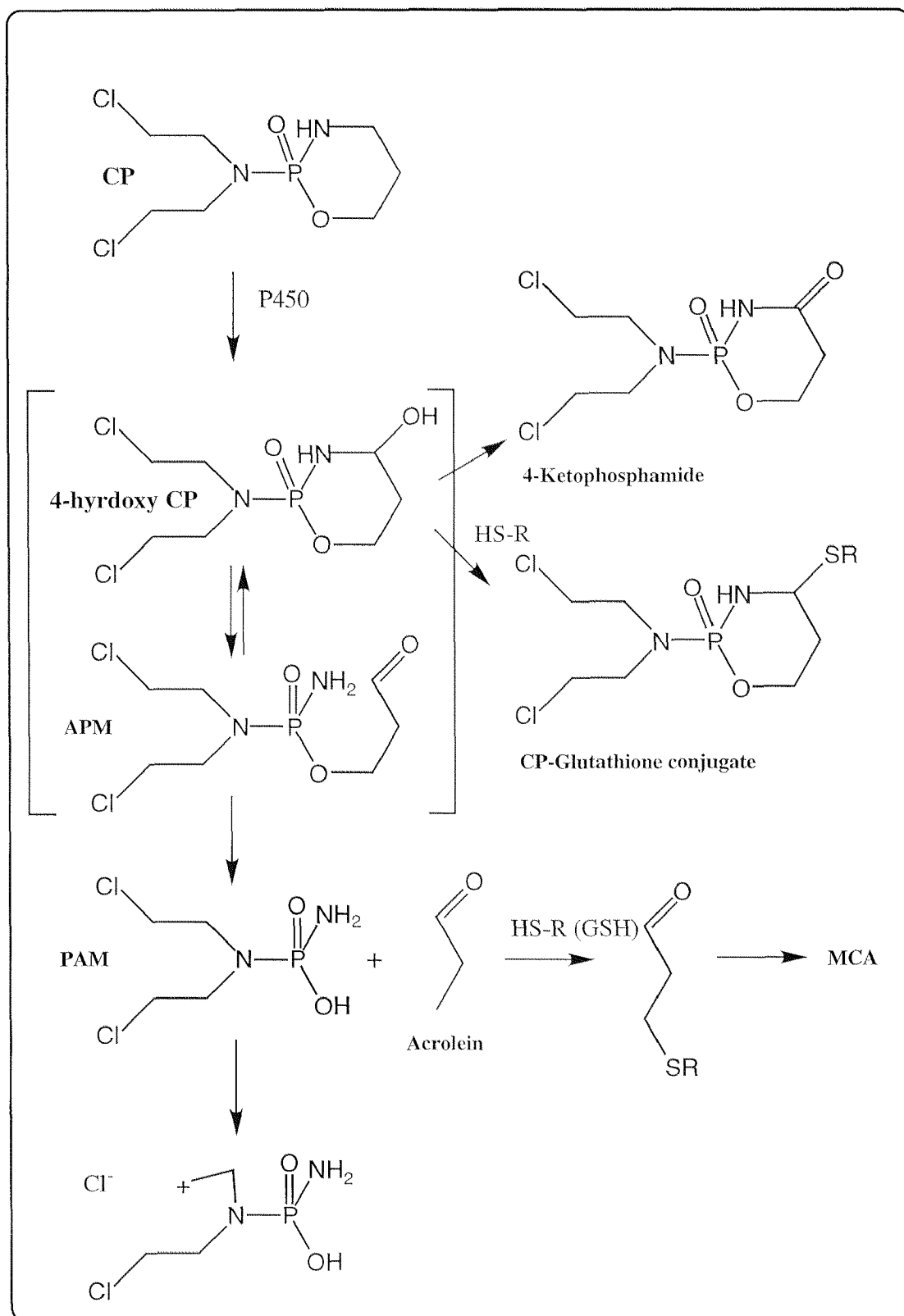


**Fig. 2.8:** Schematic illustration of the metabolic degradation of CP in the human body: CP is metabolized by P450 to 4-hydroxy CP, which spontaneously breaks down to the reactive intermediates PAM and acrolein. Alternatively 4-hydroxy CP may be inactivated either to 4-Ketophosphamide by an aldehyde dehydrogenase or to a glutathione (GSH) conjugate.

necessary for cell proliferation (Ramu, Perry et al. 1996). Overall the metabolite of CP are cancerogenic, teratogenic, cytotoxic and immunosuppressive.

In humans CP is used in a concentration range of 2-8 mg/kg/d as an antitumor agent. Immunosuppression was observed at 5-10 mM in cocultures of splenocytes and hepatocytes (Kawabata, Chapman et al., 1990).

## 2.9. Cell-spreading and cell-death

In traditional biochemical assays the measuring principle is based upon a defined process within the cell. However, the basic idea of this biosensor is that spreading includes information about the viability and metabolic state of the cell.

### Epithelial cells

It was shown by Shingvi that the degree of spreading is essential for growth and survival of primary rat hepatocytes (Shingvi, Sthepanoloulos et al. 1993); cells held in suspension enter apoptosis and die. Hepatocytes were plated on laminin-coated substrata of defined size (2-80  $\mu\text{m}$ ), such that cell-cell contact was largely prevented. The spreading of the cells was limited by the size of the protein-adhesive islands and the hepatocytes conformed to the shape of the underlying islands. The study showed an increasing DNA-production with an increasing size of the islands. Only 3% of the hepatocytes cultured on the smallest islands entered the S-phase<sup>10</sup>. In contrast to the hepatocytes cultured on unpatterned surface, which secreted high levels of albumin, the spreading restricted hepatocytes maintained a normal level of albumin secretion for at least three days.

### Endothelial cells

In another study, the degree of cell spreading on growth and apoptosis of bovine capillary endothelial cells was investigated (Chen, Mrksich et al. 1997). Cells were plated on cell-adhesive islands with different-sizes. Significantly more cells entered apoptosis when spreading was limited by the size of the fibronectin-coated islands than spreading on homogeneously fibronectin coated surfaces. Furthermore DNA synthesis correlated directly with the projected cell area measured. In a similar study the shape of the 3T3 cells was controlled by variation of substratum adhesiveness (Folkman and Moscona 1978). The DNA-synthesis (<sup>3</sup>H-thymidine incorporation) was found to be inversely proportional to the height of the cell in confluent 3T3 cells. Serum and other extracellular matrix molecules such as collagen and vitronectin were able to modulate the cellular response to a shape distortion (Ingber 1990). However, the mechanism by which cells transduce changes in cell shape into different responses remains unclear. In

---

<sup>10</sup> The different phases of cell division have several names such as S-, G<sub>0</sub>-, G<sub>1</sub>-, G<sub>2</sub>- and M-phase. During the S-phase, which may last several hours, the DNA is duplicated.

conclusion, the cell shape represents a switch between life and death, and it is hypothesized that the cytoskeleton may herein play a fundamental role.

### 3. Optical Waveguide Lightmode Spectroscopy

#### 3.1. Basic principles

Snell's law describes the reflection of light at the boundary of two dielectrics F and A with the refractive index  $n_F$  and  $n_A$  (Eq. 3.1). For  $n_F > n_A$ , a beam of light propagating in the dielectric medium F with an angle  $\alpha_F$  to the normal of the dielectric-interface is refracted at the interface with an angle of  $\alpha_A$  to the normal of the interface. This is called *external reflection*.

$$n_F \sin \alpha_F = n_A \sin \alpha_A$$

Equation 3.1

For  $n_F < n_A$  the light beam traveling in F is not refracted but is reflected at the dielectric boundary. This phenomena is called *total internal reflection* and is the basis for many practical applications in integrated optics.

In the case of the waveguide the light beam propagating in the external medium must be coupled into a dielectric with higher refractive index. Both prisms and grating have been used as coupling devices. If a laser beam impinges on the diffraction grating it can excite a guided mode with the effective index N. The coupling condition for gratings is described by the following equation:

$$N = n_{air} \sin \alpha + l\lambda / \Lambda$$

Equation 3.2

where  $l = \pm 1, 2, \dots$  is the diffraction order which amounts to  $l = 1$  for monomode waveguides,  $\Lambda = 2400$  lines/mm for the ASI-waveguide 2400 and  $\lambda = 633$  nm for the He-Ne laser.

Once trapped in the dielectric the light in the guided mode is reflected with a phase shift as if the light were reflected only at a distance  $\Delta z_{F,A}$  from the interface.

$$\Delta z_{F,A} = \frac{1}{|k_{z,F}| \left[ \left( \frac{N}{n_F} \right)^2 + \left( \frac{N}{n_A} \right)^2 - 1 \right]^\rho}$$

Equation 3.3

where  $k_{z,F} = (2\pi/\lambda) * n_F * \cos \alpha$  is the wave component perpendicular to the waveguide and  $\rho$  equals 0 and 1 for transverse electric (TE) and transverse magnetic (TM) field

respectively. For the red He-Ne laser light used in the OWLS application the  $\Delta z_{F,A}$  amounts to about 100 nm as illustrated in Fig. 3.1.

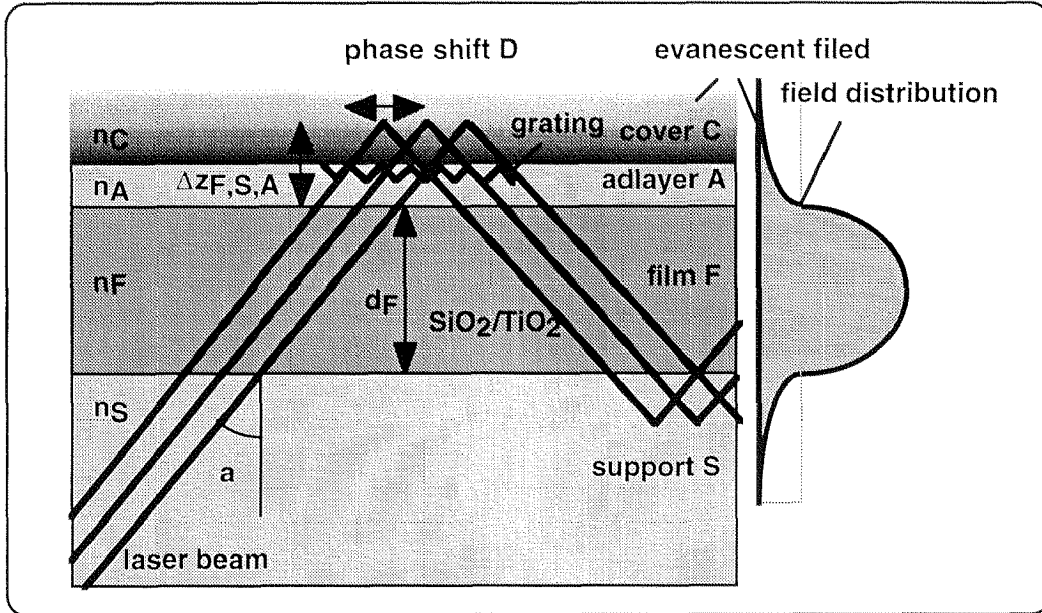


**Fig. 3.1:** OWLS-principle: The laser beam is coupled by a grating into the  $\text{SiO}_2/\text{TiO}_2$ -film. The light is totally reflected at the upper and lower boundary of the dielectric film F, where it undergoes a phase shift D. In spite of the fact that the light is totally reflected, there is still an electromagnetic wave field in the region beyond the interface, called the evanescent wave. The field distribution of the perpendicular component is shown on the left side and amounts to 100 nm for the ASI-waveguide and  $N(\text{TE})$ .

The field distribution of the perpendicular component for the three mode equation can be described by the following equation, where the field outside the waveguide represents the evanescent wave.

$$\tan(k_{z,F}, d_F) = \frac{(|k_{z,C}| + |k_{z,S}|) * k_{z,F}}{k_{z,F}^2 - |k_{z,C}| |k_{z,S}|}$$

Equation 3.4

The evanescent wave can be used for sensing the adsorption of molecules. When molecules adsorb on the surface of the waveguide, the phase shift of the guided mode is changed depending on the amount and polarizability of adsorbed molecules. In order for a ray to propagate with the highest intensity along the waveguide, its phase shift must be equal to zero or an integral multiple of  $2\pi$  radians. This condition is

summarized in the mode equation for asymmetric waveguides<sup>11</sup>:

$$d_F k_{z,F} + \Phi_{F,S} + \Phi_{F,A,C} = 2\pi m \quad \text{Equation 3.5}$$

where  $\Phi_{F,S}$  is the phase shift at the S,F-interface,  $\Phi_{F,A,C}$  is the phase shift at the adlayer A and the medium C and  $d_F \cong 180$  nm is the thickness of the waveguide. Due to the phase-shift the light intensity of both the transverse electric (TE) and transverse magnetic (TM) fields attain each a maximum at certain angles (coupling angles) between the waveguide and the laser beam.

$$r_{F,J} = \exp(i\Phi_{F,J}) = \frac{(k_{z,F} / n_F^{2\rho} - k_{z,J} / n_J^{2\rho})}{(k_{z,F} / n_F^{2\rho} + k_{z,J} / n_J^{2\rho})} \quad \text{Equation 3.6}$$

where  $\rho$  equals 0 and 1 for transverse electric (TE) and transverse magnetic (TM) fields respectively and  $k_{z,F} = k(n_J^2 - N^2)^{1/2}$ . Taking the expression of the mode equation for asymmetric waveguides (Eq. 3.5) and substituting the expression for  $\Phi$  by the Fresnel reflection coefficients for reflection at the interface F-J (J = S, C) (Eq. 3.6), we finally obtain the complete mode equation for the four-mode layer waveguide:

$$\pi m = \frac{2\pi}{\lambda} \sqrt{(n_F^2 - N^2)} \left[ d_F + d_A \frac{n_A^2 - n_C^2}{n_F^2 - n_C^2} \right] \left[ \frac{(N/n_C)^2 + (N/n_A)^2 - 1}{(N/n_C)^2 + (N/n_F)^2 - 1} \right]^\rho - \arctan \left[ \left( \frac{n_F}{n_S} \right)^{2\rho} \left( \frac{N^2 - n_S^2}{n_F^2 - N^2} \right)^{1/2} \right] - \arctan \left[ \left( \frac{n_F}{n_C} \right)^{2\rho} \left( \frac{N^2 - n_C^2}{n_F^2 - N^2} \right)^{1/2} \right] \quad \text{Equation 3.7}$$

where  $\rho$  equals 0 and 1 for transverse electric (TE) and transverse magnetic (TM) fields respectively.

The coupling angles are measured by the ASI system and used for calculations of the refractive mode indices  $N(\text{TE})$  and  $N(\text{TM})$  of the  $\text{SiO}_2/\text{TiO}_2$ -layer with the adlayer of the adsorbed molecules. A proprietary software (ASI company) has been used for this purpose (Eq. 3.6). In the case of an isotropic protein monolayer the shifts of these refractive mode indices are functions of the refractive index and thickness of the adlayer,  $n_A$  and  $d_A$ .

The refractive index of a protein solution  $n_A$  depends linearly upon its concentration according to

<sup>11</sup> The asymmetric waveguides have at one side the substrate and at the other side the medium with adsorbed molecules.



$$n_A = n_C + c_A * dn/dc$$

Equation 3.8

where  $n_c$  is the refractive index of the solvent and the coefficient  $dn/dc$  depends on the polarizability of the protein and has a quasi-universal value of  $0.182 \text{ cm}^3/\text{g}$  for all proteins (Ramsden 1993).

According to the Gibbs convention, the surface excess of the proteins *i.e.* the mass density of adsorbed proteins is for  $c_A \gg c_C$  defined as

$$M = c_A d_A$$

Equation 3.9

Using the first equation to eliminate  $c_A$  it becomes

$$M = d_A (n_A - n_C) / (dn/dc)$$

Equation 3.10

Using Eq. 3.10 the mass of adsorbed protein can be calculated. In comparison to proteins, the structure of the cell is much more complicated and heterogeneous and the coefficient  $dn/dc$  is different for each constituent of the adlayer. In the situation, where molecules with different coefficients adsorb at the same time on the ASI-biosensor the mass can not be calculated anymore. However, in the case of cell adhesion it is not necessary to know exactly the mass adsorbed in the adlayer. What is needed is only an indication that a mass is being adsorbed or desorbed. And for that the information obtained from the change of any one of the refractive mode indices is sufficient. For sensitivity reasons (Tiefenthaler and Lukosz 1989), the N(TE) mode was chosen in all our measurements.

### 3.2. Sensitivity

Due to different sizes of proteins and cells the signals of the ASI-biosensor have different meanings. BSA adsorbs as an isotropic monolayer, whose thickness is far below the penetration depth of the evanescent field, and the OWLS can measure the total amount of BSA adsorbed. In contrast, the height of an adsorbed and fully spread cell is in the range of several  $\mu\text{m}$  and therefore only a part of the cell mass is located within the 100 nm penetration depth of the evanescent field (Figure 3.2).

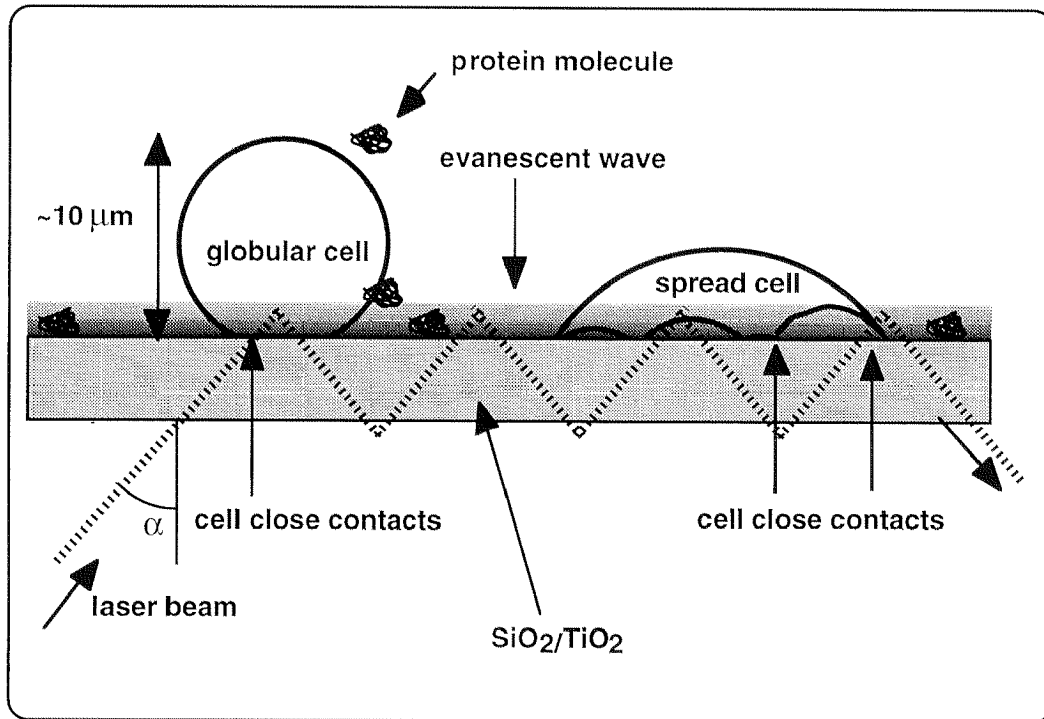


*Fig. 3.2: The OWLS-sensitivity regarding the size and shape of proteins and cells. Compared to the penetration depth of the evanescent field, the protein molecules are small and lie completely within the penetration depth of the evanescent wave. Instead, the cells are in the order of micrometers and therefore the OWLS only detects the regions of close contacts.*

In this case the OWLS-signal depends upon the cell morphology and shape in close contact with the chip surface. In the process of cell transformation from a globular (*e.g.* after cell dissociation) to a flat shape the contact area between the ASI-chip and the cell increases. Since the change of the refractive mode index is proportional to the contact area of the cells, this change in the cell shape can be detected, although the adsorbed mass can not be calculated.

### 3.3. Time-dependent selectivity

The process of adhesion and spreading of cells occurs normally in the presence of medium containing serum proteins. However, waveguide spectroscopy is nonspecific, and both protein adsorption and cell adhesion with spreading contribute effectively to the OWLS-signal (Fig. 3.3). As we are interested only in measuring cell adhesion and cell spreading, a procedure had to be found, where the effect of protein adsorption can be eliminated or accounted for. This procedure consists in separating protein adsorption (and cell settling) from cell adhesion and spreading on the time scale and it is based on the very different diffusion rates of protein molecules and cells in solutions.

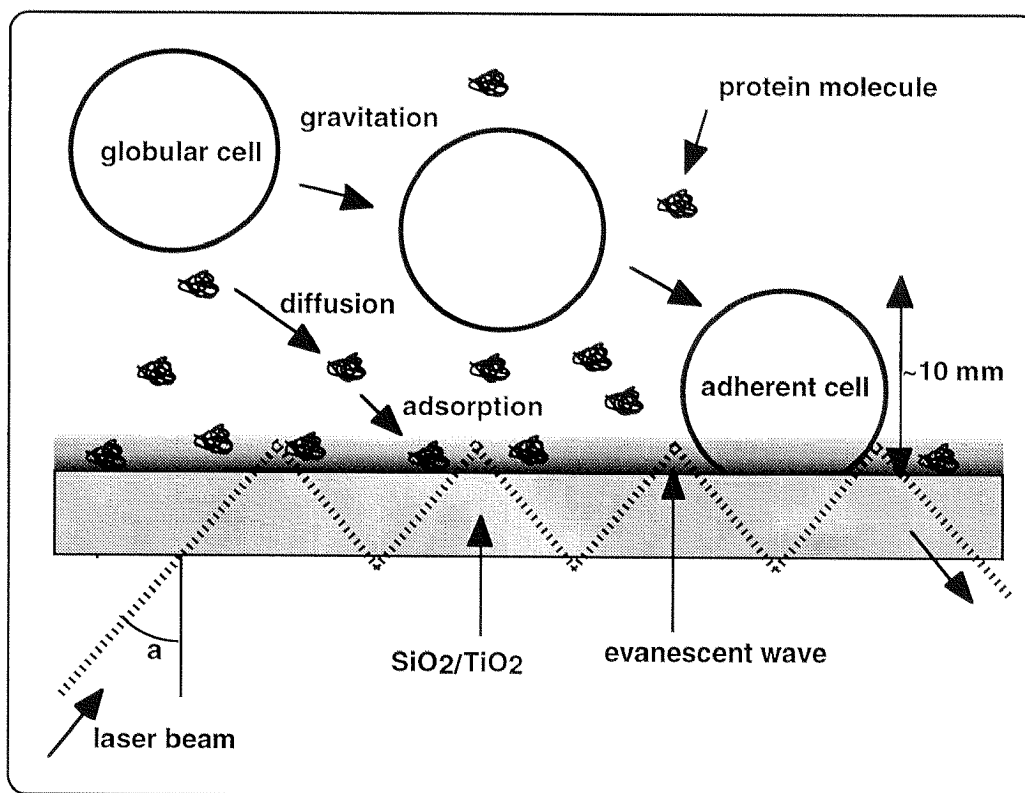


**Fig. 3.3:** *Competitive adsorption of serum proteins and cells: If the flow through the measuring chamber is stopped both proteins adsorb and cells adhere on the waveguide. The transport of proteins is controlled by diffusion and the adsorption process, whereas cell settling is driven by gravitation.*

To be able to distinguish between protein adsorption on one side and cell adhesion and spreading on the other, the process of protein adsorption and the process of cell adhesion were separated on the time scale. To achieve this all the cells in the measuring chamber must settle by the time protein adsorption occurs. After ten minutes when protein adsorption (see 5.1. Protein adsorption) and cell settling is nearly completed,

the sensor signal is mainly due to cellular adhesion of the settled cells and then the cell spreading kinetics is followed.

#### Cell settling

To control the settling time, which is proportional to the settling distance, the height of the measuring cell had to be calculated. The settling of suspended cells is mainly driven by the gravitational force and the settling velocity of a suspended cell  $u_t$  (cm/s) is given by (Vunjak-Novakovic, Obradovic et al. 1998):

$$u_t = \frac{d_p^2}{18\mu} (\rho_p - \rho_f) g = 3.89 * 10^{-4} \frac{cm}{s}$$

Equation 3.11

where  $d_p = 10 \mu m$  is the diameter of the cell,  $\rho_p = 1.05$  is the density of a cell,  $\rho_f = 1 g/cm^3$  is the density of fluid and  $\mu = 0.7$  cP is the fluid viscosity. Therefore, in order to have a settling time of no more than ten minutes, the height of the measuring cuvette should not exceed 2 mm.

#### Flow conditions

The transport mechanisms at continuous flow conditions for proteins and cells are different. Due to the laminar flow within the measuring cuvette, protein transport from the bulk to the  $SiO_2/TiO_2$  surface is mainly controlled by diffusion. In contrast, the settling of cells is best described by gravitation. The continuously tilting measuring cuvette and the circular shape of the measuring cuvette have not been considered.

In order to reach reproducible cell and proteins concentration, the best flow conditions had to be found. It is supposed that the cells are accumulated within the measuring cuvette by settling before reaching the outlet. To obtain a homogeneous cell distribution within the measuring chamber, the settling rate must thus become negligible and a high flow rate (5 ml/h) was chosen to introduce the cells into the measuring cuvette. In a cell experiment the flow was stopped after 3 min, which corresponds exactly to the filling of the inlet tube and the measuring cuvette. Once the flow was stopped, all the cells present in the cuvette settle to the waveguide. At this moment the protein adsorption had already started and was nearly finished within 8 min. The height of the measuring cell was chosen such that the cells settling time was of the same order as the protein adsorption time. For the settling time of eight minutes, the height of the measuring cell was found to be 2 mm (Eq. 3.11).

#### Cell adhesion and spreading

After cell settling and completed protein adsorption, the cells adhere and spread. In contrast to the time of protein adsorption and cell settling the time of cell adhesion and spreading in the order of hours. The contact area of the cells with the waveguide chip

increases for several hours until the *fully spread state* of the cells, *the steady state*, is reached. Therefore, the selectivity between proteins and cells is based upon different rates of protein adsorption and cells adhesion and spreading respectively.

## 4. Materials and Methods

### 4.1. Materials

Potassium monopersulphate triple salt, neutral red, cyclophosphamide and colchicine were all purchased from Fluka-Chemie AG (Buchs, Switzerland). HEPES, Gentamicin, trypan blue, the tetrazolium salt for the MTT assay and the 25 cm<sup>2</sup>-culture flasks were from Sigma (Fluka-Chemie AG, Buchs, Switzerland). Optimem was obtained from Life Technologies (Basel, Switzerland) and fetal calf serum was from Oxoid (Basel, Switzerland). Trypsin was from Gibco (Life Technologies, Switzerland). ASI-2400 chips were obtained from Artificial Sensing Instruments (ASI, Switzerland). The BCA protein assay reagent A was purchased from Pierce (Socochim, Lausanne, Switzerland). The acid-detergent cleaner for the ASI-chips was from Hoffmann-La Roche (Basel, Switzerland). The MVQ-caoutchouc for the measuring chamber was supplied by Angst & Pfister (Zürich, Switzerland).

### 4.2. Cell culture

The L-M(TK-) fibroblasts (L-fibroblasts, ATCC CCL1.3) were obtained from the University Hospital of Zurich. Two different Swiss-3T3 fibroblasts cell-line were used: embryo fibroblasts (E-fibroblasts, ATCC CCL 92) were from Masaryk University, Brno and Swiss 3T3 j2-fibroblasts (J-fibroblasts, (Rheinwald and Green 1975)) were from the Karolinska Institute, Stockholm. The hepatoma cells (Hep-G2, ATCC HB8065) were from the Institute of Toxicology, ETH Zurich. This cell-line originates from a human liver carcinoma showing epithelial-like morphology.

These cell-lines grow rapidly and form monolayers. They were cultured in Optimem supplemented with 4% (v/v) FCS and 2 ml/l Gentamicin in 25 cm<sup>2</sup>-culture flask. The cells were grown in culture flasks placed in a humidified, CO<sub>2</sub>-controlled (5%) incubator at 37°C. After reaching confluency the cells were subcultured using 0.5 % (w/v) trypsin-5.3 mM EDTA.

Cell suspensions for the cell adhesion experiments were prepared by detaching the cells from the culture flask bottom with trypsin-solution. Trypsinization was stopped by adding FCS containing medium. After centrifugation they were suspended in the HEPES-buffered medium supplemented with 4% (v/v) FCS. The cell suspension was then diluted to approximately 250,000 viable fibroblasts/ml and 450,000 viable hepatocytes/ml. The cell viability was determined by the trypan blue dye exclusion method.

### 4.3. Viability measurements

For the viability assays between 200,000 and 300,000 cells were seeded in 24-multiwells. When adhesion and spreading was completed after 4 - 8 hours, the cells were exposed to the drug or in the case of serum deprivation, the medium containing FCS was replaced by serum-free medium. Each measurement was performed in duplicate. A protocol of the viability measurements and the solutions (MTT-, NR-lysis buffer, Karnovsky) are listed in the *Appendix*.

For the tetrazolium assay, 300  $\mu$ l MTT-solution was added to each well and the multi-well plate was incubated at 37°C for about 1 h. Then all solution was depleted and 100  $\mu$ l lysis solution was added. When the color was developed after some 15 min the OD was measured at 560 nm.

For the neutral red assay, 90  $\mu$ l NR-solution was added to each well and the multi-well plate was incubated at 37°C for about 1 h. Then all solution was removed completely and the cells were fixed by adding 30  $\mu$ l Karnovsky solution into each well. After 10 min the cells were washed with 100  $\mu$ l PBS buffer and 100  $\mu$ l lysis buffer was added. When the color was fully developed the OD was fluorimetrically measured at 540 nm.

For the total protein assay, the cells were fixed by adding 600  $\mu$ l Karnovsky solution to the medium in each well. Then the cells were washed with PBS. To the fixed and dried cells 300  $\mu$ l of the freshly prepared BCA protein assay solution was added. When the blue color was fully developed the OD was measured spectrophotometrically at 560 nm.

### 4.4. The OWLS-Setup and the measuring cuvette

The pump, the ASI-waveguide and the tubes with medium and cells were all kept in a thermostated box at 37°C as illustrated in Fig. 4.1. The waveguide position was controlled by a personal computer. The key element of the optical biosensor is the sensor chip mounted on a turnable table. The optical waveguides from the Artificial Sensing Intelligence, Zurich (ASI) consist of a glass-chip upon which a  $\approx$ 180 nm thick layer of SiO<sub>2</sub>/TiO<sub>2</sub> was spincoated. By a grating embossed into this layer a polarized laser light is coupled into the SiO<sub>2</sub>/TiO<sub>2</sub> layer propagates within this layer by total internal reflection due to its high refractive index of SiO<sub>2</sub>/TiO<sub>2</sub> ( $n_r = 1.75-1.82$ ).

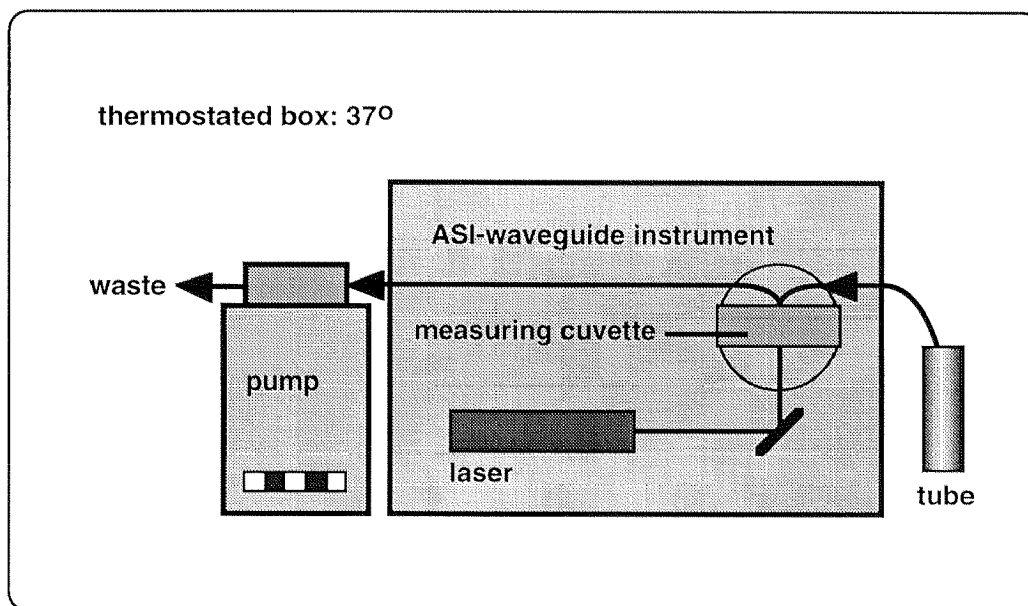


**Fig. 4.1:** *OWLS-setup: The waveguide, the pump and the tube containing either medium alone or medium with cells and serum were all hold in thermostated box at 37°C.*

#### Measuring cuvette

A new measuring chamber made of a food grade MVQ silicon-caoutchouc was constructed for the cell experiments. To prevent gradients within the ASI sensing region a circular shape for the measuring chamber was chosen. The chamber of a cylindrical shape of 190  $\mu\text{l}$  ( $r = 5.5$  mm,  $h = 2$  mm) was sandwiched between the ASI chip and an ocular micrometer plate which was used as a window for microscopy (Figure 4.2). In this way, the cells inside the measuring chamber could be also observed by inverted phase-contrast-microscopy. Through the inlet-tube with a total volume of 50  $\mu\text{l}$ , medium and cells were sucked into the chamber by a peristaltic pump with an outlet into the waste.

#### Waveguides

The waveguides ASI-2400 were initially etched in a 1% (w/v) permonosulphuric acid ( $\text{H}_2\text{SO}_3$ ) overnight to increase hydrophilicity of the chip as well as cell adhesion. At the end of each experiment the ASI chip was washed in an ultrasonic cleaner first with an acid-detergent cleaner, and after that with acetone for 15 min. The chips could be used up to ten times, before the grating became so much damaged that the ASI software rejected the chip. The inlet and outlet tubes were rinsed and sterilized with 70% ethanol.



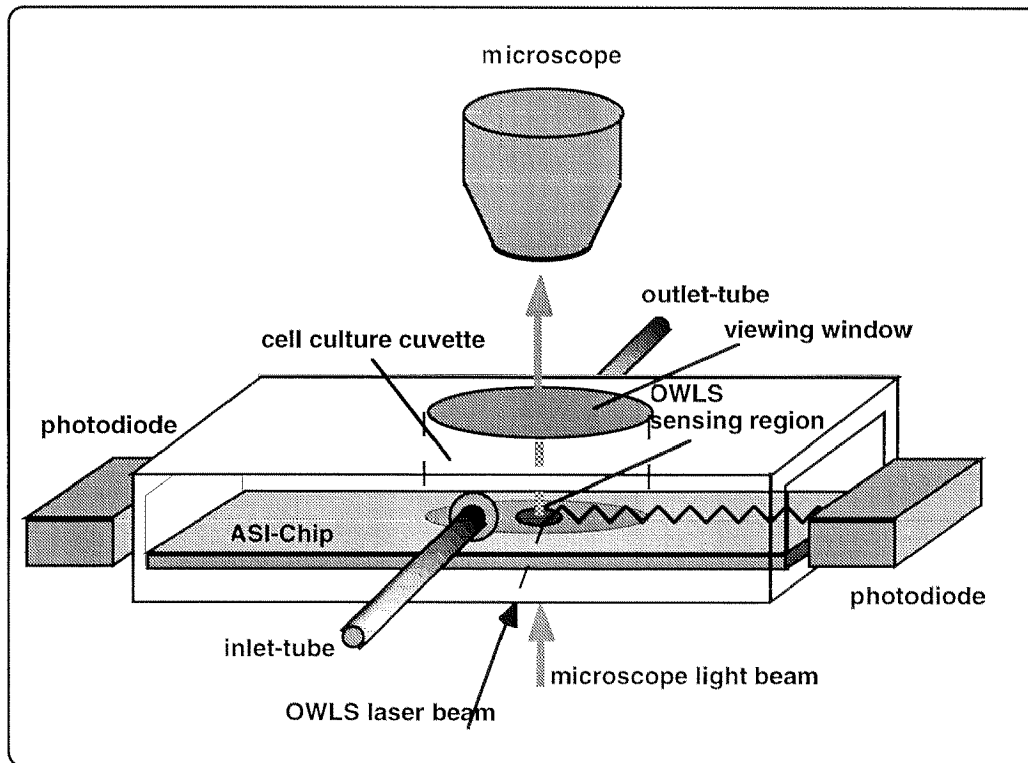


**Fig. 4.2:** *The OWLS-measuring cuvette: All parts of the measuring chamber are fixed in the sample holder. The measuring cuvette consists of an cylindrical, 2 mm high caoutchouc piece, sandwiched between the ASI waveguide and the ocular micrometer plate. Syringe needles for the inlet and the outlet were pierced through the caoutchouc.*

#### Cell culture medium

Due to the surface charge of the hydroxyl-groups of the  $\text{SiO}_2/\text{TiO}_2$  surface, the OWLS is sensitive to pH drifts (Kurrat, Prenosil et al. 1997). Accordingly, the medium for the OWLS experiments was buffered with 50 mM HEPES. To prevent gas-bubbles, which disturb the measurements, the medium was degassed at 500 mbar prior its use in the OWLS. Since serum proteins adsorbed on the ASI chip decrease the sensitivity, the FCS content of the Optimem-medium was reduced to 4% (v/v). When the buffer was changed or the FCS content was decreased, cell survival and growth was not affected. Unless the flow was stopped to allow cell settling and adhesion on the waveguide, all measurements were performed during continuous flow through the measuring chamber. No visible changes in cell morphology grown on the waveguide under continuous flow or in the culture flask were observed by inverted phase-contrast microscopy.

#### Light sensitivity

Since light is known to induce the depolymerization of MT in a dose-dependent manner, the laser-beam was interrupted unless the waveguide was measuring (Sporn and Foster 1992). The light quantity in the study of Sporn is comparable to the laser power of

the OWLS. As demonstrated with this setup, the filled in cells within the sensing region did not spread and remained in a globular shape as shown in Fig. 4.3, if the laser was not interrupted .

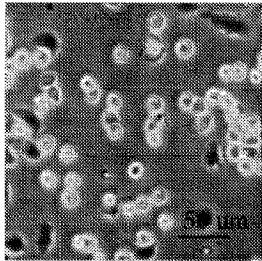


**Fig.4.3:** *Influence of light exposure on cell morphology: If the cells were continuously exposed to the laser beam, the cells within the sensing region did not spread and remained in a globular shape.*

To reduce the light exposure of the cells further to the lowest possible level, the measurement frequency was reduced. At the beginning of the experiment, where the OWLS-signal was steadily increasing the measuring period was 30 s. After 10 min, the measuring period was increased to 5 min and after one hour to 20 min.

#### **4.5. Experiments**

Each experiment started with serum-free medium flowing through the measuring chamber at 5 ml/h to establish the baseline. To measure serum adsorption, the flow was switched to medium supplemented with 4 % (v/v) FCS.

##### **Cell experiments**

For the cell experiments the trypsinized cells were diluted to different cell concentrations. To determine the cell-concentration a Neubauer counting chamber was used. The cell suspension prepared earlier was pumped through the measuring chamber for 3 min at a rate of 5 ml/h. This was needed to transport a suspension volume corresponding approximately to the filling of the measuring chamber of 190 μl and the inlet tube 50 μl together. After that, the flow was stopped to induce cell settling.

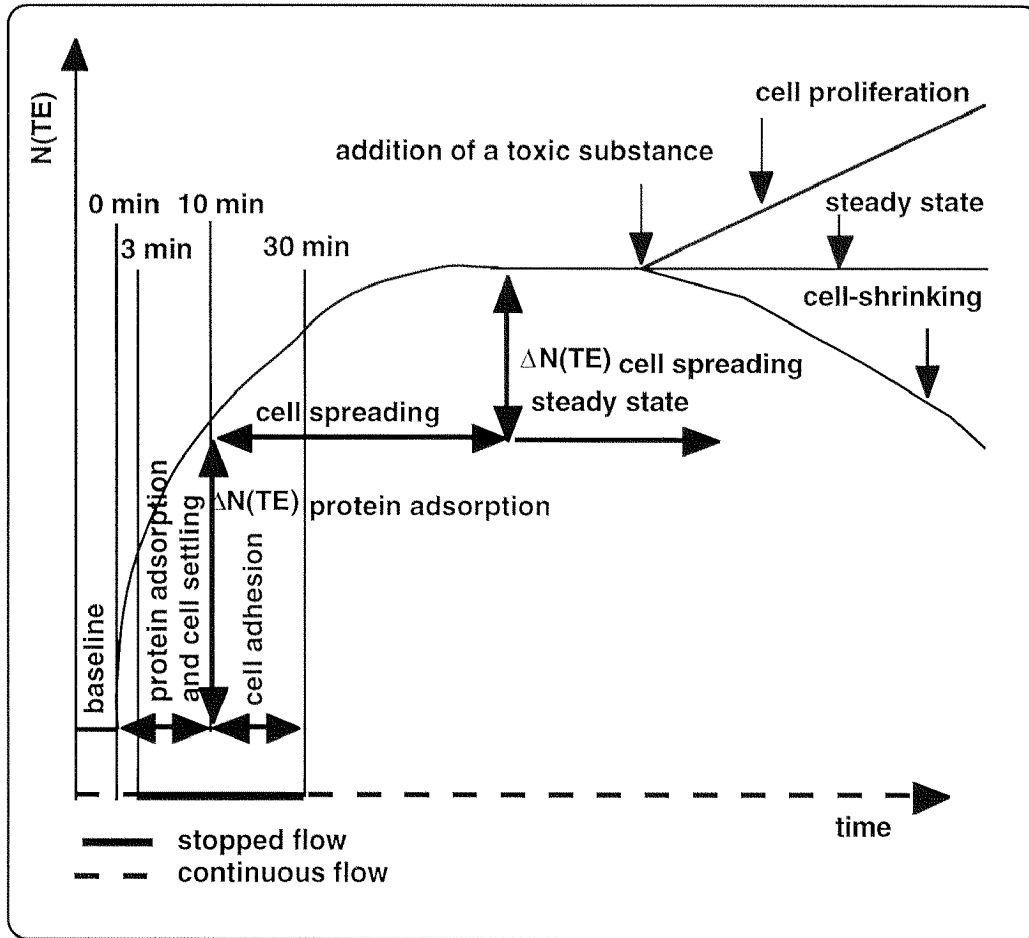


**Fig. 4.4:** *OWLS-experiment: An OWLS experiment consisted of four phases: The first phase was the baseline, where pure medium was flown through the measuring cuvette. Then the flow was switched to medium with serum and cells. After three minutes the flow was stopped such that cells could adhere. After 30 min the flow was resumed at a five times lower rate of 1 ml/h to keep the medium conditions constant. After having reached a constant signal for several hours, a toxic substance could be added.*

As the cell suspension entered the measuring chamber, the OWLS-signal increased sharply due to the adsorption of serum proteins. In the case of purely serum containing Optimem the signal reached a constant level after approximately 10 min because proteins adsorb very fast. In the case of a mixture of serum containing Optimem and cells the OWLS-signal increased steadily. After 30 min all the viable cells adhered tightly and the flow of medium, this time without cells, was resumed at a flow rate of 1 ml/h. A continuous flow guaranteed stable pH and reproducible medium conditions. During experiments no infection was ever observed.

To show the effect of FCS on cell spreading, cells suspended in serum-free medium were flown into the measuring chamber. When the OWLS-signal became constant the flow of the medium containing 4 % (v/v) FCS was resumed. When the fully spread

state was reached, the cells were again deprived of serum by a flow of serum-free medium.

#### Longterm experiments and test compounds

After 4 - 6 h cell spreading was ususally completed (*fully spread state*) and in the case of the fibroblasts the OWLS-signal became almost constant for up to 48 h. The hepatoma cells remained at the steady state only for a short time, and then the OWLS-signal started to increase further again but at a lower rate.

The reproducible long-term behavior of the OWLS-signal was the key for the experiments with toxic substances such as colchicine and BAC. At steady state any drug can be added to the medium flowing through the measuring cell. Due to the flow of only 1 ml/h the residence time of the cell culture amounted to about 20 min. The duration of an experiment with a test compounds was limited to one day and thus the time of the drug exposure was between 12 to 18 h, which covered nearly all toxic cellular event initiated by the test compounds.

#### **4.6. Cell visualization by microscopy**

To prove the sensitivity and the selectivity of the OWLS sensor it was necessary to correlate cell density and morphology with the OWLS-signal. Through *the viewing window* of the measuring chamber the cells could be observed at any time using the inverted phase-contrast microscope.

#### Image analysis

Quantification of the covered cell area with the aid of the phase-contrast microscopic pictures and image analysis (IA) was considered for a quantitative comparison with the OWLS-signal. Although the depth profile of cell adhesion is not taken into account, the determination of the covered area was expected to be a simple indicator of cell adhesion. An algorithm for the quantification of covered cell area must recognize borders and areas of different darkness. By matrix operations the borders and areas can be combined into the resulting cell coverage. Since the cell-lines used in the experiments displayed a different morphology, an adaptation of the program to each cell-line was necessary.

At regions of close adhesion the picture observed by phase-contrast microscopy become similarly dark as the background, whereas the more globular cells display bright and white borders in contrast to the dark background. Thus the quantification of weakly adhering cells is easier than that of tightly adhering cells. Using inverted phase-contrast microscopy the precise quantification becomes increasingly difficult with increasing cell adhesion and therefore another method such as CLSM would be needed. One of the major shortcomings of CLSM is the fluorescence staining and thus the measurements

would only be possible at the end of an experiment. Moreover, the CLSM is restricted to single cells.

#### Cell density

Owing to the above mentioned reasons, the cell density was selected as a simple and easily accessible indicator of the covered cell area. However, as shown in 5.2.3. *OWLS-signal in long-term cultures*, the cell-covered area is not linearly dependent on the cell density.

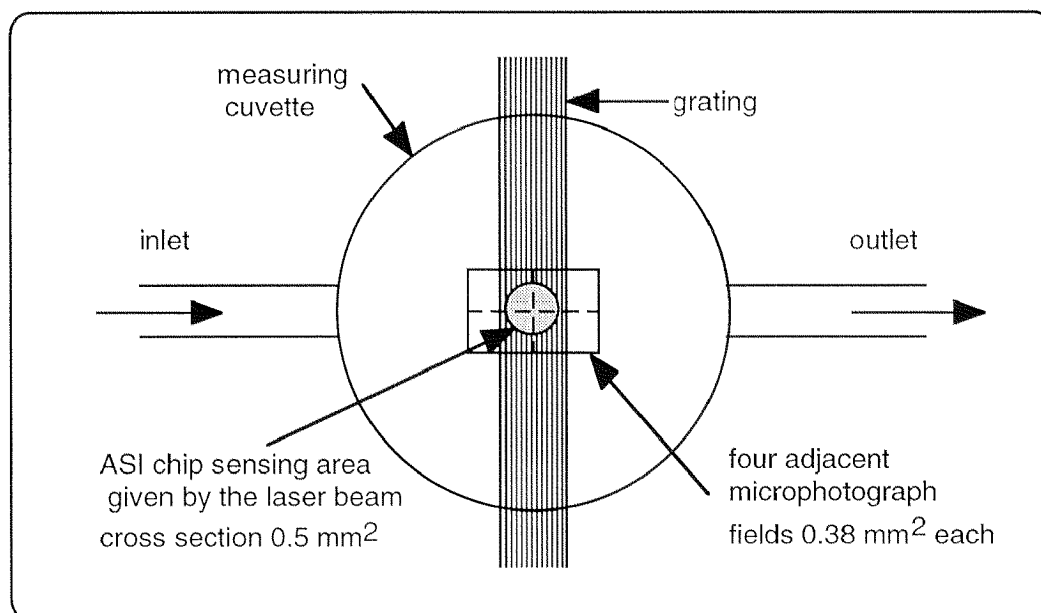


**Fig. 4.5:** *Top-view of the measuring cuvette: The cell-density within the sensing region was determined by taking four adjacent microphotographs in the area of the sensing region.*

To monitor cell density and cell morphology in the sensing region of the ASI-chip, microscopic pictures of four adjacent squares ( $0.32 \text{ mm}^2$ ) over the ASI sensing area were taken. The area of the circular sensing region of the ASI chip was  $0.50 \text{ mm}^2$  and the four pictures together covered a rectangle of  $1.28 \text{ mm}^2$ . Schematically it is shown in Figure 4.5. To determine the cell density, the number of cells in every picture was counted (Fig. 4.6). In a typical experiment the OWLS-signal encompassed an area with 300-500 fibroblasts and 600-1000 hepatoma cells respectively.

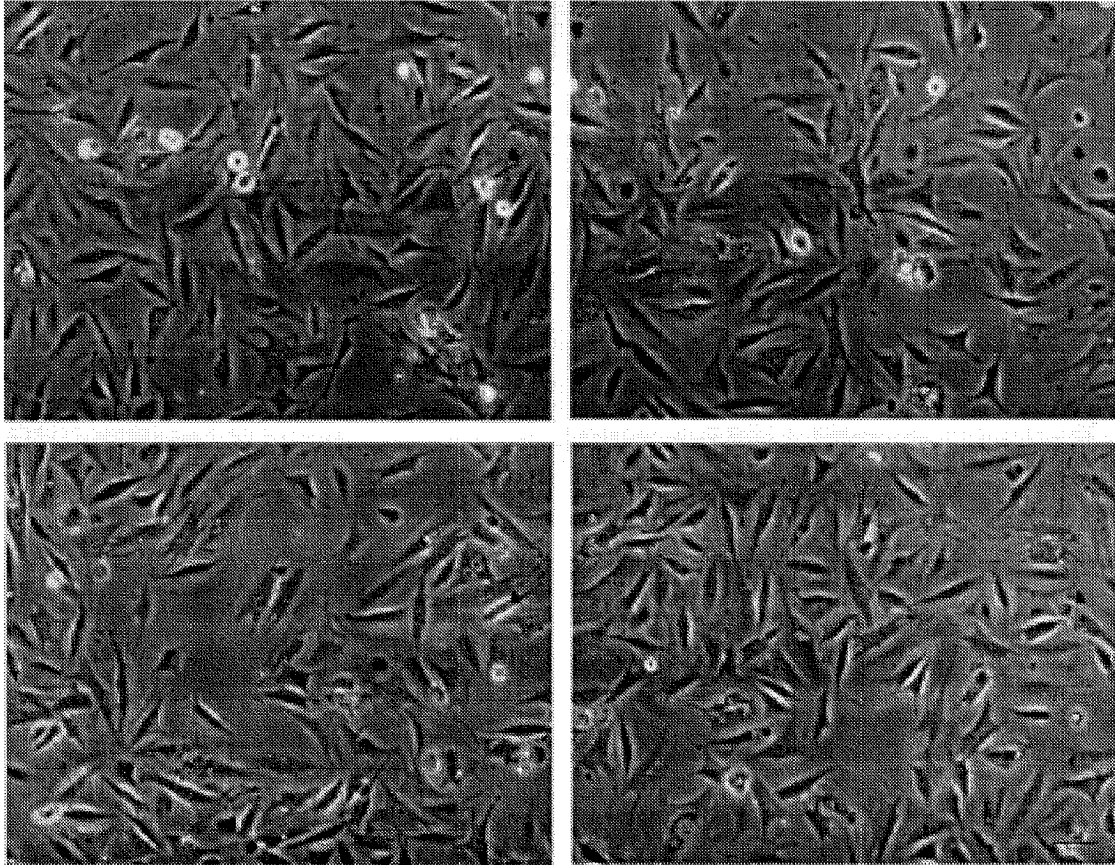


**Fig. 4.6:** *Four adjacent microphotographs: The random influence on the variation of cell density increases with decreasing picture area. The cell distribution within the micropictures and the sensing region varied to some extent: The picture on the upperleft side represents 83 cells, the picture on the upper right side 98, the picture on the lower left side 104 and the picture on the lower right side represents 108 cells. Bar indicates 50  $\mu\text{m}$ .*

## 5. Results

### 5.1. Protein adsorption

As outlined in section 3.3. *Time-dependent selectivity*, the OWLS is not selective and thus both serum proteins adsorb and cells adhere on the waveguide. Since serum proteins can not be excluded in cell experiments, it was first necessary to study the adsorption kinetics of serum proteins at biologically realistic concentrations. Second, the influence of the stopped flow on protein adsorption as used in the cell experiments was investigated. Finally, it was not only interesting to study the addition of FCS to adherent cells but also to study the effect of serum deprivation on fully spread cells. Consequently, the desorption kinetics of serum proteins in Optimum medium was measured with the OWLS.

#### 5.1.1. Adsorption of serum bovine albumin and serum proteins

All cell experiments were performed in Optimum containing 4 % (v/v) FCS, composed as listed in Table 5.1. Principally, FCS consists of two third of albumin and one third of globulin.

*Table 5.1: Main protein components of FCS*

<i>Albumin</i>	<i>2.6 g/dl</i>	<i>61 %</i>
<i>Globulin</i>	<i>1.3 g/dl</i>	<i>31 %</i>
<i>Total protein</i>	<i>4.2 g/dl</i>	<i>100 %</i>

#### BSA model

Kurrat et al. established a model for the adsorption kinetics of BSA by combining the RSA model with the theory of reversibly and irreversibly bound proteins. In the following the model of Kurrat is referred to as the BSA model. This model is based on adsorption measurements with the OWLS, which were performed at an albumin concentration of only 85  $\mu\text{g/ml}$  compared to the total protein concentration of 1680  $\mu\text{g/ml}$  in the cell experiments. Taking advantage of the existence of the BSA adsorption model, it was possible to predict the adsorption behavior of serum proteins at considerably higher concentrations as used in the cell experiments.

#### Boundary conditions

The comparison of the adsorbed mass of proteins in two different buffer-systems has to be taken with caution. The experiments for the BSA adsorption model were done with a

10 mM HEPES buffer at 25°. In contrast, the adsorption of serum proteins was studied in the cell medium containing various inorganic salts buffered with a 50 mM HEPES-buffer at 37°C. The buffer-system has not only an influence on the adsorbed mass of proteins at saturation but also on the adsorption kinetics. It was shown that the adsorption kinetics of BSA was drastically altered if the buffer was changed from a phosphate buffer to a HEPES buffer (Ramsden, Roushet al., 1995). This striking effect of the buffer system is not surprising since counterions play an important role in protein adsorption.

### Albumin

As shown in *Table 2.1.* the maximal surface concentration varies from one protein to the next. Regarding the sensor sensitivity, the maximal surface concentration of globulin was found to be considerably higher than albumin. However, a contribution of globulin to the OWLS-signal was not accounted for, because the competitive adsorption of albumin and globulin was never studied and thus no such model exists. In addition, the adsorption of albumin is much faster than that of globulin. According to the Vroman-effect, the albumin surface concentration passes a maximum and the reversibly bound albumin is continuously replaced by globulin. Due to these discrepancies only the albumin part of the FCS was compared with the corresponding BSA-concentration of the model; *e.g.*, 4% (v/v) FCS contains 1040 µg/ml albumin.

Therefore, the comparison of the BSA model and the serum adsorption experiments are purely qualitative. In addition, for compatibility reasons with the cell experiments, the y-axis is represented in N(TE) units for the serum adsorption and the y-axis in the BSA model is represented in mass units.

Fig. 5.1.1 shows the adsorbed mass of BSA calculated according to the BSA model after 5, 10 and 30 min. It can be predicted from the BSA model that the adsorption of proteins at high bulk concentration is very fast and 90 % surface saturation is reached within minutes. Moreover the maximal surface concentration does not significantly change with bulk protein concentration higher than 500 µg/ml.



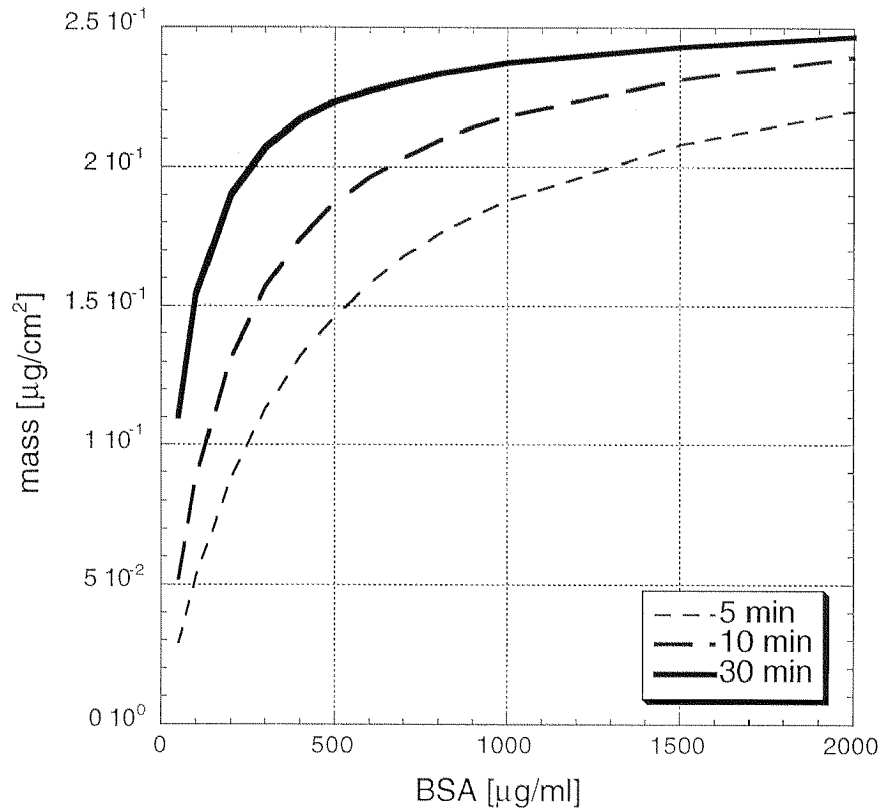


**Fig. 5.1.1:** Adsorbed mass of BSA at different bulk concentrations and different times calculated by the BSA model. The plot shows the adsorbed mass after 5, 10 and 30 minutes as a function of the bulk concentration. The model is based upon BSA adsorption experiments in a 10 mM HEPES buffer at 25°C.

An identical behavior was also found for serum proteins (Fig. 5.1.2). For four different concentrations 1, 2, 4 and 6 % (v/v) of FCS its surface concentration is plotted at different times. In accordance with the BSA model, 90 % surface saturation was reached within ten minutes at bulk protein concentration higher than 520 µg/ml and 2 % (v/v) FCS respectively.

It can be concluded that the surface concentration of adsorbed proteins varies within a small range at FCS concentrations between 2 - 6 % (v/v). This is not surprising as the mass of dissolved proteins at 1000 µg/ml BSA in a small volume of 1 mm height represents more than forty times the mass of adsorbed proteins on the corresponding surface at its saturation. Thus, any higher excess of dissolved proteins has only a minor influence on the mass of adsorbed proteins.

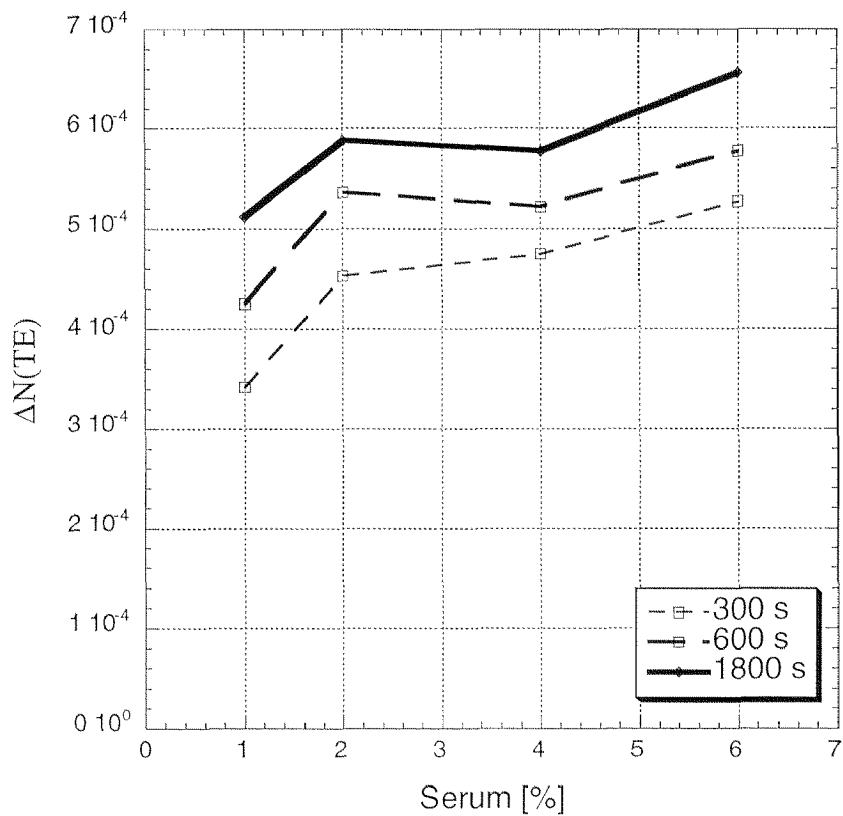


**Fig. 5.1.2:** Adsorption of serum proteins at different bulk concentrations. The figure shows the  $\Delta N(TE)$  after 5, 10 and 30 min for 1, 2, 4 and 6 % FCS buffered with 50 mM HEPES in Optimem medium at 37°C. The data are the average of three measurements.

Despite different boundary conditions, the BSA adsorption model was fully sufficient to estimate the adsorption rate of serum proteins between 1 - 6 % (v/v) FCS in Optimem.

### 5.1.2. Dynamics of serum adsorption at high bulk concentrations

In order to start cell settling and adhesion the flow through the measuring cuvette was stopped after 3 min. The influence of stopped flow was studied with both the BSA model and with serum protein adsorption measurements. As described in section 3.3. *Time-dependent selectivity*, the bulk protein concentration only reached a fraction of its maximum value, when the flow was stopped after three minutes.

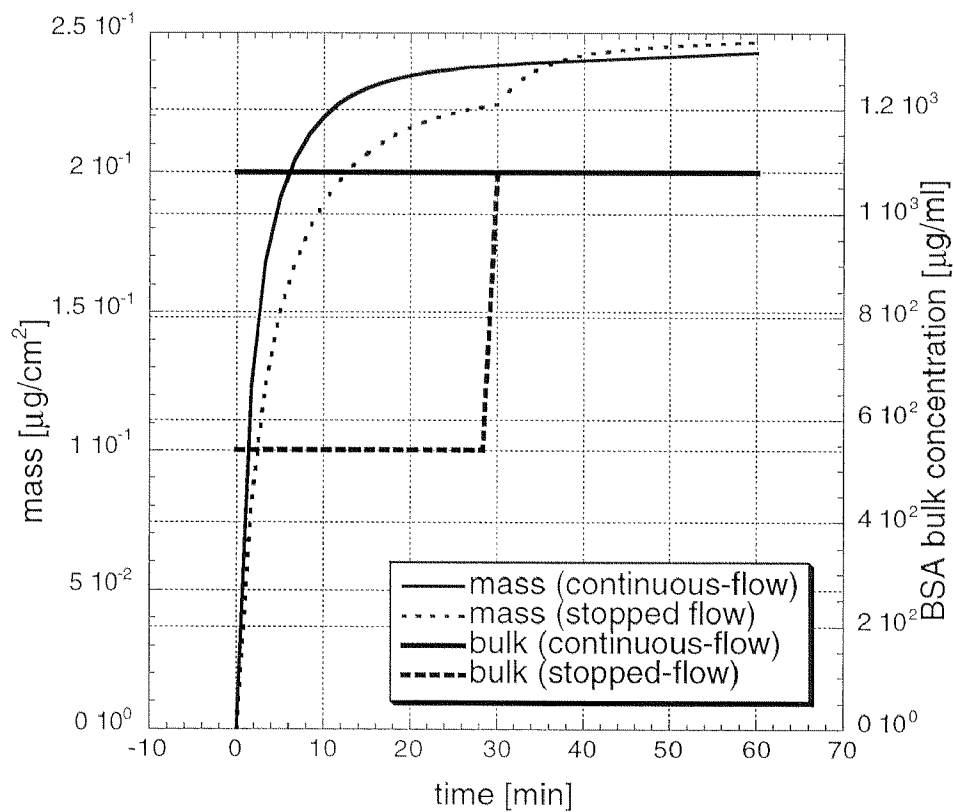


*Fig. 5.1.3: Influence of flow conditions on the adsorbed mass of proteins calculated by the BSA model at 1040  $\mu\text{g}/\text{ml}$  BSA. On the left hand axis the mass of adsorbed BSA is plotted as a function of time at continuous and stopped flow conditions. On the right hand y-axis the BSA bulk concentration for both cases continuous and stopped flow is plotted. The fact, that the bulk concentrations has a comparatively small influence on the adsorbed mass of proteins, became obvious in the adsorption kinetic as well.*

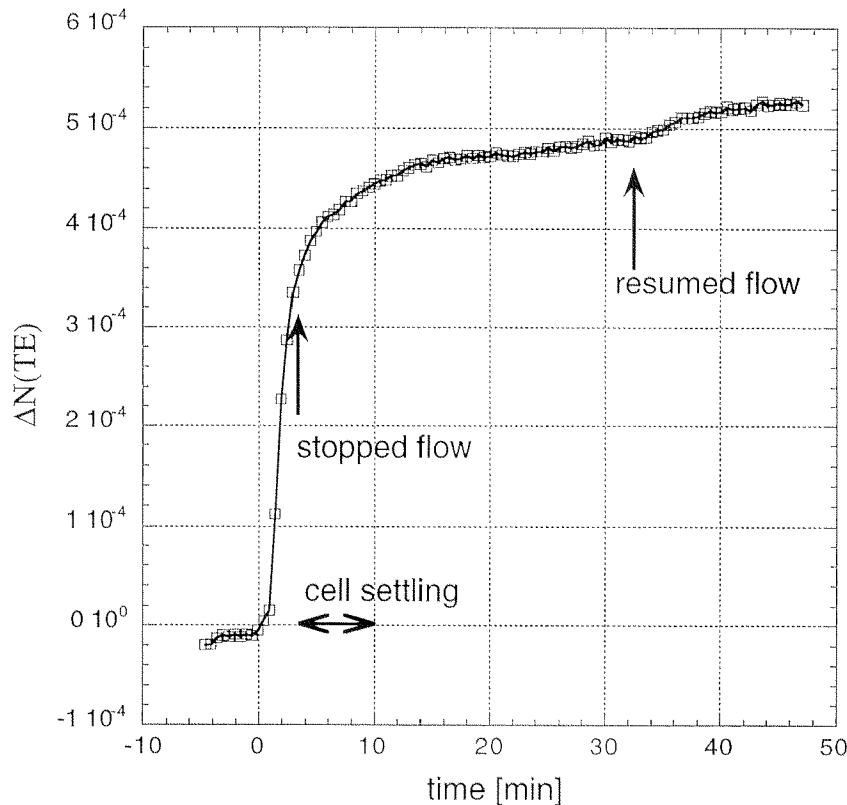


**Fig. 5.1.4:** *Influence of flow conditions on the adsorption of serum proteins: The cell settling starts when the flow is stopped and was calculated to last about 8 min. By the time cell settling starts, the protein adsorption is nearly completed. When the flow is resumed after 30 min, only a minor increase of the OWLS-signal is observed. The data are the mean of three measurements.*

Using the same model for BSA it is shown in Fig 5.1.3 that the adsorption of BSA at  $1040 \mu\text{g/ml}$  is a very fast process. In order to simulate the stopped flow in the model, the bulk concentration was first set to  $520 \mu\text{g/ml}$  BSA, which had only a minor influence on the adsorption kinetics. After 30 min the bulk concentration was set to  $1040 \mu\text{g/ml}$  BSA, which corresponds to the albumin concentration in 4 % FCS. The doubling of the bulk concentration lead to an increase of approx. 10 % of the BSA surface concentration.

In parallel, the influence of stopped flow was studied with proteins at the same FCS concentration as used for the cell experiments (Fig. 5.1.4). From the previous result it was expected, that the bulk protein concentration between 2 - 6 % (v/v) FCS had only

a negligible effect on the amount of adsorbed proteins. Indeed, when the flow of medium with 4 % (v/v) FCS was stopped, the serum proteins showed the very same adsorption kinetics as at continuous flow conditions. After the flow was resumed 30 min later, only a minor increase of the  $N(TE)$  was observed.

Again, the predictions of the BSA adsorption model were in good agreement with the OWLS measurements of serum protein adsorption. In both cases an increase of the bulk concentration lead to a negligible additional adsorption of proteins.

### 5.1.3. Protein adsorption and desorption

Figure 5.1.5 shows the adsorption and desorption kinetics of BSA predicted by the model for several bulk concentrations. The bulk concentrations of 260, 520, 1040 and 1560  $\mu\text{g/ml}$  BSA correspond to the albumin part of 1, 2, 4 and 6 % (v/v) FCS in Optimem. For desorption the bulk concentration was set to 0  $\mu\text{g/ml}$  and for readsorption to its initial value.

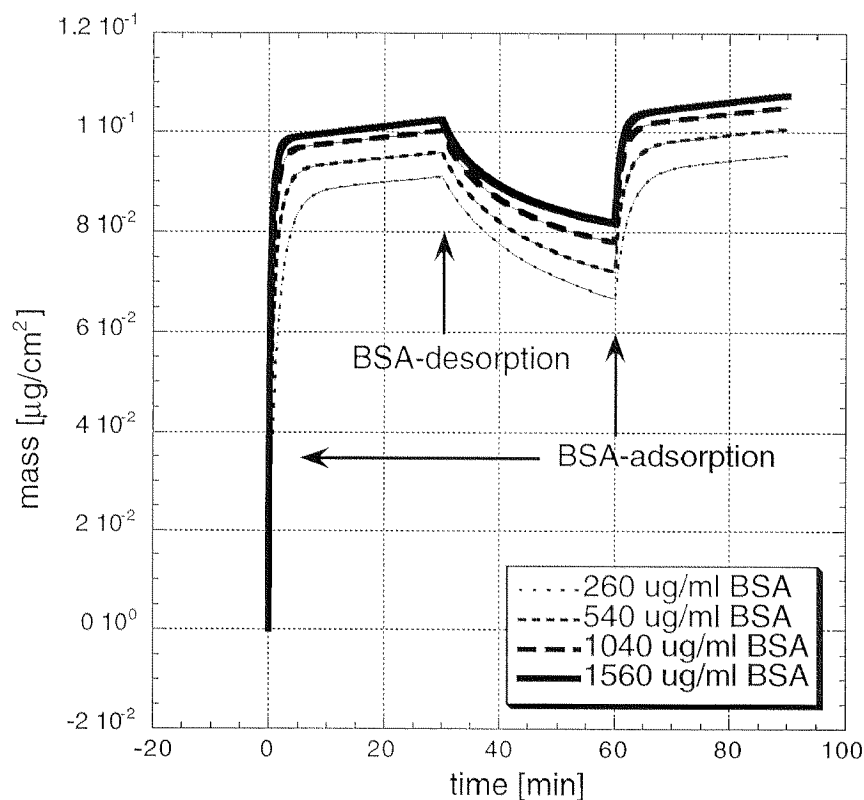


*Fig. 5.1.5: Influence of several bulk concentrations on the adsorption and desorption kinetics of BSA as described by the BSA model. The BSA adsorption was modelled using four different bulk concentrations. To model the desorption process, the bulk concentration was set to 0  $\mu\text{g/ml}$  after 30 min. For the readsorption of BSA the protein bulk concentration was set to its initial value after 60 min.*

Figure 5.1.6 shows the adsorption and desorption of serum proteins at the corresponding albumin concentrations as used in the model. For adsorption Optimem

medium with 1, 2, 4, 6 % (v/v) FCS was flown through the measuring cuvette and for the subsequent desorption the flow was switched to pure Optimem. Finally, Optimem containing the initial serum concentration was flown again through the cuvette.

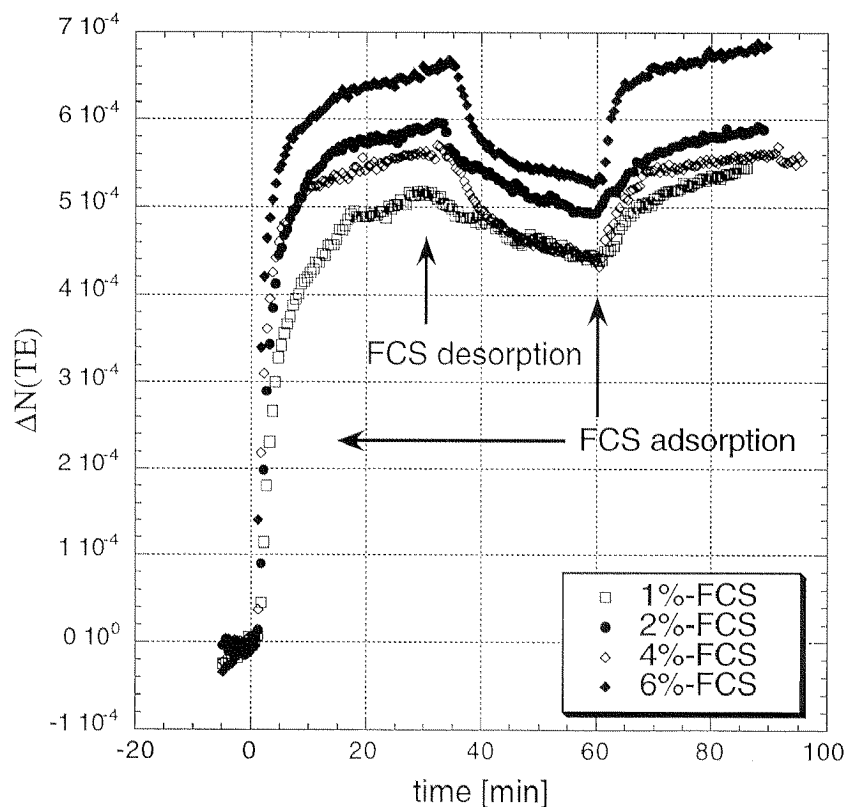


**Fig. 5.1.6:** *Influence of bulk concentration on the adsorption and desorption kinetics of serum proteins measured with OWLS. If the flow was switched from medium with FCS to pure medium to start the desorption phase, the time between the switch (30 min) and the start of the desorption phase increased slightly with FCS concentration. With increasing FCS concentration, the protein concentration in the measuring cuvette decreased more slowly and the process of protein desorption was delayed. If the flow was switched to the initial medium containing FCS after 60 min, the OWLS-signal reached a similar  $\Delta N(TE)$  as before desorption. The data are the mean of three measurements.*

### Reproducibility

Principally, the serum adsorption and desorption measurements were in good agreement with the BSA model predictions. Although the adsorption of 2 % (v/v) FCS displayed higher  $\Delta N(\text{TE})$  than the  $\Delta N(\text{TE})$  of 4 % (v/v) FCS, the curves of the 2 % (v/v) and 4 % (v/v) FCS measurements are not in contradiction but naturally lie within a certain range of error. Protein and plasma adsorption measurements showed that the OWLS protein adsorption measurements include an quantitative mass error of at least  $\pm 10\%$  (Kurrat, Walivaara et al., 1998), which was essentially confirmed by the serum measurements in this work.

### Desorption

The desorption process was in the same order of time as the adsorption process and was nearly completed after 10 min. The desorption process in the model started immediately, if the bulk concentration was set to 0  $\mu\text{g/ml}$  BSA. Since the desorption of proteins starts only at low bulk protein concentrations, the start of the desorption process was delayed with increasing serum concentration in the OWLS-experiments. At 4 % (v/v) FCS in medium the desorption started after 5 min and was mainly finished after 20 min. The decrease for 4 % FCS was in the order of  $\Delta N(\text{TE}) = 1.2 \cdot 10^{-4}$ . During desorption process the reversibly adsorbed proteins are removed and re-adsorb in the subsequent adsorption phase. When the flow was switched again to the initial serum concentration, both the OWLS-signals with serum proteins and the BSA model reached the same level as before serum desorption, which confirmed the theory of reversibly and irreversibly bound proteins.

### Bulk concentration: Serum adsorption measurements, BSA and SPT model

However the negative  $\Delta N(\text{TE})$  of desorption was dependent on the previous serum concentration (Figure 5.1.6), whereas the negative  $\Delta \text{mass}$  of desorption in the BSA model did not depend on the previous BSA concentration (Figure 5.1.5). In the BSA model the amount of reversibly bound BSA decreased with time (not shown) in favor of the irreversibly adsorbed protein. The reversibly bound BSA is not a function of the bulk protein concentration. Consequently, the negative  $\Delta \text{mass}$  of desorption is only proportional to the adsorbed mass at saturation for different FCS concentrations.



In this point the experimental results differed from the BSA model. In fact, the negative  $\Delta N(\text{TE})$  of desorption, after the adsorption at different FCS concentration, was proportional to the protein bulk concentration. This result indicated that the amount of proteins, which were *reversibly* adsorbed and desorbed was a function of their bulk concentrations. In summary, the amount of reversibly adsorbed proteins seems to depend on the bulk concentration in the serum experiments, whereas the BSA model did not predict any bulk-concentration dependency.

#### OWLS-signal and protein relaxation

Furthermore, both the OWLS-signal and the BSA model did not reach a stable plateau but drifted progressively towards higher mass and  $\Delta N(\text{TE})$  respectively. This drift were also found for the desorption process, but they were quantitatively different for the experiments and the model, indicating some inconsistencies in the BSA model. The drift behavior in the model originates from the continuously increasing replacement of reversibly bound proteins in favor of irreversibly ones. The serum adsorption and desorption experiments further indicated a bulk concentration dependency of the reversibly bound proteins. Together the BSA model was found insufficient to describe this behavior, whereas the SPT model, which states that the unfolding of proteins is dependent on time and competes with the additional adsorption of proteins can explain the expected behavior.

## 5.2. Cell Adhesion and Spreading

### 5.2.1. Adhesion and spreading of different cell-lines

For the experiments three fibroblast and one hepatocyte cell-lines were used. Accordingly, the fibroblasts-lines are named *L-*, *E-* and *J-fibroblasts*, whereas the Hep G2 are named *Hepatocytes*. In the preliminary experiments the adhesion and spreading characteristics of all four cell-lines were tested at the same conditions and the results are shown in Figure 5.2.1.

The cell suspensions in medium containing FCS were flown through the measuring cuvette and after 3 min the flow was stopped. When cell settling and protein adsorption was finished after 10 min, cell spreading was observed (Fig. 5.2.1: curves (ii-v)). The cell density was determined as described in 4.6. *Cell visualization by microscopy*. The curves of the fibroblasts corresponded to a similar cell-density. Since the covered area of fully spread hepatoma cells was much smaller than in the case of fibroblasts, the cell density of the hepatoma cells was approximately twice as high as that of fibroblasts.

Following the selectivity model, all curves (ii-v) were identical for the first ten minutes, after which cell serum adsorption and settling are almost completed. In the second phase of the experiments the slopes of  $N(TE)$  values were much lower and varied due to the different adhesion behavior of each cell-line. In comparison to the curves (iii-v) the slope of the curve (ii) was much smoother in the second phase. After 2 – 6 h a fully spread state was reached and the OWLS-signal remained constant.

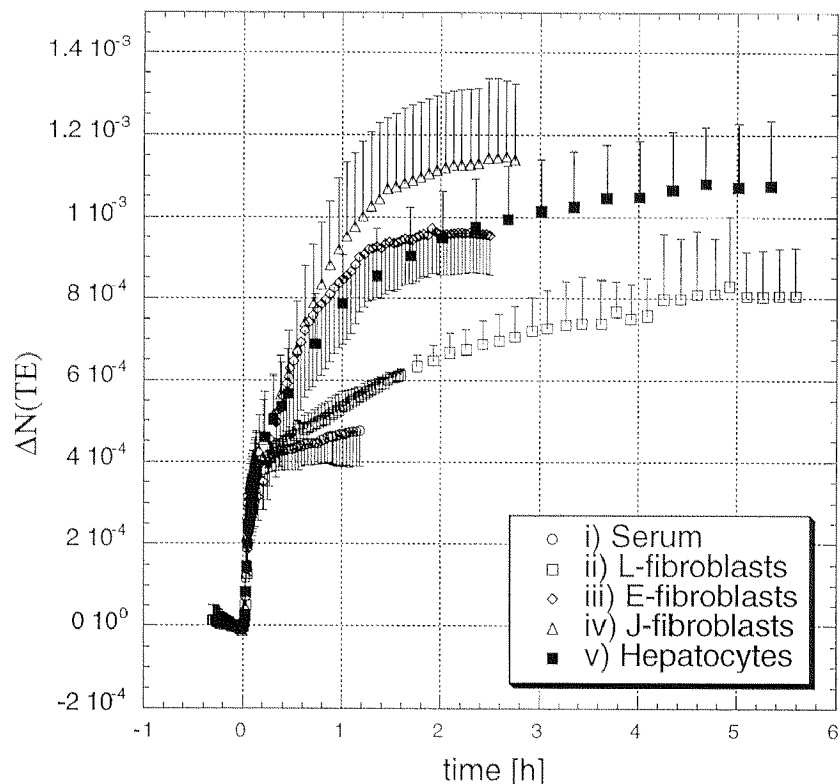


*Fig. 5.2.1: Serum adsorption and adhesion of different cell-lines: Curve (i): Optimem with 4% (v/v) serum; the OWLS-signal reached a quasi steady-state after about ten min. Curve(ii-v): The spreading of four different cell-lines displayed significant differences in the OWLS-signal. Each curve represents the average of at least four experiments with comparable cell density. The curve (ii) is the average of four experiments with the average of 243,000 cells/ml corresponding to the cell density of 377.6 cells/mm<sup>2</sup>. The curve (iii) is the average of ten experiments with the average of 266,000 cells/ml respectively 360.4 cells/mm<sup>2</sup>. The curve (iv) is the average of seven experiments with the average of 244,000 cells/ml respectively 309.8 cells/mm<sup>2</sup>. The curve (v) is the average of five experiments with 445,000 cells/ml respectively 771 cells/mm<sup>2</sup>.*

The different OWLS responses for the different cell-lines can be explained by their different morphology after adhesion observed by inverted phase-contrast microscopy (Figure 5.2.2). The J- and E-fibroblasts displayed a rather flat morphology indicating a firm adhesion, whereas the L-fibroblasts remained globular with small filapodia. The hepatoma cells showed a fully spread morphology similar to the J- and E- fibroblasts.

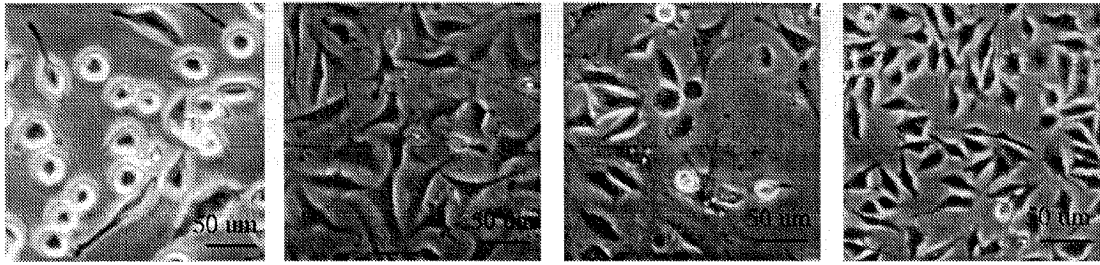


**Fig. 5.2.2:** *Morphology of different cell-lines: From the left to the right: L-fibroblasts, E-fibroblasts, J-fibroblasts and hepatoma cells.*

The OWLS-signal for serum adsorption was in the order of  $\Delta N(\text{TE}) = 4.5 \cdot 10^{-3}$  and the 95%-confidential interval was  $\Delta N(\text{TE}) = 5 \cdot 10^{-5}$ . The OWLS-signal displayed a different steady state  $\Delta N(\text{TE})$  for all cell-lines at the fully spread state. Among the fibroblasts, the J-fibroblasts showed the highest  $\Delta N(\text{TE})$  due to a strong adhesion. The E-fibroblasts having a similar morphology as the J-fibroblast spread with an equal rate but did not reach the same adhesion. The L-fibroblasts spread slowly and reached the lowest  $\Delta N(\text{TE})$ . Finally, the hepatoma cells spread with a rate comparable to the J- and L-fibroblasts and attained a similar final  $\Delta N(\text{TE})$  as the J-fibroblasts.

The 95%-confidential interval for the cell experiments was in the range of  $\Delta N(\text{TE}) = 1 \cdot 10^{-4}$  and thus approximately twice as large as the 95%-confidential interval for serum adsorption. The possible sources of error for the reproducibility of the cell experiments were cell-size and cell density distributions on the waveguide.

### 5.2.2. OWLS sensitivity and cell density

In a series of experiments the OWLS-signal sensitivity of several cell densities was investigated. The cell density on the chip was controlled by changing the cell concentration in the suspension. The cell-concentration in the suspension was in close correlation to the cell-density measured with microscopy (Fig. 5.2.3).

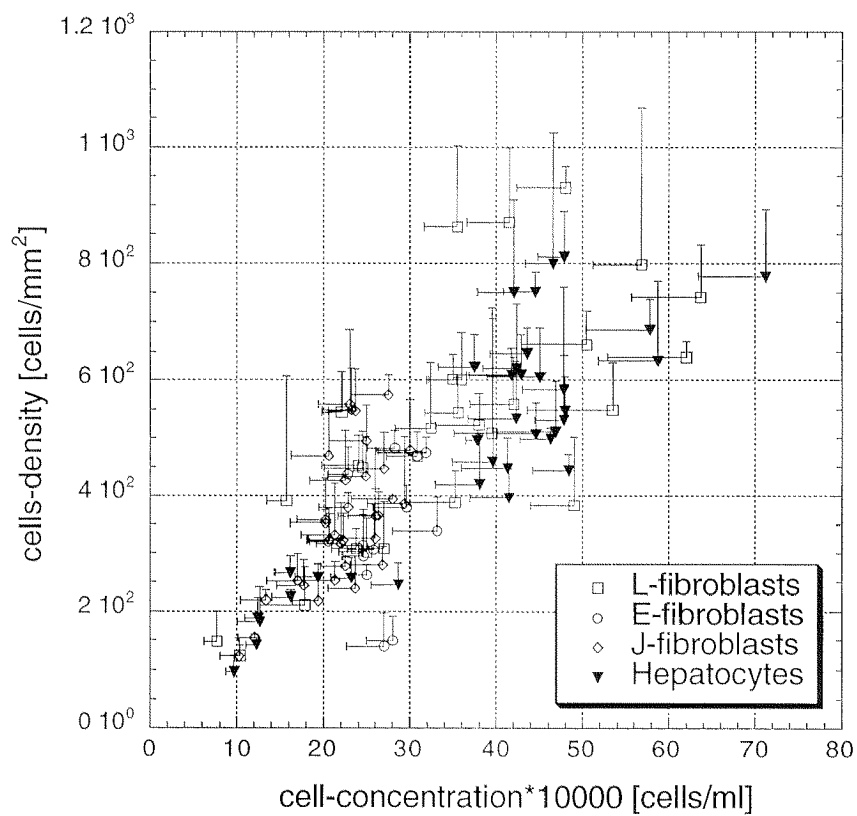


*Fig. 5.2.3: Correlation of cell concentration flown into the measuring cuvette and cell density at fully spread state. The cell concentration was determined by counting eight fields of the Neubauer chamber. The cell density was determined as described in section 4.4. Experiments.*

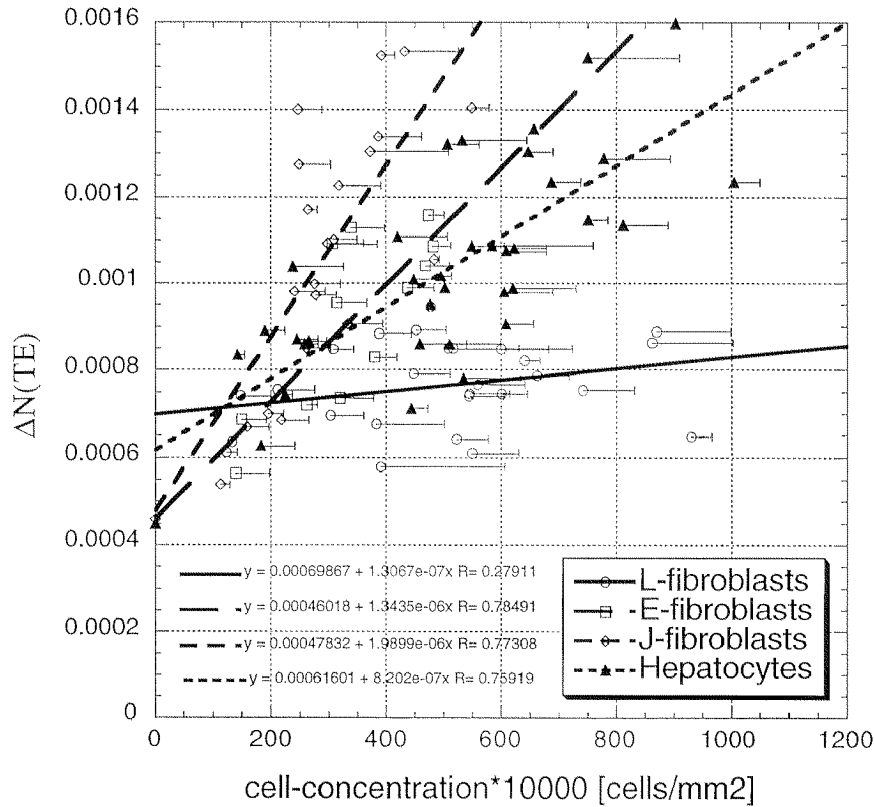


**Fig. 5.2.4:** Correlation of the OWLS-signal  $N(TE)$  at the fully spread state and the cell density for each cell-lines: The cell density determined by inverted phase-contrast microscopy correlated quantitatively to  $\Delta N(TE)$  of the OWLS-signal. The different fibroblast cell-lines showed clearly a different adhesion behavior. In the case of the J-fibroblasts the strongest adhesion was observed. The hepatoma cells displayed a firm adhesion as well but about the double the cell density was needed to attain a similar  $\Delta N(TE)$  as for J-fibroblasts.

Steady state  $\Delta N(TE)$  was correlated to the actual cell density as shown in Fig. 5.2.4. As shown in the previous section 5.2.1. Adhesion and spreading of different cell-lines, the contact area between the cell and the waveguide depends on the cell-line. For the case of a strong adhesion a good correlation between  $\Delta N(TE)$  at the fully spread state and the cell-density was found: J-, E-fibroblasts and hepatoma cells. As a consequence of the lower cell size, the slope of the cell-density- $\Delta N(TE)$  correlation for the hepatoma cells amounts only about half of the slope of the J-fibroblasts. For the case of L-fibroblasts with weak cell adhesion a rather low correlation was found.

The 95%-confidential interval of the cell concentration was within a narrow range. In contrast, the 95%-confidential interval for the cell-density measurements varied from one measurement to the next. The source of error was mainly the naturally occurring inhomogeneous cell distribution on small areas. The confidential interval calculated from the four pictures of  $0.32 \text{ mm}^2$  indicated that the cell-distribution within the sensing region  $0.5 \text{ mm}^2$  is difficult to be determined exactly. The correlation of the cell-density and the OWLS-signal did not respect the cell size and the state of the cell, which may affect the contact area as well.

Since a high response of the OWLS-signal is essential to detect smallest changes in cell morphology, the J-fibroblasts and the hepatoma cells were chosen for the subsequent experiments.

### 5.2.3. OWLS measurements of long-term cultures

To study the effect of chemical substances on cell-spreading and shrinking, it was necessary to examine long-term behavior of the two selected cell-lines with the OWLS biosensor.

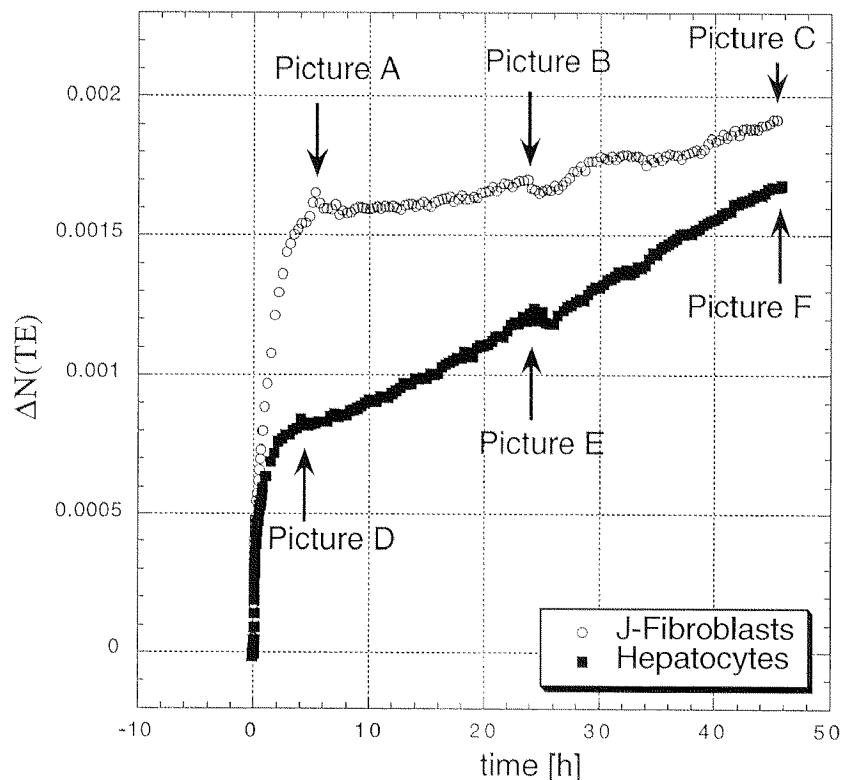


**Fig. 5.2.5:** OWLS measurements of long-term cultures with J-fibroblasts and hepatoma cells. The J-fibroblasts cells were seeded with concentration of  $187,500 \pm 6,050$  cells/ml attaining a cell density of  $269.33 \pm 32.13$  cells/mm<sup>2</sup>. The hepatoma cells were seeded with a concentration of  $173,400 \pm 98,100$  cells/ml attaining a cell density of  $220,990 \pm 51,288$  cells/mm<sup>2</sup>. Both cell-lines reached the steady state after about 4-6 hours. The J-fibroblasts proliferated rather slowly and the OWLS-signal remained almost constant or increased slightly up to 48 h. In contrast the fast proliferation of the hepatoma cells resulted in an increasing OWLS-signal. The data are the average of three measurements.

The long-term effects of the two cell-lines were found to be fundamentally different as illustrated in Fig. 5.2.5. When the J-fibroblasts had reached the fully spread state, the OWLS-signal remained almost constant. The OWLS-signal drifted towards higher



values. Accordingly, the cell density increased slightly during 48 h (Fig 5.2.6) and the contact area of a single fibroblasts was strongly dependent on the cell-density.

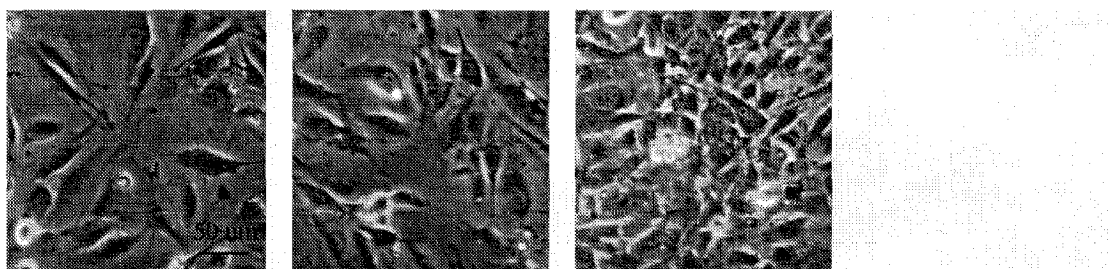


**Fig. 5.2.6:** Cell density of J-fibroblasts after 4, 24, 48 h (Picture A-C). The first picture from the left shows the fully spread J-fibroblasts after 4 h. The second picture shows the cell-density after 24 h from the beginning of the experiment. The third picture shows the cell density after 48 h.

In contrast, when the hepatoma cells had reached the fully spread state, the OWLS-signal continued to increase, but at a lower rate. The microscopic pictures at different times (Fig. 5.2.7) showed that the hepatoma cells proliferated fastly. As expected, an exponential cell growth was observed (Fig. 5.2.8). Within 24 h the cell density was multiplied by a factor of almost three and the cells grew to high confluency within 48 hours. No sign of cell-density inhibited growth was observed for up to 48 h. Similar as the fibroblasts, the contact-area of one single hepatoma cells was cell-density dependent.

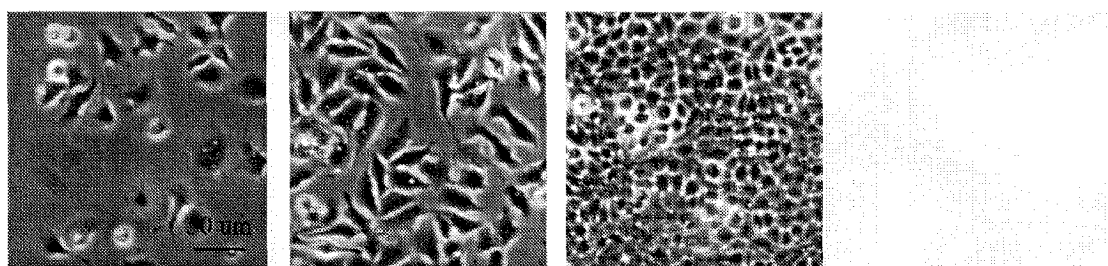


**Fig. 5.2.7:** Cell density of hepatoma cells after 4, 24, 48 h (Picture E-F). The first picture from the left shows the cells at the fully spread state after 4 h. The second picture shows the cell-density after 24 and the last picture after 48 h. Within 48 hours the cell-density had exponentially increased to complete confluency.

Although the hepatocyte cell density increased exponentially (Fig. 5.2.8), the OWLS-signal increased approximately linearly (Fig. 5.2.9). Together these findings suggest a cell-density dependent behavior of the contact-area.

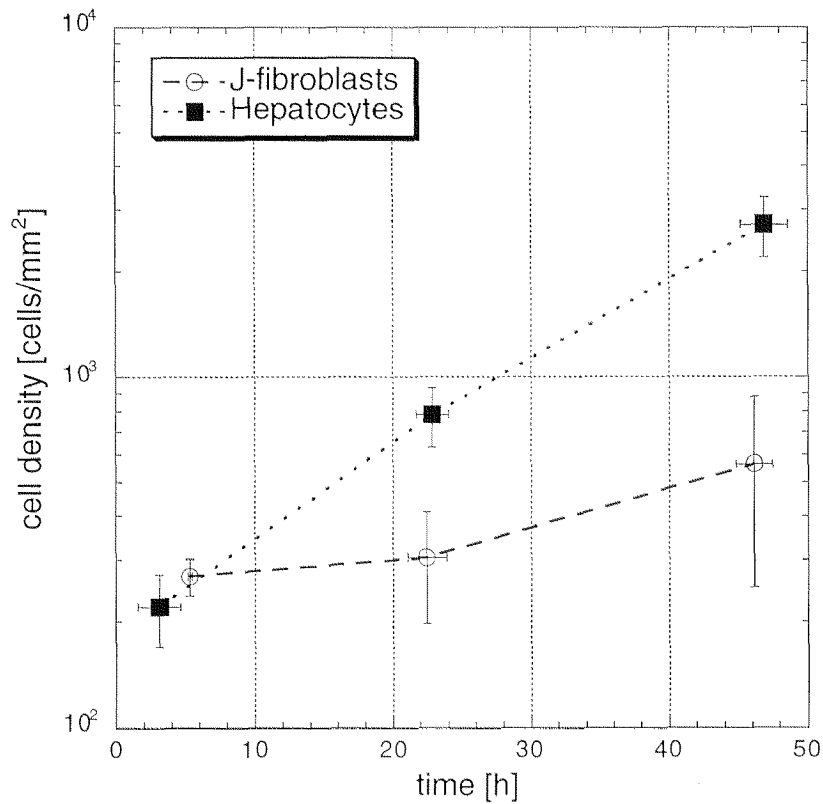


**Fig. 5.2.8:** Proliferation of J-fibroblasts and hepatoma cells. The cell-density of fibroblasts was slightly increasing over 48 h, whereas the cell-density of hepatoma cells displayed clearly the exponential growing cell number. The data are the mean of three experiments.

Although the growth of hepatoma cells was not contact-inhibited, the contact area of single cells decreased clearly with increasing cell-density (Fig. 5.2.7). Nevertheless, the total contact area of spread cells increased due to exponentially growing cell number. Obviously the second trend predominated leading to an constantly increasing OWLS-signal.

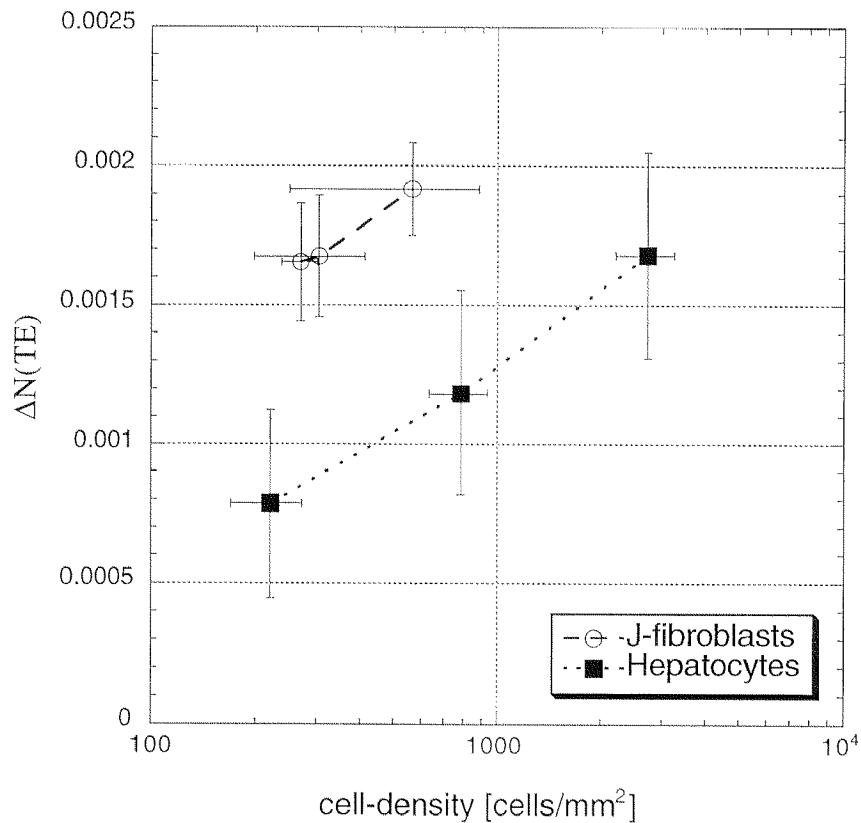


**Fig. 5.2.9: Correlation of cell density and  $N(TE)$ .** The logarithmic representation of the cell-density confirmed the cell density-dependent contact area. The data are the mean of three experiments.

#### Contact guidance

As mentioned in 2.3. *Cytoskeleton* fibroblasts exhibit contact-inhibition at a certain confluency. Cell-cell interactions are intensified and the cells pile up. This phenomena was also observed with fibroblasts at very high cell densities with the OWLS (Fig. 5.2.10). As expected the OWLS-signal increased initially sharply to a high  $\Delta N(TE)$ . The OWLS-signal did not reach a steady state but started to decrease indicating the cells attaining a more globular shape. In contrast to the fibroblasts, contact-inhibition was not observed with hepatoma cells except in one case where the OWLS-signal reached a plateau after over 40 hours at a very high cell density.

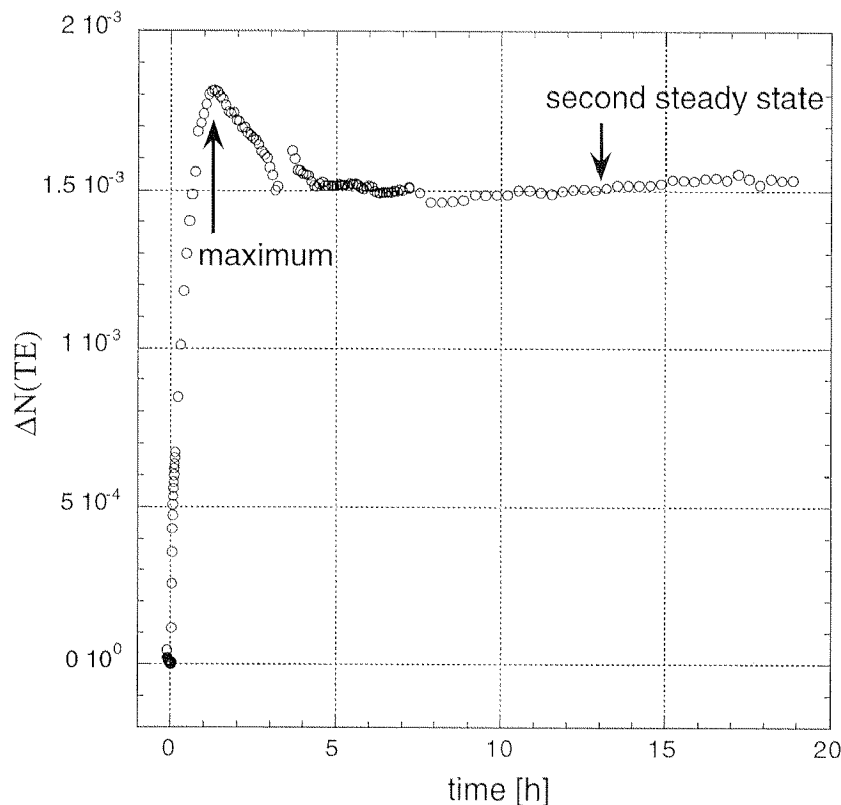


**Fig. 5.2.10:** *Effect of contact-inhibition on the OWLS-signal with J-fibroblasts.* J-fibroblasts were seeded on the waveguide at a cell-concentration of  $882,500 \pm 57,913$  cells/ml. Due to contact guidance the OWLS-signal did not reach the steady state but started to decrease after having passed a maximum (1 h). Finally, it reached a steady state at a lower level after approximately 5 h.

In contrast to the results of 5.2.2. *OWLS sensitivity and cell density*, where the contact area at the fully spread state was found to be proportional to the cell density for both hepatoma cells and J-fibroblasts, the OWLS-signal for long-term culture experiments was cell-density-dependent for both cell-lines:

- Both J-fibroblasts and hepatoma cells are suggested to pile up with increasing cell density. The contact area per cell was thus dependent on the cell-density.
- In the case of fibroblast contact inhibition limited cell spreading. Since the cell growth of fibroblasts was relatively slow, both the OWLS-signal and the overall cell contact area remained almost constant for up to 48 h.

- In the case of hepatoma cells the proliferation rate was considerably high and independent of the cell-density. While the contact area of individual hepatoma cells decreased, the OWLS-signal increased due to the predominating cell growth.

#### 5.2.4. Effect of serum on cell adhesion spreading and the contact area

Serum contains growth factors such as fibroblast growth factor (FGF), which stimulate the formation of F-actin as well as stress fibers within minutes. Thus the serum induced spreading was investigated with OWLS.

If fibroblasts or hepatoma cells were seeded without serum they adhered but hardly spread (Fig. 5.2.11). As a consequence the contact area of an individual cell was smaller than at the fully spread state. Consequently, when the OWLS-signal reached a low steady state value after only one hour (Fig. 5.2.12). When the flow of medium with serum was started again, the addition of growth-factors induced cell spreading.

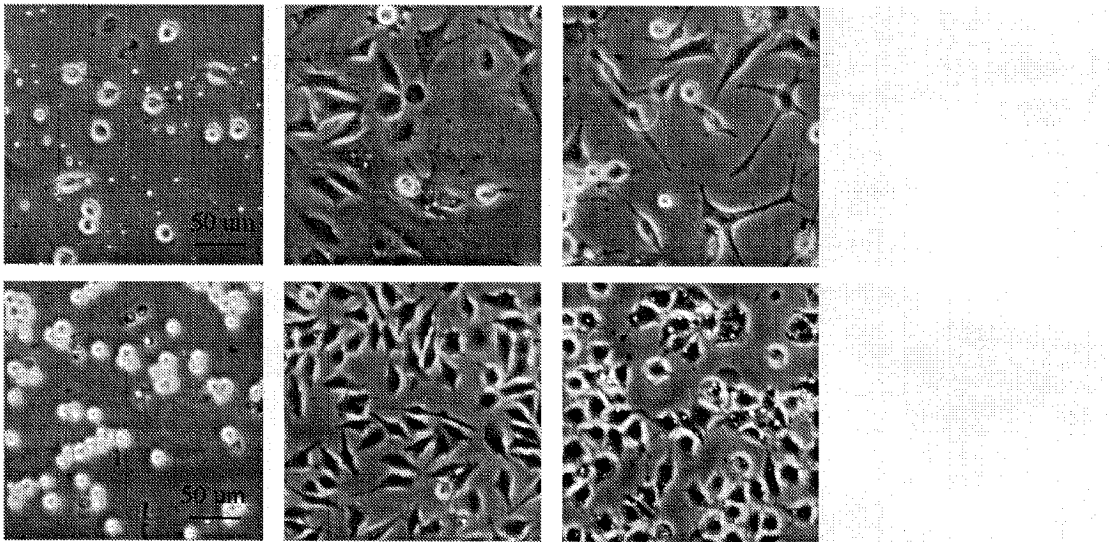


*Fig. 5.2.11: Morphology of J-fibroblasts and hepatoma cells at different serum conditions. The three pictures in the first row represent fibroblasts and the three pictures in the second row hepatoma cells. The pictures in the first column show purely adherent cells after seeding without serum. The pictures in the second column show the fully spread cells. The pictures in the third column illustrate the cell morphology after serum deprivation for at least 12 h.*

Accordingly, an increasing contact area was monitored with the OWLS within minutes. By microscopy it was observed that individual cells started spreading at different time points after seeding, which indicated the different metabolic state of the cells. After 4 – 6 h the OWLS-signal reached the usual high level of fully spread cells.

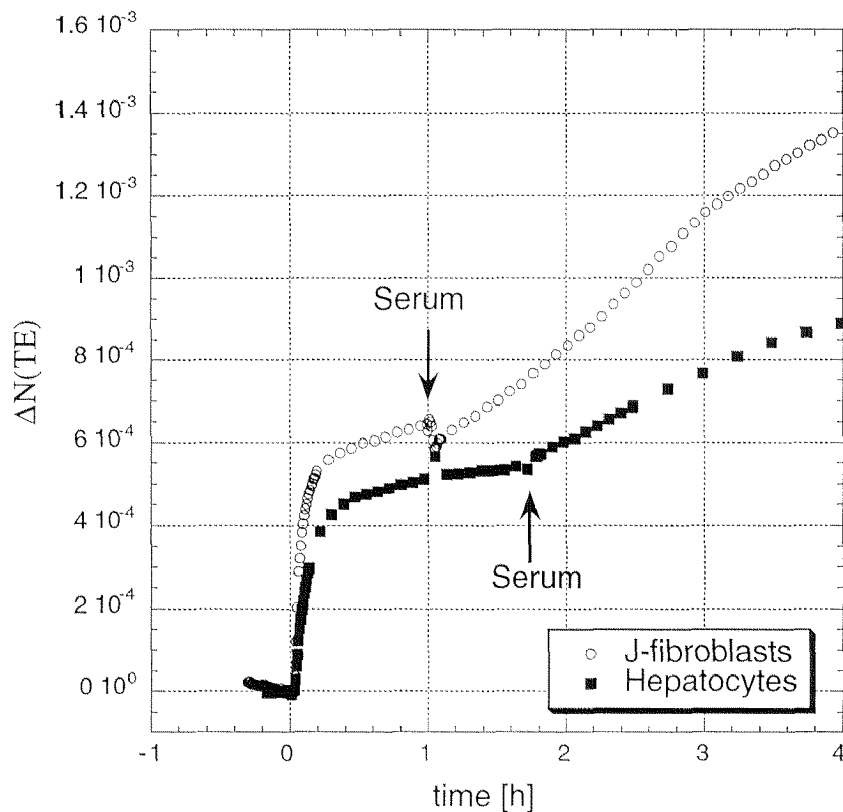


*Fig. 5.2.12: Influence of serum on adherent cells and the OWLS-signal. The addition of serum induced cell spreading within minutes in both cell-lines, which was reflected by the respective increase of the OWLS signal.*

### 5.2.5. Effect of serum deprivation on cell adhesion

Serum removal is known to reduce stress fibers and induce apoptosis after several hours, and therefore it was first investigated with three biochemical assays namely NR, MTT and BCA. The viability tests were performed after 2 and 16 h of serum removal (Fig. 5.2.13 & 14). Principally, similar results were found for both cell-lines: The NR test was not sensitive to serum removal in both cases. However, the MTT and the BCA test were sensitive and showed a slight decrease after 2 h and a clear decrease after 16 h. In the case of the fibroblasts the reduced activity correspond to a lower viability, whereas in the case of the hepatoma cells the lower proliferation rate was principally responsible for the reduced viability.

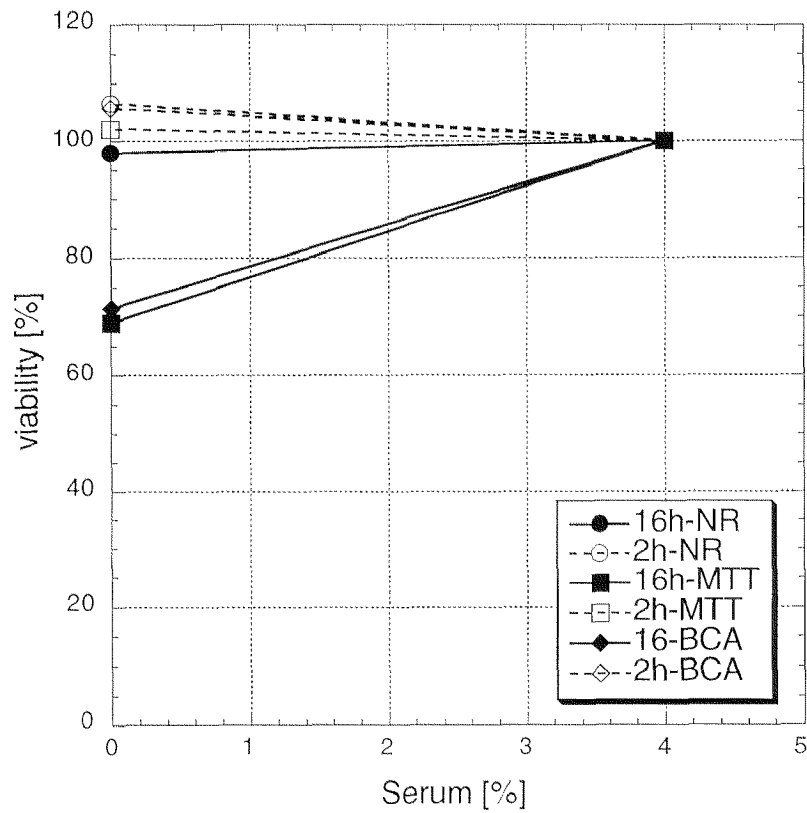


*Fig. 5.2.13: Effect of serum removal on the viability of J-fibroblasts determined by NR, MTT and BCA. After 2 h no difference between serum presence or serum absence was observed. However after 16 h a clearly reduced activity was monitored with MTT and the BCA assay. The NR assay was hardly sensitive to the removal of serum.*

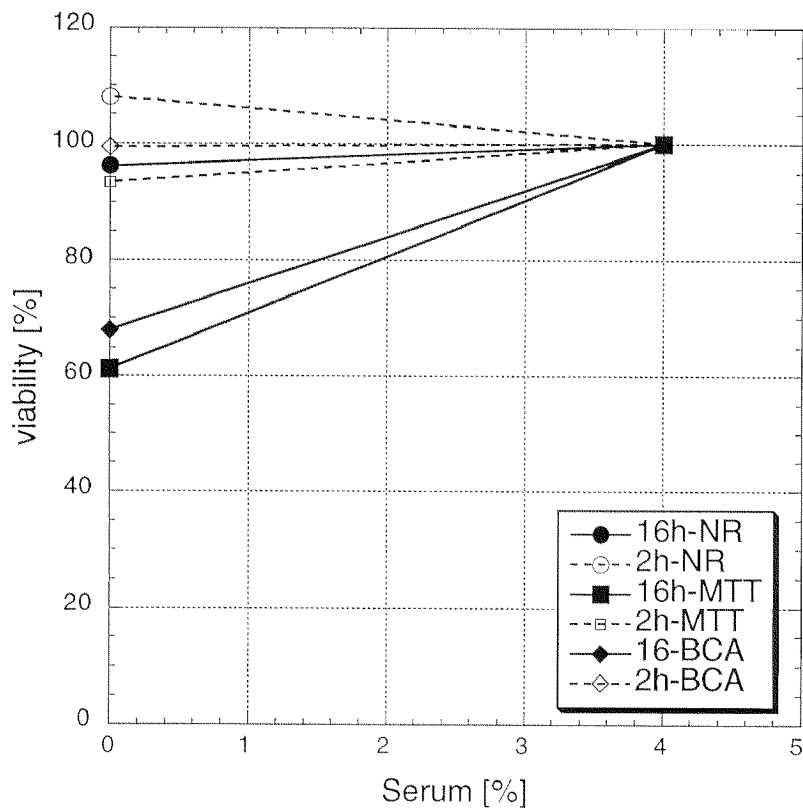


**Fig.5.2.14:** *Effect of serum removal on the viability of hepatoma cells determined by NR, MTT and BCA. After 2 h no difference between serum presence or serum absence was observed. However after 16 h a clearly reduced activity was monitored with MTT and the BCA assay. The NR assay was hardly sensitive to the removal of serum.*

The morphology of serum-deprived fibroblasts (Fig. 5.2.11) showed a higher contact area than cells plated without serum. Most of the cells lost volume displaying extensive retraction fibres. In contrast, the morphology of serum-deprived hepatoma cells did not indicate a considerable loss of adhesion or loss of contact area (Fig. 5.2.11).



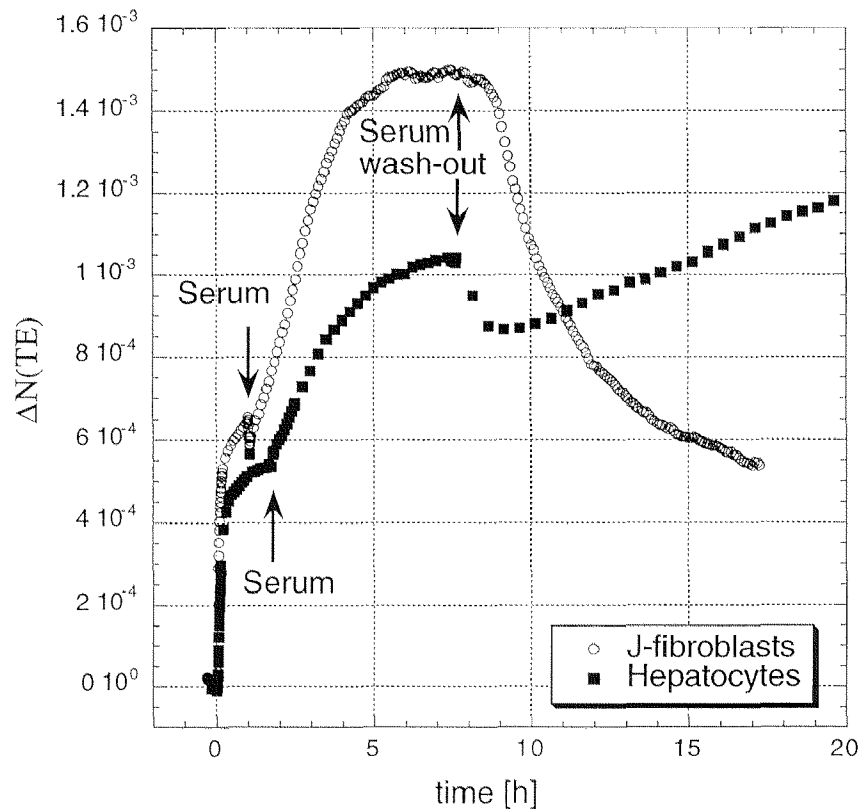


**Fig. 5.2.15:** *Effect of serum removal on the adhesion behavior of fibroblasts and hepatoma cells:* In the case of fibroblasts the OWLS-signal decreased to a similar level as before spreading, whereas in the case of hepatoma cells the OWLS-signal decreased in a smaller range and started to increase about an hour later.

The effect of serum deprivation on cell adhesion of both cell-lines was investigated using OWLS. Figure 5.2.15 shows an experiment, where the flow of serum-medium was replaced by a flow of serum-free medium at the steady state of fully spread cells. In the case of fibroblasts the influence of serum on cell-adhesion and spreading was almost reversible. The OWLS-signal started to decrease after about 1 h and reached a similar level as before spreading. The time to reach the second steady state was of the same order of magnitude as the time needed for spreading. In accordance with the microscopic pictures (Fig. 5.2.11) the OWLS-response suggests a weak cell adhesion due to the different pattern of stress fibers observed in the serum-starved cells (Fig. 5.2.11). Thus the reduction of cell adhesion indicated a loss of viability and may be an early indicator of cell death.

In contrast to the fibroblasts the effect of serum deprivation on the adhesion of hepatoma cells was completely different (Fig. 5.2.15): If the flow of medium containing serum was switched to pure medium the OWLS-signal decreased immediately. The decrease looked rather alike the desorption of serum proteins than a cellular response. The decrease was in the order of  $\Delta N(\text{TE})=2 \cdot 10^{-4}$  and after 1 h the signal started increasing again at a lower rate than observed with serum, which suggested a certain lower proliferation rate of the hepatoma cells in serum-free medium. This result is in agreement with the viability tests as well.

In conclusion serum-removal may influence the cytoskeleton, cell adhesion and the proliferation rate. Both experiments with serum addition and removal show nicely that although the sensor does not possess any selectivity, the process of protein adsorption, cell adhesion, spreading and growth can be separated on the time-scale.

In the case of the fibroblasts, the OWLS measurements, the viability tests and the cell morphology observed microscopically were in good agreement. After 2 h only a minor reduction of both OWLS-signal and viability tests was observed. After 16 h the OWLS had reached a constant level and equally the viability tests showed strongly reduced levels of about 60 - 70 %.

In the case of the hepatoma cells, the interpretation must respect the proliferation rate resulting in a continuously increasing OWLS-signal. This way the smaller decrease of the OWLS-signal after serum removal becomes obvious and the viability tests of the hepatoma cells can be equally correlated to the OWLS-signal.

### 5.2.6. Effect of colchicine

After the addition of a microtubuli-disrupting agents such as colchicine, the microtubuli depolymerize within minutes and the cells, display a different morphology. As a consequence, the contact area of the cells is reduced (Fig. 5.2.16).

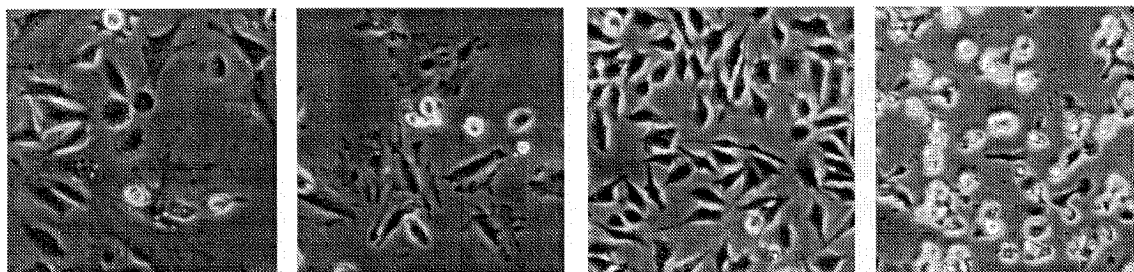


*Fig. 5. 2. 16: Morphology of J-fibroblasts and hepatoma cells after exposure to 2.5 mM colchicine: The first picture from the left shows fully spread J-fibroblasts. The second picture shows J-fibroblasts after exposure to 2.5 mM colchicine for several hours. The third picture shows fully spread hepatoma cells and the last picture hepatoma cells after exposure to 2.5 mM colchicine for several hours.*

The effect of colchicine on cell viability at different concentrations was first investigated using the NR, MTT and BCA assays. For fibroblasts and hepatoma cells similar results were obtained (Fig. 5.2.17 and 5.2.18): With hepatoma cells no dose-response relationship was observed with the MTT and BCA assay. However, the situation with NR and the hepatoma cells displayed a dose-effect relationship with all three assays. A strongly reduced activity was found after 16 h. Since colchicine completely inhibits the proliferation but is not cytotoxic, the reduced cell number of the hepatoma cells may be responsible for the reduced activity observed in the viability tests.

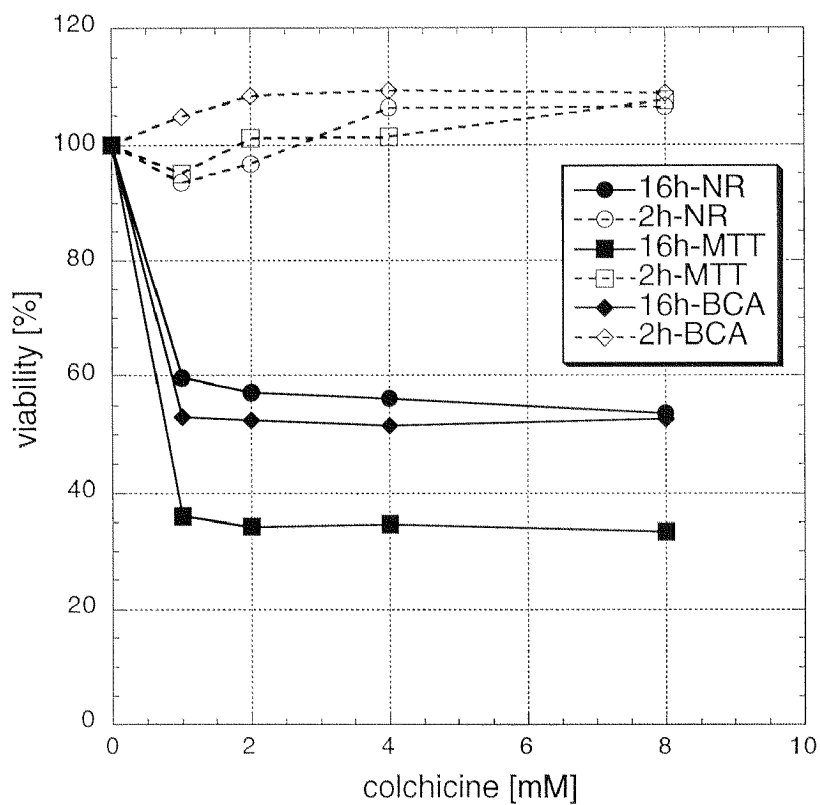


*Fig. 5.2.17: Effect of colchicine on the viability of fibroblasts determined by NR, MTT and BCA determined after 2 and 16 h. No dose-response relationship was found between 1 and 8 mM colchicine. After 2 h no effect was observed, whereas after 16 h a reduced activity was monitored.*

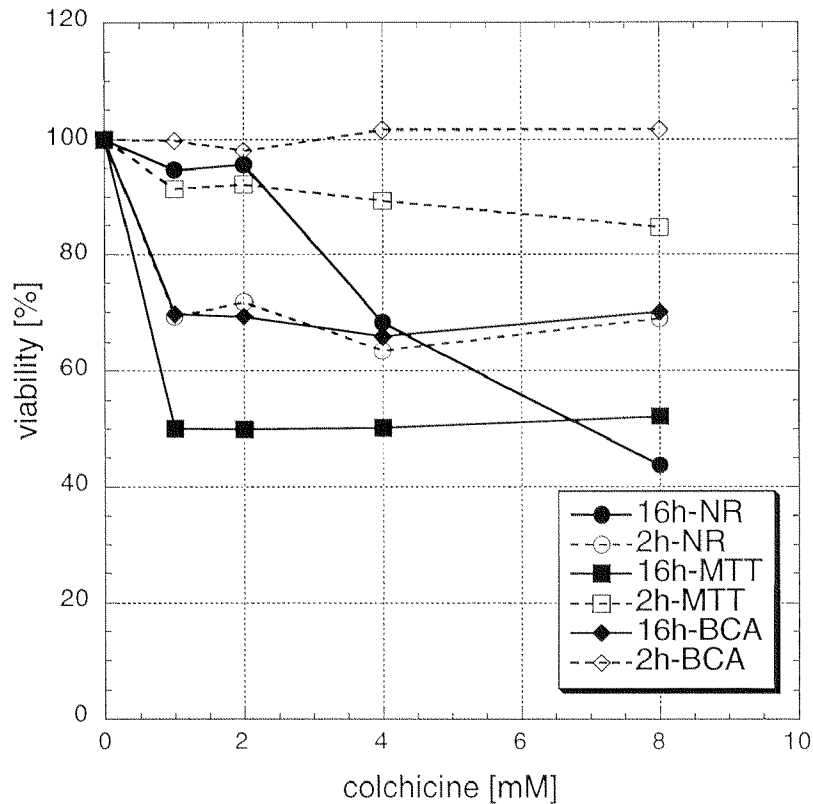


*Fig. 5.2.18: Effect of colchicine on the viability of hepatoma cells determined by NR, MTT and BCA after 2 and 16 h. With one exception, no dose-response relationship correlation was found between 1 and 8 mM colchicine. After 2 h no effect was observed, whereas after 16 h a reduced activity was monitored.*

Figure 5.2.19 shows two OWLS experiments with colchicine (2.5 mM) with each cell-line. Since the effect of colchicine can be observed under the microscope within minutes (Fig. 5.2.16), the measuring frequency was set to 5 min. At steady-state (4 – 6 h) the medium was switched to medium with 2.5 mM colchicine. After a delay of 20 min due to the residence time of the medium in the inlet tube, colchicine reached the measuring cell and the OWLS-signal decreased sharply until a second steady-state was attained after several hours. The behavior was identical for fibroblasts and hepatoma cells. The negative  $\Delta N(\text{TE})$  from the first to the second steady state varied to a large degree by repeating the same experiments. This is most probably because the individual cell densities and the cell-cell contacts influence the colchicine induced retraction of the cells.

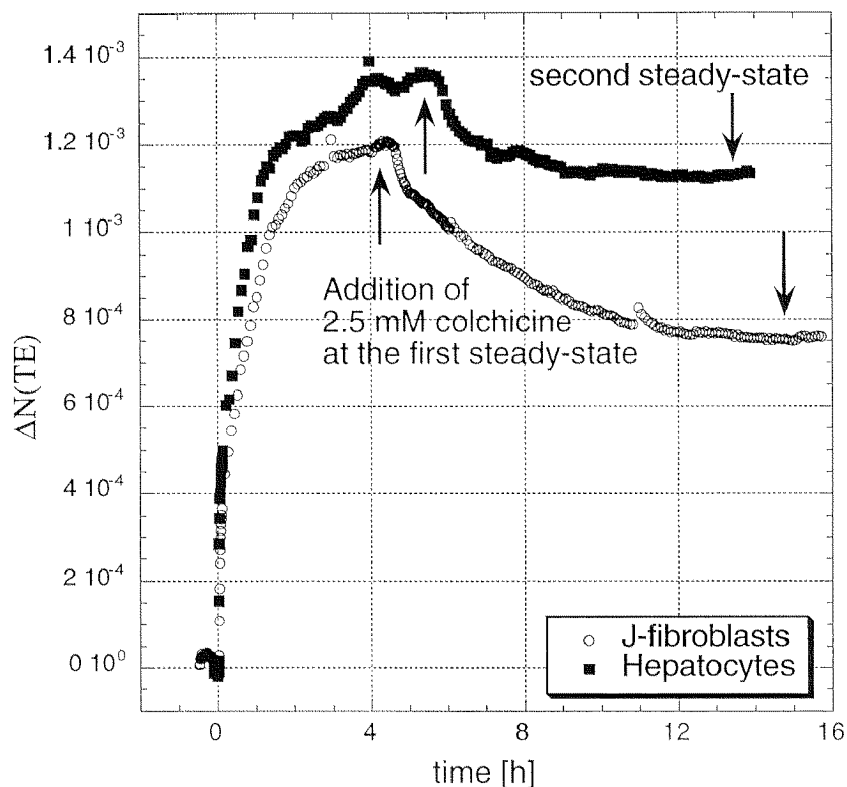


*Fig. 5.2.19: OWLS response of fully spread cells after the exposure to the cytoskeletal-disrupting agent colchicine. Both fibroblasts and hepatoma cells showed a clear decrease of the OWLS-signal as soon as colchicine had reached the measuring cuvette.*

The strength of the OWLS method became specially obvious in the experiments with colchicine, because cytoskeletal activity may not have a direct influence on the metabolic activity but rather on adhesion. In fact, the OWLS-signal and the viability measurements both detected the effect of colchicine. However, the time response of both methods showed no correlation at all. The prominent effect of the cytoskeleton-modifying substance colchicine was detectable with OWLS within minutes, whereas the effect of colchicine on viability as measured with the MTT, NR and BCA assay were only visible after more than 2 h. However, the OWLS results are not in direct contradiction to the biochemical assays but confirm the microscopic observations. Accordingly, the OWLS may be an ideal tool for the on-line observation of alterations

of induced or inherent cytoskeletal activity. This represents a considerable advantage in comparison to biochemical assays.

### 5.2.7. Effect of benzalkonium chloride

Surfactants are used in many cosmetic and dermatologic preparations and formulations such as shampoos, tonics and conditioners. However, surfactants such as sodium dodecyl sulphate or benzalkonium chloride (BAC) act as a membrane perturbing agent. By lowering the interfacial surface tension cell membranes are damaged and lysed. Thus, it was of interest to study the irritation potential of BAC on fibroblasts using the OWLS technique in comparison with microscopic observations.

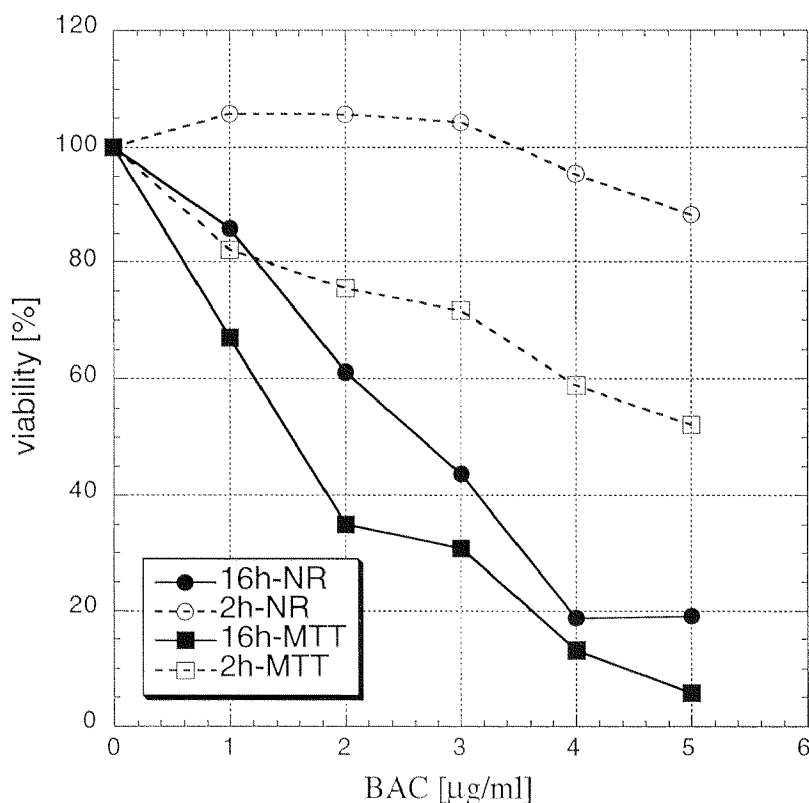


*Fig. 5.2.20: Effect of different concentrations of BAC on the viability of fibroblasts determined by the NR and MTT assay. After exposure to BAC a dose-response relationship was observed. This effect became stronger with longer exposure time.*

The cytotoxicity of BAC was first studied with the same three viability tests as for the situation with serum removal and colchicine (Fig. 5.2.20). The dose-response relationship became more prominent with time (2 and 16 h). Moreover the MTT test was more sensitive than the NR test.



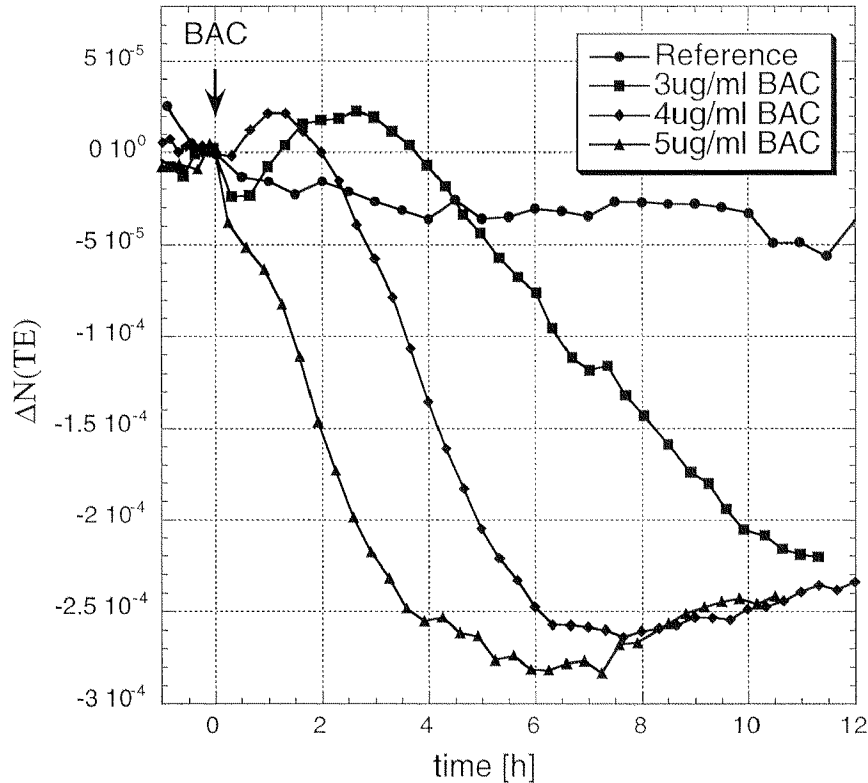


*Fig. 5.2.21: Effect of different concentrations of BAC on the OWLS-signal of fully spread fibroblasts. The OWLS-signal displayed a dose-dependent decrease. The data are the mean of at least four measurements.*

Figure 5.2.21 shows the result of a series of experiments with several concentrations of BAC. The medium was supplemented with BAC at the steady state (time=0). At the end of each experiment the fibroblasts were observed under the inverted phase-contrast microscope. Due to a different cell density within the ASI sensing region, the intensity of the OWLS response after BAC-exposure was varying from one experiment to the next. To eliminate this effect at least four experiments were performed for each BAC concentration. At 5 and 4  $\mu\text{g/ml}$  BAC the fibroblasts were found all dead and lysed at the end of an experiment (Fig. 5.2.22). At 3  $\mu\text{g/ml}$  BAC about half of the cells were still spread whereas the other half assumed globular shape. When the fibroblasts were exposed to 5  $\mu\text{g/ml}$  BAC the OWLS-signal started to decrease almost immediately. After about 5 h the signal became constant again. A similar behavior was also observed for the other concentrations. But at 4  $\mu\text{g/ml}$  and 3  $\mu\text{g/ml}$  BAC the OWLS-signal started

to decrease only after about 2 and 4 h hours respectively, and in both cases it exhibited a small maximum before the final decrease. This effect may be due to an initially increased cell activity due to a stress response.

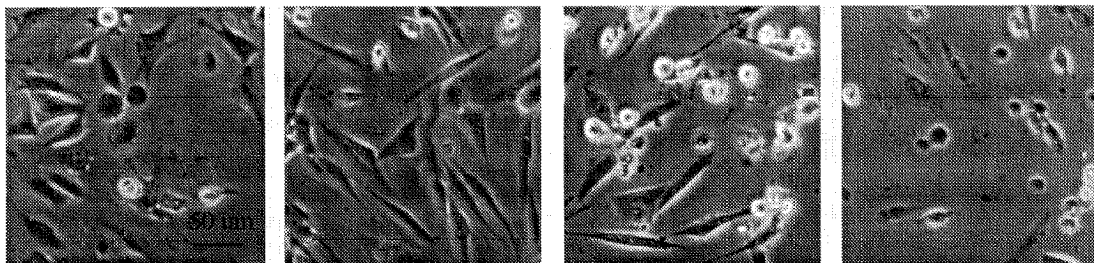


**Fig. 5.2.22:** *Morphology of J-fibroblasts after exposure to different concentrations of BAC. The first picture from the left side shows the fully spread J-fibroblasts without BAC, the second picture with 2 µg/ml, the third picture C with 3 µg/ml and the last picture with 4 µg/ml BAC. With increasing BAC concentration the fibroblasts were lysed and died, which became visible by a typical morphology.*

In conclusion, the results of the OWLS measurements, the viability tests and the cell morphology correlated quite well. It was found that OWLS may also serve as a method to study the membrane perturbing potential of skin irritants and surfactants.

### 5.2.8. Effect of cycloheximide

Cycloheximide (CY) inhibits protein synthesis by binding to the 80 S ribosome. Protein synthesis is indirectly essential in almost any cellular process. Lack of protein synthesis becomes visible especially in fastly proliferating cells such as hepatoma cells. Fig. 5.2.23 shows the result of the viability measurements using MTT, NR and BCA tests.

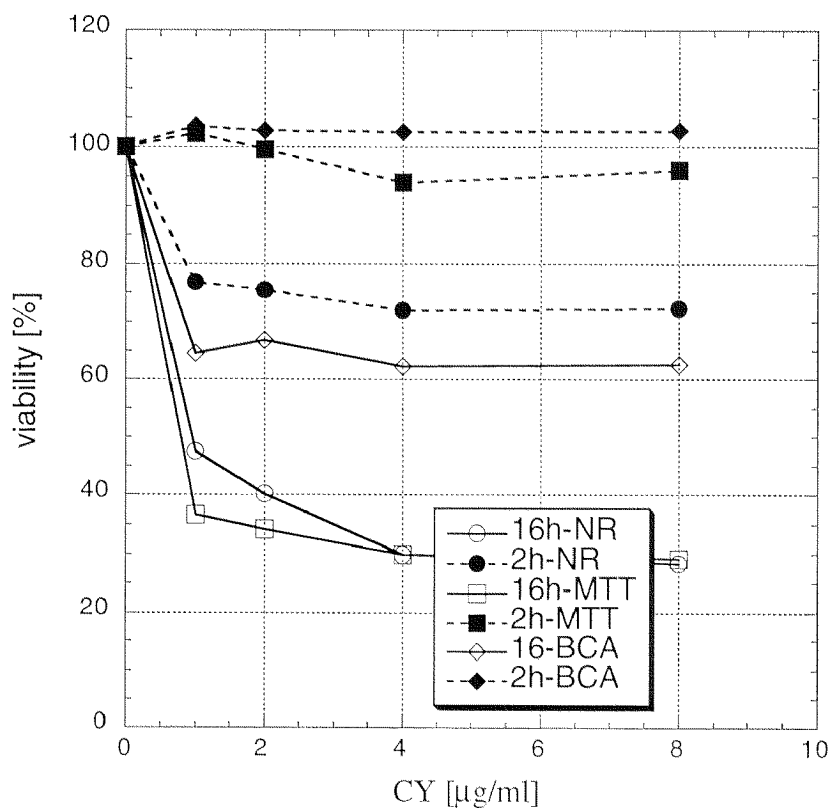


*Fig. 5.2.23: Effect of CY on the viability of hepatoma cells determined by the NR, MTT and BCA assay. No dose-response relationship was found between 1 and 8  $\mu\text{g/ml}$  CY. Except for the NR assay, no effect was observed with MTT and BCA assay after 2 h. In contrast, a reduced activity was monitored by all tests after 16 h.*

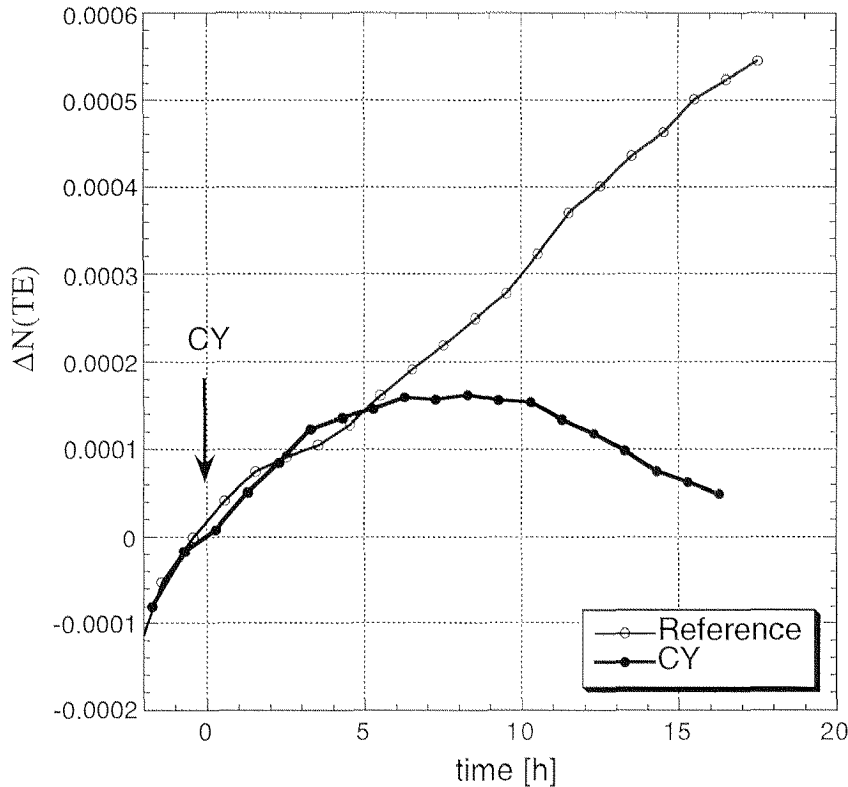
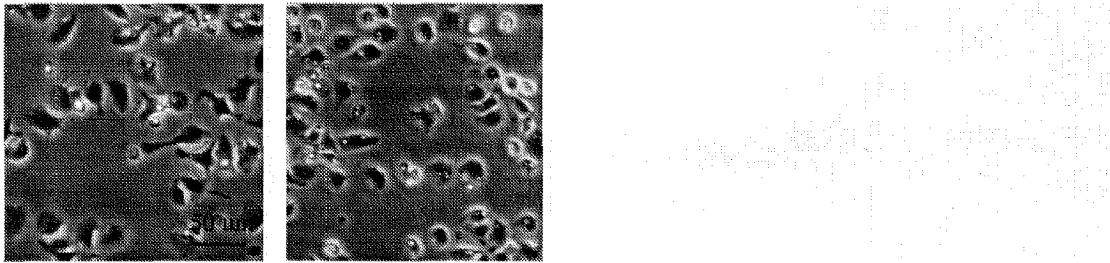


**Fig. 5.2.24:** *Effect of CY measured by the OWLS. A clear change of the OWLS-signal with respect to the reference after administration of CY (time=0) was detectable after 5 h. In the case of CY-exposure the cell-density remained constant and thus the decrease of the OWLS-signal after 10 h is due to weaker cell adhesion. The data are the mean of four experiments.*

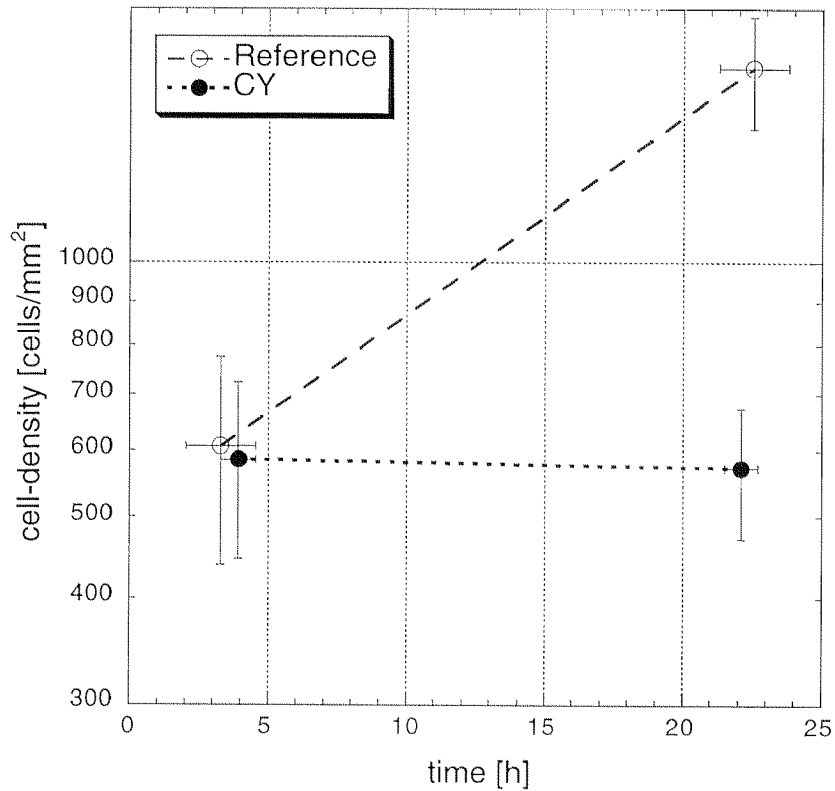
CY was used in a concentration range as described in the literature in order to completely block protein synthesis. Accordingly, no dose-response relationship was found at this high range. In accordance with the proliferation rate of hepatoma cells, all tests indicated a slightly reduced activity after 2 h and a strongly reduced activity after 16 h.

Fig. 5.2.24 shows the influence of CY on the OWLS-signal. When the hepatoma cells had fully spread the cell density was determined. One hour later (time=0), 4  $\mu\text{g/ml}$  CY in medium was flown through the measuring cuvette. During the first 5 h the OWLS-signal was identical for both situations. A clear difference between the reference and the OWLS measurements was only visible after 5 h, when the signal reached a plateau indicating the arrested proliferation. After 10 h the signal started to decrease pointing

towards a weaker cell adhesion, which was also confirmed by by microscopy. Fig. 5.2.25 shows the morphology of hepatoma cells after exposure to CY for at least 15 h. Most cells had lost their filapodia and some cells became round. Remarkably, the cell density remained almost constant (Fig. 5.2.26), meaning that the alteration of the OWLS-signal can be purely described by cell adhesion. In fact, this transient maximum could indicate a cellular stress as in the situation with of 3 and 4  $\mu\text{g/ml}$  BAC. In accordance to the OWLS-signal, it is suggested, that this stress is expressed as an increase in the cytoskeleton synthesis.



*Fig. 5.2.25: Morphology of hepatoma cells after exposure to 4  $\mu\text{g/ml}$  CY for 16 h. The picture on the left side shows the morphology before administration of CY. The picture on the right side shows the morphology of the hepatoma cells after exposure to 4  $\mu\text{g/ml}$  CY for 16 h.*



*Fig. 5.2.26: Effect of CY on the proliferation of hepatoma cells. After exposure to CY the proliferation rate of hepatoma cells is arrested. The data are the mean of four experiments.*

It is concluded that the inhibition of cell proliferation can be observed with all three methods, light microscopy, OWLS and the viability tests. The on-line character of the OWLS allows to detect a difference already after 5 h, a time interval after which the cell adhesion started to decrease.

### 5.2.9. Effect of cyclophosphamide

The antitumor prodrug CP needs metabolic activation through the P450 monooxygenase system, which is mainly expressed in liver cells. The active metabolite 4-hydroxy-CP and breaks down into phosphoramidate mustard and acrolein, which show an alkylating and cytotoxic potential.

The concentration range of CP-toxicity was first tested using the three biochemical assays (Fig. 5.2.27). In all tests a clear dose-effect relationship was observed, which became more prominent with increasing exposure time. The reduced proliferation rate is mainly responsible for the observed reduced viability signals.

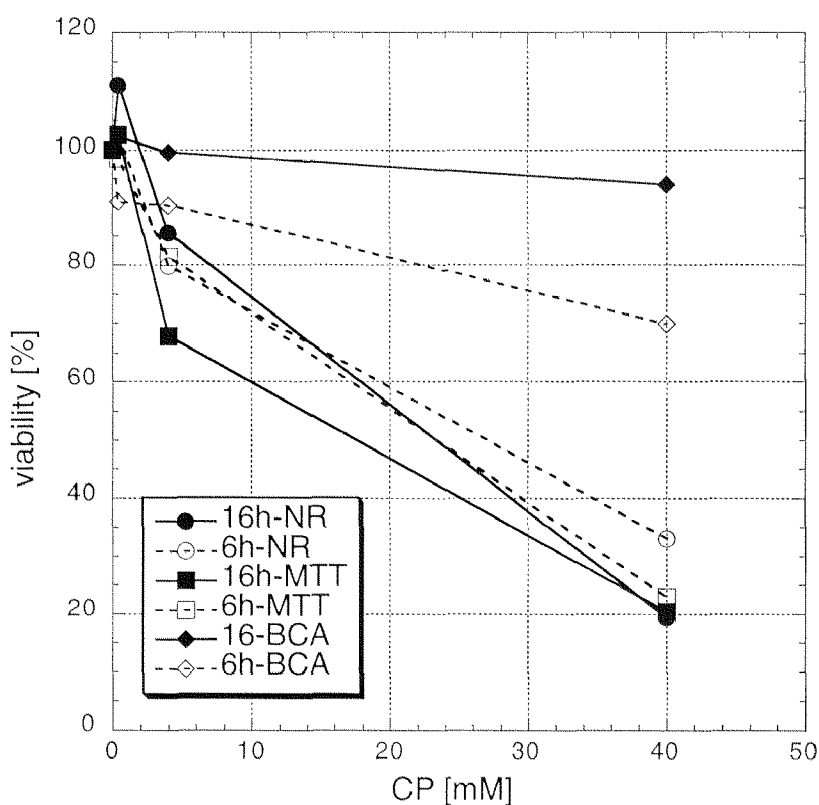


*Fig. 5.2.27: Effect of different concentrations of CP on the viability of the hepatoma cells determined by the NR, MTT and BCA assay. All three tests showed a clear dose-effect relationship between 0.4-40 mM CP. With increasing exposure time the reduced cell activity became even more obvious.*

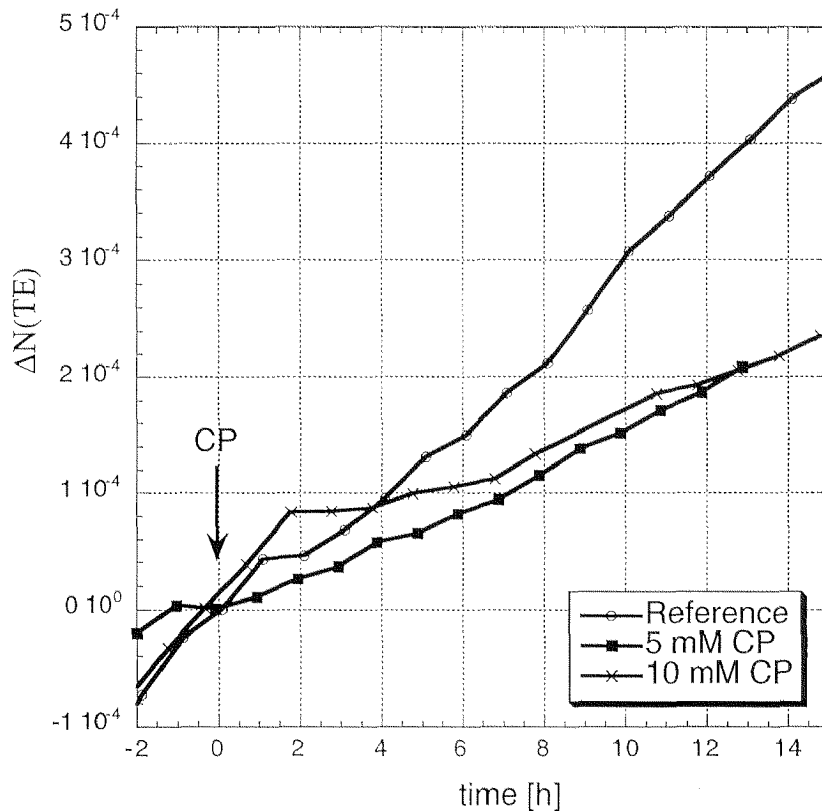


**Fig. 5.2.28:** Effect of CP measured by the OWLS. A clear difference of the OWLS-signal after administration of CP was only detectable after 5 h for both 5 and 10 mM CP. Surprisingly no clear dose-response relationship was found. The data are the mean of three experiments.

Fig. 5.2.28 shows the effect of 5 and 10 mM CP on the OWLS-signal. When the hepatoma cells had reached the fully spread state (4–6 h) and the cell density had been determined, medium containing CP (5, 10  $\mu\text{g}/\text{ml}$ ) was flown through the measuring cuvette.

The morphology of hepatoma cells after exposure to 10 mM CP for at least 12 h is shown in Fig. 5.2.29. No obvious difference in cell adhesion could be observed. However, the cell proliferation was inhibited in a dose-dependent way (Fig. 5.2.30) and could be detected by the OWLS.



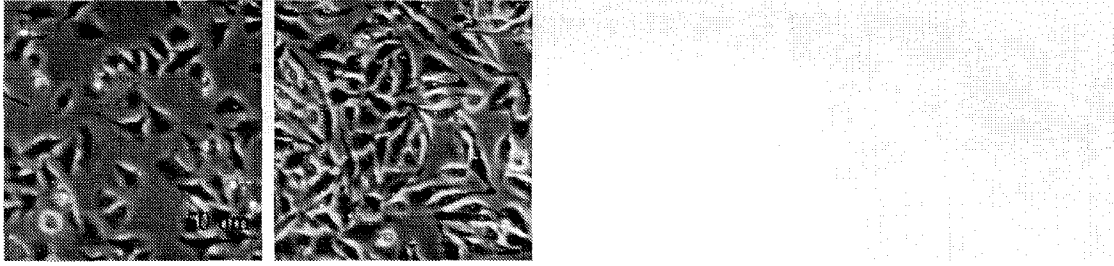


**Fig. 5.2.29:** Morphology of hepatoma cells after exposure to 10 mM CP for at least 12 h. The picture on the left side shows the morphology before administration. The picture on the right side shows the morphology of the hepatoma cells at the end of an OWLS experiment.

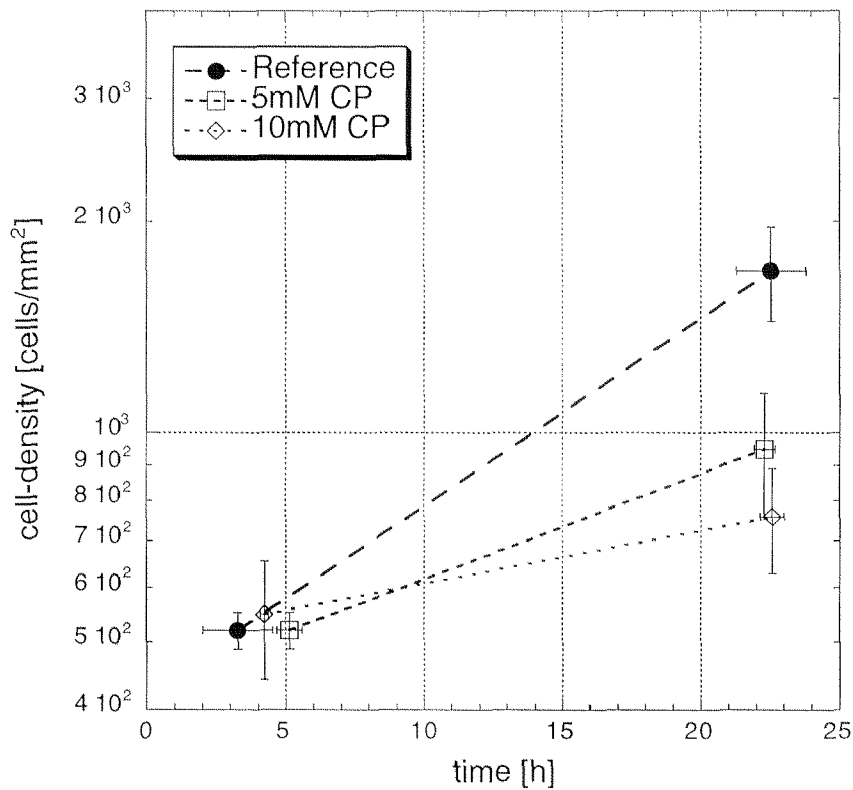


**Fig. 5.2.30:** Influence of CP on the proliferation of hepatoma cells. After exposure to 5 and 10 mM CP the proliferation rate of hepatoma cells is reduced in a dose-dependent way. The data are the average of at least three experiments.

In conclusion, results from the OWLS measurements, the viability test and the observations by inverted phase-contrast microscopy were in good agreement. After

exposure to CP the proliferation rate of the hepatoma cells was reduced, which was detectable by the OWLS and by the viability tests after 5 - 6 h.

## 6. Discussion

In previous studies the OWLS was used for monitoring the spreading of BHK cells. Cell adhesion and spreading is a fundamental process for cell survival. It interacts with many essential processes within the cell and vice versa is affected by cellular metabolism. Hence the scope of this work was to test whether or not the OWLS may be used as a cell-based biosensor to study cell adhesion as an indicator of the metabolic state of a cell population. After having established conditions for reproducible measurements, several representative applications were studied. The investigations followed the guidelines according to Koeter in order to fulfill the requirements for validation (Koeter 1994), (Koeter 1995):

### Standard Operation Procedures (SOPs)

The first part of this work consisted in finding SOPs for reproducible and quantitative OWLS measurements of cell adhesion. This included the study of protein adsorption at biologically realistic conditions in order to elucidate the selectivity and specificity of the biosensor in combination with cells. A new design of the measuring cuvette allowed parallel observations with light microscopy, which was needed for the validation of the results. By optimization of the cell-medium and the fluid conditions stable measurements could be carried out for up to 48 h. In addition the height of the measuring cuvette was redesigned such that cell settling occurred simultaneously with protein adsorption.

An OWLS experiment included three phases: The first phase lasted approximately ten minutes and was defined by the time needed for the almost complete adsorption of proteins present in the medium. The second phase comprised the time needed to complete cell spreading and was individual for each cell line. The length of the second phase was between two and six hours. The third phase was used for detection of the cell response to special environmental agents. Its duration was dependent on the concentration and nature of the chemical. In the case of hepatoma cells proliferation was observed during the third phase.

### Applications

In the second part of the present study cell adhesion was studied in detail. This included the OWLS response following the adhesion of representative cell-lines with increasing cell densities. The different adhesion behavior of the different cell-lines and the correlation of the cell-density and the OWLS-signal allowed the measuring principle of the OWLS in whole cells layers to be characterized. This consisted in measuring the contact area between the waveguide and the cell. The significance of the contact area can be compared to the endpoint of biochemical assays. Based on these experiments, two

fundamentally different anchorage-dependent cell-lines but both with a strong adhesion to the waveguide were chosen.

### Experiments

In the following step the best strategy for measuring the effect of toxic substances on cell adhesion had to be found. Originally a change of cell spreading was considered to be the best strategy. During spreading the OWLS-signal increases dramatically and thus minor toxic influences on the OWLS-signal may become visible within a short time. Nevertheless, the toxicity of most substances at relevant concentrations can only be observed after several hours. Moreover, the confidential interval for measurement of cell spreading was considerably high such that toxic effects were expected to be smaller than the experimental error. For both reasons the strategy of measuring spreading as an indicator of metabolic state was finally abandoned.

Unlike spreading, the reproducibility of the long-term behavior of both selected cell-lines was considerably higher; the OWLS-signal of the fibroblasts reached a reproducible steady state after spreading, whereas the signal of the rapidly growing hepatoma cells was reproducibly increasing with time. In both situations the toxic chemical is added after spreading and minor toxic changes could be observed with OWLS even after hours. It is suggested that trypsinization comprises many sources of error and a reproducible metabolic state of the cells is only obtained after spreading (4 – 6 h). Thus the strategy of the steady-state before exposure to test substances was chosen for the experiments.

Several model compounds were identified in the literature. The criteria for the selection of the substances were on one side the elucidation of the endpoint of the OWLS (colchicine, serum) and on the other side the demonstration of possible OWLS applications (BAC, CY, CP). For the fibroblasts the evaluation of the irritation potential of BAC was selected as a representative example. In the case of the hepatoma cells, monitoring growth inhibiting substances such as CY and CP was of special interest, including the metabolic capacity of the hepatoma cells.

### Validation of the OWLS

Since the OWLS-signal is not selective, it was necessary to elucidate the relationship to biological events such as protein adsorption and cell adhesion. A number of input parameters were studied in this respect, including reproducibility, selectivity and sensitivity. For the validation of the OWLS, the results were compared with inverted light microscopy and biochemical assays. With the aid of microscopic pictures the contact area was found to be the underlying unit of this assay when compared with endpoints of viability assay.

### 6.1. Sensitivity

For the cell experiments the direct response of the ASI instrument in the form of  $N(\text{TE})$  was selected, because it is not possible to calculate the adsorbed mass or its relative changes in a situation with both protein adsorption and cell adhesion.

Moreover, for the best possible sensitivity of the OWLS-signal towards the cell spreading it was desirable to keep the overall contribution of the serum as low as possible. For this reason the serum concentration in the medium was reduced to 4 % (v/v) instead of 10 % (v/v) as often used in cell culture.

From the preliminary experiments it was found that the protein contribution under such conditions was  $\Delta N(\text{TE}) = 4.5 \cdot 10^{-4}$  and it was thus assumed that the contribution of proteins remains stable during the whole experimental period with cells. A typical OWLS-signal at the fully spread state exhibited more than twice of the value of serum measurements: The highest OWLS-signal for the fibroblasts was  $\Delta N(\text{TE}) = 1.3 \cdot 10^{-3}$  and  $\Delta N(\text{TE}) = 1.8 \cdot 10^{-3}$  for the hepatoma cells. Thus the contribution of cells to the OWLS-signal dominated by 65 - 75 % as compared to the contribution of proteins, which was in the range of 25 - 35 %. Accordingly, an experimental error of  $\pm \Delta N(\text{TE}) = 4.5 \cdot 10^{-5}$  due to adsorbed proteins represented a total relative error of 2.5 - 3.5 %, which is accepted with biological assays.

### 6.2. Time-dependent selectivity

A new measuring cuvette was designed such that protein adsorption and the cell settling were accomplished simultaneously at certain time after the entry into the cuvette. This time interval is based on the adsorption time of serum proteins, which is needed for the saturation of the ASI chip. By the BSA model, it was calculated and experimentally verified that 90 % surface saturation is reached within ten minutes. By this procedure it was possible to separate protein adsorption and cell spreading on the time scale.

Significant differences between protein adsorption and cell adhesion became obvious in several experiments: First the adhesion of the different cell-lines showed the identical OWLS-signal within the first phase (Fig. 5.2.1). Due to different adhesion and spreading, the OWLS-signal differed in the second phase. Second, triggering spreading by the addition of serum indicated that the increase of the contact area was detectable within minutes for both cell-lines fibroblasts and hepatoma cells (Fig. 5.2.12). Since the cells were introduced in serum-free medium, it was expected that the addition of serum would result in an immediate increase of the OWLS-signal due to protein adsorption. However, if FCS containing medium was flown through the measuring cuvette with the purely adhering, non-active cells, the OWLS-signal did not increase.

Apparently no further adsorption of proteins took place meaning that the chip surface was already completely covered with proteins and cells. There are two explanations for this phenomena: Either the excretion of proteins by the cell was considerably fast and covered the free surface with proteins within 1 h and the protein content in the serum-free medium was artificially enlarged due to the part of dead cells and digested extracellular matrix in serum-free medium with the cells.

### 6.3. Protein adsorption

Protein adsorption gained enormous interest in the development of new biomaterials. It includes many processes such as transport in solution, adsorption and unfolding due to thermodynamic instabilities. Many factors such as surface charge of the protein and the surface, counterions and the nature of the proteins may play a fundamental role and completely change the adsorption behavior. Most research was performed with single protein systems such as albumin. Although competitive protein adsorption is the most realistic case, it is hardly possible to study it experimentally due to the lack of selective experimental methods. Therefore most research in the area of competitive protein adsorption remains on a theoretical level. It can be concluded, that although protein adsorption has been studied in detail, no coherent theory has been developed yet.

Due to non-specific adsorption of proteins and adhesion of cells, the influence of protein adsorption on the waveguide was studied in details. Based on the BSA model it was possible to predict the protein adsorption dynamics at higher concentrations as used in the experiments with cells. Although the comparison between the BSA model and the serum adsorption measurements was on a qualitative level due to the different measuring conditions for BSA and serum, the correlation of the measured serum adsorption measurements and the model predictions were in good agreement:

- It was shown both theoretically and experimentally that at biological serum concentration protein adsorption is fast and 90 % surface concentration is reached within ten minutes.
- Within a serum bulk concentration of 2 - 6 % (v/v) only a negligible influence on the surface concentration of adsorbed proteins was monitored. Consequently if the flow through the measuring cuvette is stopped before the protein concentration has reached its final value, the amount of adsorbed proteins is only marginally affected.

As described in the BSA model and found in the serum protein adsorption measurements, the OWLS-signal did not reach a final constant level, but increased

constantly. The increasing trend of the BSA model is a consequence of the slow replacement of reversibly bound proteins by irreversibly bound proteins. The scaled particle theory (SPT) results in a similar trend due to structural rearrangements, which occur with respect to the bulk concentration. Both models describe the real adsorption behavior of serum proteins. Regarding the protein bulk concentration, the SPT model was found to produce better results though.

#### **6.4. Extracellular matrix**

Since the cell experiments lasted up to 48 h, it was desirable to know the fate of adsorbed proteins. For the experiment with the ASI waveguide, the following scenario may take place: Medium with serum proteins and suspended cells are introduced into the measuring cuvette. First the proteins adsorb on the ASI waveguide. After the cell settling the fibroblasts adsorb through nonspecific binding to adsorbed proteins. Through adsorbed serum proteins such as fibronectin and vitronectin focal contacts are formed by the fibroblast. By the clustering of integrin and laminin receptors spreading is induced through the reorganization of the cytoskeleton. Later the fibroblasts remove the initial protein and secrete a new ECM of different protein composition and form new focal contacts (Dewez 1999), (Brash and Horbett 1995). Finally, the matrix is remodelled by cell-surface bound and cell-released enzymes.

Although the principal phenomena such as protein replacement and structural rearrangement are known from the literature, it is impossible to study a complex sequence of events in a qualitative nor in a quantitative way. In addition to the unfolding of proteins, cells secrete protein modifying enzymes. It was generally accepted that protein unfolding processes have a negligible effect on the OWLS-signal compared to the adhesion of cells. This assumption was largely confirmed by the long-term measurements suggesting that protein adsorption, replacements or structural rearrangements did not play a significant role. For the cell experiments, it was therefore assumed that the contribution of protein adsorption to the OWLS-signal remained in all experiments within the same range of  $\Delta N(\text{TE}) = 4.5 \cdot 10^{-4}$ .

#### **6.5. Cell adhesion**

By several experiments it was shown that the OWLS-signal is proportional to the contact area between the adsorbed cells and the surface of the ASI-chip. The OWLS-signal of all cell-lines showed a qualitative correlation with the microscopically visible morphology of the cells.

Equally, the correlation with the OWLS-signal at steady state was dependent on the adhesion of the cells for several cell-densities. Accordingly, a strong correlation was found for firm adhesion, whereas cell density and OWLS-signal were almost

---

uncorrelated in the situation of weak cell adhesion. The long-term behavior of the two selected cell-lines was different:

- After having reached the fully spread state, the contact area of J-fibroblasts remained almost constant for up to 48 h. At high cell-density the contact-inhibition became so strong that cells piled up in a way that the OWLS-signal decreased significantly and stabilized after hours at a considerably lower  $\Delta N(\text{TE})$ .
- In contrast, the hepatoma cells proliferated exponentially fast and a constantly rising OWLS-signal was the consequence. In fact, two opposing trends were observed. On the one hand the number of hepatoma cells tripled every 24 h and on the other hand the contact area per cell decreased due to the increasing cell-density. Consequently, the correlation of the cell-number and the OWLS-signal changed with increasing cell-density. Apparently, the influence of proliferation predominated.

Finally, it was shown in two scenarios with both fibroblasts and hepatoma cells that the OWLS-signal corresponded to morphological alterations within minutes: If serum was added to adherent cells, the spreading process could be monitored over several hours. The activity of the cytoskeleton could be visualized in real-time when the cells were exposed to colchicine. The changes of the cell-shape due to the microtubuli-disrupting agent were observed with both inverted phase-contrast microscopy and OWLS.

### 6.6. Reproducibility

The reproducibility of the OWLS measurements was impaired by several sources of errors. To identify them, four correlations and their corresponding confidential interval are discussed:

- Quantitatively, the *adsorption of proteins* was determined in our study within a range of about  $\pm 10\%$ . The same range of error was also observed by other investigations with for plasma adsorption experiments (Kurrat, Walivaara et al. 1998). In their study, the waveguides were additionally exposed to an oxygen plasma before each use. It is of interest that despite extraordinary cleaning, the serum and plasma adsorption experiments showed the same error. The true source of this error remains unknown. It may be either due to different surface properties of the waveguide or a different quality of the serum proteins leading to a different



organization of the adsorbed proteins from one experiment to the next. The serum was of the same batch and stored at equal conditions though.

Compared to protein adhesion the quality of the waveguide played a minor role in the cell experiments. Regarding the cells, other sources of errors such as the metabolic state and the distribution of cells might be more important:

The *cell concentration* was determined by counting the number of cells in sixteen squares of the *Neubauer* cell counting chamber. This way the cell concentration could be reproducibly determined with a 95 % confidential interval amounting to 5 % of the total cell concentration. The error of the cell concentration was in an acceptable range. Increasing the number of counted squares of the *Neubauer* counting area did not decrease the 95 % confidential interval. In order to further reduce the confidential interval a professional cell counter would be necessary.

- In contrast, the 95 % confidential interval of the *cell density* varied between 5 and 30 % of the total cell density. Since a random distribution of cells shows locally a very inhomogeneous distribution, it is difficult to obtain a homogeneous cell density on a small spot such as the sensing area. Generally, the smaller the selected area, the bigger are the random deviations. The cells become objects with dimensions comparable to the sensing area.
- The third source of error are the different *metabolic states of the cells*, leading to different cell adhesion and cell contact area. The different metabolic state of the cells may originate from a different cell-density in the T-flask, different trypsinization time and different cell-cycle stage. In the case of hepatoma cells the metabolic state of a cell population may have an effect on the lag-time before proliferation starts. Such biological factors are hard to control unless the experiments are run with growth-synchronized cell cultures in parallel. Therefore the intensity of the OWLS-signal showed a broad confidence interval. Again the small number of cells within the sensing area represents a random influence

Consequently, the changes of the OWLS-signal after the addition of colchicine and BAC were influenced by the same sources of error. Nevertheless, the influence of these chemicals was clearly determined and could be used for further studies.

Most sources of errors could be simply eliminated by performing the OWLS measurements in parallel with control on the same chip with a larger sensing area. These two basically easy technical improvements would solve most problems

concerning the reproducibility: The waveguide surface quality problem would disappear in parallel measurements. The problem of the varying state of the cells from one measurement to the next would be solved as well. The random factor on the inhomogeneous cell distribution could be minimized by the larger sensing area. A higher reproducibility instantaneously leads to the observation of smaller effects and would strengthen the advantages of OWLS again.

### **6.7. Applications**

The development of artificial skin represents a preliminary conditions for *alternative* skin corrosion and irritation assessment. *In vivo* data of animals and *in vitro* data of artificial skin are in close correlation. Artificial skin is one of the first examples in which the use of animals for risk assessment was successfully replaced.

It consists of several layers of fibroblasts and keratinocytes. Compared to keratinocytes the cell culture of the widespread 3T3-fibroblasts is simple because fibroblasts are not very sensitive regarding cell survival after seeding. Moreover, fibroblasts display a strong adhesion. For the OWLS application, it was thus attractive to start with a fibroblast cell-line.

For instance, artificial skin was used to study the skin irritation potential of surfactants such as BAC. In our experiments, the BAC dose-response relationship was in close relation with the viability tests. The promising results of the BAC experiments suggest further experiments with other irritants and human fibroblasts in order to fully evaluate the OWLS also for the detection of skin irritants in fibroblast cultures.

In contrast, the selection of hepatoma cells was especially interesting due to their wide spectra of xenobiotic metabolisms. Tumor hepatocytes with their fast proliferation rate may be used in experiments with growth inhibiting substances. Using inhibition of cell proliferation as an indicator of toxicity, the reduced proliferation can be monitored on-line and became detectable within 5 h with CY and 4 h with CP respectively.

### **6.8. Cytoskeletal activity and its relation to the metabolic state**

For both fibroblasts and hepatoma cells it was shown experimentally that cell adhesion is an indicator of the metabolic state of cells. Cell adhesion is mediated by cytoskeletal activity, which depends also on the cell-cycle stage of the cell. The important role of the cytoskeleton on cell adhesion was shown directly with both the cytoskeleton-disrupting agent colchicine and serum effects:

- Immediate decrease of the OWLS-signal after the exposure to colchicine demonstrated the cytoskeletal dependence of cell adhesion. The significance of the results was increased by carrying out the experiments using the cell-lines of

different species, namely from mouse and man. For both cell-lines the same effects on the OWLS-signal were observed.

- The activation of the cytoskeleton through growth factors is regulated through biochemical pathways. The effect of cell spreading after the addition of growth factors was observed with both fibroblasts and hepatoma cells.
- Serum removal is known to reduce cell viability. After a time interval of hours a process between apoptosis and necrosis is induced. The OWLS-signal decreased within 1 h after serum removal indicating a loss of cell adhesion. In contrast serum deprivation did not significantly decrease the adhesion of hepatoma cells, and accordingly the OWLS-signal remained constant. It was also confirmed by microscopy. The OWLS-signal decreased only due to serum desorption and became stable after 1 h.

All results of the OWLS experiments were in good correlation with the viability measurements and with the microscopical observations. This clearly indicated a close relation between the metabolic state of the cell measured by viability assays and its adhesion measured and observed by either OWLS or by microscopy.

A more indirect clue as to viability-dependent adhesion are the results with BAC, CY and CP. The dose-effect relationship of the OWLS-signal after administration of BAC correlated with the viability test and the microscopical observations. In the case of the hepatoma cells, cell proliferation becomes the most important indicator for viability.

Thus, it was demonstrated that vital cellular processes could be identified and monitored on-line by the OWLS. However, compared to the viability assays such as the MTT and NR assay *the endpoint* in the OWLS depends on the specific situation and can not be simply expressed in percent as for the standard viability assays. Furthermore, it is obvious that the role of the reference is different for fibroblasts and hepatoma cells.

### **6.9. Validation**

The idea to use the OWLS measurements to quantify cell adhesion as an indirect indicator of the metabolic state was fully verified. From the comparison between the methods to measure viability namely OWLS, microscopy and the three biochemical assays the following conclusions can be drawn:

- In several scenarios as summarized in *Table 1.6*, the cell adhesion was changed and measured with OWLS. It was found that OWLS detects the contact area between the

cell and the waveguide. It can be regarded as an endpoint unlike the mechanism of other biochemical assays.

- In the situation of fibroblasts and a surfactant such as BAC a similar dose-response relationship for all three methods, the OWLS measurements, the microscopic observations and the viability test was observed.
- CY inhibits protein synthesis and thus inhibits proliferation. The metabolites of CP alkylate the DNA. In both situations, where hepatoma cells were exposed to either CY or CP, the reduction of cell viability and cell adhesion became visible by the reduced proliferation rate in all three methods.

The OWLS combines several advantages: OWLS is an *on-line* method, which needs no additional labelling. The technique contains quantitative information about the adhesion of several hundred cells at the same time. Although the process of cell adhesion is far from being fully understood, it could be shown that it may be used as a quantitative indicator of viability. Furthermore cell adhesion covers a broad spectra of adverse effects and toxic events.

### 6.10. Biokinetic modelling

OWLS measures cell adhesion and the corresponding metabolic state on-line and may thus be useful to collect data for biokinetic modelling. The relationship between exposure time, dose and OWLS response is a complex interaction of several processes. The development of biologically based kinetic (BBK) modelling as a tool in the analysis of the kinetics of chemicals in biological systems has progressed rapidly in the last decade. Biokinetics describes the absorption, distribution, metabolism, storage and excretion of the chemical. It includes also the rates of transport processes such as transport to the tissue and through the cell membrane. The aim of biokinetics studies is to obtain a quantitative measure of the pharmacological and toxicological activity of the chemical at the tissue target (Frazier, 1995).

Chemical binding of macromolecular ligands in the plasma, such as albumin, has several consequences. First the total concentration of the chemical in the plasma compartment increases the affinity of the ligand for the chemical. Second by the lower concentrations of free molecules the toxicity is increased (Benoit, Cormier et al., 1987). The OWLS measurements carried out at continuous flow conditions may be useful to study the influence of protein binding on the toxicity by varying the albumin content of the medium flowing through the measuring cuvette. Especially detergents such BAC are known to have a high affinity to albumin.

### 6.11. Outlook

The experimental results obtained in the present study, demonstrate that OWLS is a simple and a powerful method to quantify cell adhesion under various conditions. It may be used to study the effect of growth factors as well as cytotoxic substances. On-line measurements provide a deeper insight into the context of cell shape and viability. More sophisticated experiments such as repeated exposure of toxic substances may be envisioned. The continuous flow conditions represents realistic *in vivo* conditions and allow biokinetic modelling.

The present number of the cells (150-250 fibroblasts/300-400 hepatoma cells) encompassed by the sensing area of the chip is considered to be statistically too small. The sensing region area should therefore be enlarged to increase both sensitivity and reproducibility of the measurements. In addition, reproducibility of the measurements could be improved by a chemical modification of the ASI-chips, e.g. protein-adhesive regions combined with protein-repulsive regions in a well-defined fashion could help to overcome the problems of the irregular cell distribution.

On the cell culture side a growth-synchronized cell culture may reduce the effect of different cell size or cell volumetric density. Alternatively, parallel measurements on the same chip would help to overcome these problems by a technical approach.

The OWLS combined with other optical methods has also potential for high-throughput screening. Future research includes further elucidation of the relation between the contact area and the state of the cytoskeleton as well as the cell viability.

## Abbreviations, Symbols and Indices

### Abbreviations

AP	Acid-phosphatase
ASI	Artificial sensing instruments
APM	Aldophosphamide (APM)
ATP	Adenosintriphosphate
BBK	Biologically based kinetic
BCA	Bicinchoinic acid
BHK	Baby hamster kidney
BAC	Benzalkonium chloride
CY	Cycloheximide
CP	Cyclophosphamide
CHO	Chinese hamster ovary
DNA	Deoxynucleic acid
ECM	Extracellular matrix
EDTA	Ethylendiamintetraacetat
FGF	Fibroblast growth factor
FCS	Fetal Calf Serum
F-actin	Filamenouts actin
Fg	Fibrinogen
FGF	Fibroblast Growth Factor
Fn	Fibronectin
GTP	Guanosin-5-triphosphat
HEPES	4-(2-Hyrdoxyethyl)piperazine-1-ethanesulfonic acid sodium salt
HSA	Human Serum Albumin
IL-6	Interleukin Factor 6
IA	Image analysis
IgG	Immunoglobulin
INA	Illumination aperture
LDH	Lactatdehydrogenase
LPA	Lisophospholipid acid
MCA	Mercapturic acid
MKE	Monkey kidney epithelial
MVQ	Methyl-vinyl-silicon caoutchuc
MT	Microtubuli
MTT	3-[4,5-dimethylthiazol-2-yl]-2,5-diphenyl tetrazolium bromide
PBS	Phosphate buffered saline
PAM	Phosphoramid mustard
P450	Cytochrom P 450
Rac	GTP-binding protein
Rho	GTP-binding protein
RIT	Residual internal tension
RNA	Ribonucleic acid
NR	Neutral red
RSA	Random sequential adsorption
QCM	Quartz crystal microbalance
PS	Polystyrene
RICM	Reflectance Interference Contrast Microscopy
OWLS	Optical Waveguide Lightmode Spectroscopy
SPT	Scaled Particle Theory
TE	Transverse electric
TEER	Transepithelial electrical resistance
TM	Transverse magnetic
VERO	African green monkey cells

---

## Symbols

A	adlayer
$\Phi$	phase-shift
d	thickness, diameter
g	gravitation constant
h	height
l	diffraction order
M	mass
N	effective refractive index
n	refractive index
OD	optical density
r	radius
u	settling velocity
z	distance
$\alpha$	angle
$\lambda$	wavelength
$\rho$	density
$\mu$	viscosity

## Indices

A	adlayer
C	cover
F	fluid
J	(optical) medium
S	substratum

## References

"Final report on the safety assessment of benzalkonium chloride.", (1989) *J. Am. Coll. Toxicol.* 8(4): 589-625.

Bains, W. (1994). "A spectroscopically interrogated flow-through type toxicity biosensor." *Biosensors & Bioelectronics* 9: 111-117.

Benoit, J., M. Cormier and J. Wepierre (1987). "Effect of proteins on the assessment of surfactant cytotoxicity by an in vitro test: possible correlations with in vivo data" *Toxic. in vitro* 1: 91-96

Borenfreund, E. and J. A. Puerner (1984). "A simple quantitative procedure using monolayer cultures for cytotoxicity assays." *J. Tissue Culture Methods* 9(1): 7-9.

Brash, J. L. and T. A. Horbett (1995). "Proteins at interfaces II: Fundamentals and Applications", ACS Symposium Serie, 343.

Brown, R. A., G. Talas, R. A. Porter, D. A. McGrouther and M. Eastwood (1996). "Balanced mechanical forces and microtubule contribution to fibroblast contraction." *J. Cell Physiol.* 169: 439-477.

Clothier, G.S., S. Stipho and Y.C. Kwong (1999), "Assessment of initial damage and recovery following exposure of MDCK cells to an irritant", *Toxic. in vitro* 13:717-717

Chen, C. S., M. Mrksich, S. Huang, G. M. Whitesides and D. E. Ingber (1997). "Geometric control of cell life and death." *Science* 276: 1425-1428.

Chow, S.C., I. Peters and S. Orrenius, (1990)"Reevaluation of the role of de novo protein synthesis in rat thymocyte apoptosis" *Exp. Cell. Res.* 216: 149-159

Cornelis, M., C. Dupont and J. Wepierre (1992). "Prediction of eye irritancy potential of surfactants by cytotoxicity test in vitro on cultures of human fibroblasts and keratinocytes." *Toxic. in vitro* 6(2): 119-128.

Danowski, B.A., and K. Harris. (1988) "Changes in fibroblast contractility, morphology, and Adhesion in response to phorbol ester tumor promoter." *Exp. Cell Res.* 177: 47-59.

Danowski, B.A.(1989) "Fibroblast contractility and actin organization are stimulated by microtubule inhibitors", *J. Cell. Sci* 93: 255-266



Dejana, E., S. Colella, G. Conforti, M. Abbadini, M. Gaboli and P. C. Marchisio (1988). "Fibronectin and vitronectin regulate the organization of their respective Arg-Gly-Asp adhesion receptors in cultured human endothelial cells." *J. Cell Biol.* 107: 1255-1223.

Dewez, J.-L. (1999). "Competitive adsorption of proteins: Key of the relationship between substratum surface properties and adhesion of epithelial cells." *Biomaterials* 20: 547-559.

Dickson, F. M., J. N. Lawrence and D. J. Benford (1994). "Cytotoxicity of 12 chemicals of known human and animal skin irritation potential in human keratinocyte cultures." *Toxic. in vitro* 8(4): 661-663.

Draize, J.H., Woodard G. and H.O. Calvery, (1944) "Methods for the study of irritation and toxicity of substances applied topically to the skin and mucous membranes", *J. Pharmacol. Exp. Therapeut.* 82: 337-390

Durand-Cavagna, G., P. Delort, P. Duprat, Y. Bailly, B. Plazonnet and L. R. Gordon (1989). "Corneal toxicity studies in rabbits and dogs with hydroxyethyl cellulose and benalkonium chloride." *Fund. Appl. Toxicol.* 13: 500-508.

Dürholt, H. Steger-Hartmann, T., Wagner, J. and E. Wagner (1995). "Der Leitfähigkeitstest-ein Testsystem zur Ermittlung der membrantoxischen Eigenschaften von Substanzen, *Acta hydrochim, hydrobiol* 23 :298-302

Ehret, R., W. Baumann, M. Brischwein, A. Schwinde, K. Stegbauer and B. Wolf (1997). "Monitoring of cellular behaviour by impedance measurements on interdigitated electrode structures." *Biosensors & Bioelectronics* 12(1): 29-41.

Evans, P. F. (1994). "Updated toxicology test methods for new industrial chemicals: implication for regulatory acceptance for in vitro alternatives now and in the future." *Toxic. in vitro* 8(4): 912-922.

Fentem, J. H. and M. Balls (1994). "Why, when, and how in vitro tests should be accepted into regulatory toxicology." *Toxic. in vitro* 8(4): 923-924.

Fentem, J. H., M. K. Prinsen, H. Spielmann, E. Walum and P. A. Botham (1995). "Validation-lessons learned from practical experience." *Toxic. in vitro* 9(6): 857-862.

Folkman, J. and A. Moscona (1978). "Role of cell shape in growth control." *Nature* 273: 345-349.

## References

---

- Frazier, J.M. (1995). "Biokinetic modelling and in vitro analysis: Application of in vitro systems to the prediction of in vivo biokinetics" *Toxic. in vitro* 9(4): 527-536
- Fredriksson, C., S. Kihlmann, M. Rodahl and B. Kasemo (1998). "The piezoelectric quartz crystal mass and dissipation sensor: A means of studying cell adhesion." *Langmuir* 14: 248-251.
- Gaigalas, A. K., J. B. Hubbard, M. McCurley and S. Woo (1992). "Diffusion of bovine serum albumin in aqueous solutions." *J. Phys. Chem.* 96:2355-2359.
- Goldmann, W.-H., M. Schindl, T. Cardozo and R. Ezzell (1995). "Motility of vinculin-deficient F9 embryonic carcinoma cells analyzed by video, laser confocal, and reflection interference contrast microscopy." *Exp. Cell. Res.* 221: 311-319.
- Gryte, D. M., M. D. Ward and W.-S. Hu (1993). "Real-time measurement of anchorage-dependent cell adhesion using a quartz crystal microbalance." *Biotechnol. Prog.* 9: 105-108.
- Gueniche, A. and M. Ponc (1993). "Use of human skin cell cultures for the estimation of potential skin irritants." *Toxic. in vitro* 7(1): 15-24.
- Harris, A. K. (1998). "Polarity and polarization of fibroblasts in culture." *Adv. Mol. Cell Biol.* 26: 201-252.
- Haynes, C. A. and W. Norde (1994). "Globular proteins at solid/liquid interfaces." *Colloids Surf. B: Biointerfaces* 2: 517-566.
- He, X. M. (1992). "Atomic structure and chemistry of human serum albumin." *Nature* 358: 209-214.
- Herbert, L., S. Pandey and E. Wang (1994). "Commitment to cell death is signaled by the appearance of a terminin protein of 30 kDA." *Exp. Cell. Res.* 210: 10-18.
- Huetz, P., V. Ball, J.-C. Voegel and P. Schaaf (1995). "Exchange kinetics for a heterogeneous protein system on solid surface." *Langmuir* 11: 3145-3152.
- Ingber, D. E. (1990). "Fibronectin controls capillary endothelial cell growth by modulating cell shape." *Proc. Natl. Acad. Sci. USA* 87: 3579-3583.
- Ishiyama, M. H. T., M. Shiga, K. Sasamoto, Y. Ohkura, K. Ueno and M. Watanabe (1995). "Novel cell proliferation and cytotoxicity assay using tetrazolium salt that produces a water-soluble formazan dye." *In vitro Toxic.* 8(2): 187-190.

Jung, H. I., I. Shin, Y. M. Park, K. W. Kang and K.-S. Ha (1997). "Colchicine activates actin polymerization by microtubule depolymerization." *Mol. Cell* 7: 431-437.

Kawabata, T.T., M.Y. Chapman, D.-H. Kim, W.S. Stevens, M.P. Holsapple (1990). "Mechanisms of in vitro immunosuppression by hepatocyte-generated cyclophosphamide metabolite and 4-Hydroperoxocyclophosphamide" *Biochem. Pharmacol.* 40: 927-935

Koeter, H. B. W. M. (1994). "Principles for a pragmatic approach to the regulatory acceptance of alternative tests." *Toxic. in vitro* 8(40): 925-930.

Koeter, H. B. W. M. (1995). "Validation: a highly charged concept." *Toxic. in vitro* 9(6): 851-856.

Kunz, R. E. (1997). "Miniature integrated optical modules for chemical and biochemical sensing." *Sensors and Actuators B* 38-39: 13-28.

Kurrat, R., J. E. Prenosil and J. J. Ramsden (1997). "Kinetics of human and bovine serum albumin adsorption at silica-titania surfaces." *J. Coll Interf. Science*: 185.

Kurrat, R., J. J. Ramsden and J. E. Prenosil (1994). "Kinetic model for serum albumin adsorption: experimental verification." *J. Chem. Soc. Faraday Trans<sub>2</sub>* 90: 587-590.

Kurrat, R., B. Walivaara, A. Marti, M. Texto, P. Tengvall, J. J. Ramsden and N. D. Spencer (1998). "Plasma protein adsorption on titanium: comparative in situ studies using optical waveguide lightmode spectroscopy and ellipsometry." *Colloids Surf. B: Biointerfaces* 11: 187-201.

Lawrence, J. N., S. Starkey, F. M. Dickson and D. J. Benford (1996). "Use of human and rat keratinocyte cultures to assess skin irritation potential." *Toxic. in vitro* 10: 331-340.

Lewis, R. W., J. C. McCall and P. A. Botham (1993). "A comparison of two cytotoxicity tests for predicting the ocular irritancy of surfactants." *Toxic. in vitro* 7(2): 155-158.

Lewis, R. W., J. C. McCall, P. A. Botham and I. Kimber (1993). "Investigation of TNF-alpha release as a measure of skin irritancy." *Toxic. in vitro* 7(4): 393-395.

Li, S.-Y., J. J. Ramsden, J. E. Prenosil and E. Heinzle (1994). "Measurement of adhesion and spreading kinetics of baby hamster kidney and hybridoma cells using an integrated optical method." *Biotechnol. Prog.* 10: 520-524.

## References

---

- Loprieno, N., L. H. Bruner, G. J. Carr, M. Chamberlain, M. Cottin, O. D. Silva and S. Kato (1995). "Alternatives in cosmetics testing." *Toxic. in vitro* 9(6): 827-838.
- Lu, A. N. C. F. and K. K. Chittur (1994). "A comprehensive model of multiprotein adsorption surfaces." *J. Coll. Interf. Sci.* 168: 152-161.
- Massia, S. P. and J. A. Hubbell (1991). "An RGD spacing of 440 nm is sufficient for integrin ab-mediated fibroblast spreading and 140 nm for focal contacts." *J. Cell Biol.* 114: 1089-1100.
- Narai, A., S. Narai and M. Shimizu (1997). "Rapid decrease in transepithelial electrical resistance of human intestinal Caco-2 cell monolayers by cytotoxic membrane perturbants." *Toxic. in vitro* 11: 347-354.
- Nimeri, G., C. Fredriksson, H. Elwing, L. Liu, M. Rodahl and B. Kasemo (1998). "Neutrophil interaction with protein-coated surfaces by an extended quartz crystal microbalance technique." *Colloids Surf. B: Biointerfaces* 11: 255-264.
- Pape, W. J. W., J. Degwert, F. Steckel and U. Hoppe (1993). "Immunocompetent cells for in vitro screening of skin irritation." *Toxic. in vitro* 7(4): 389-392.
- Parish, W. E. (1990). "Inflammatory mediators applied to in vitro toxicology: studies on mediator release and two-cell systems." *Toxic. in vitro* 4(4/5): 231-241.
- Ramsden, J. J. (1993). "Review of new experimental techniques for investigating random sequential adsorption." *J. Statistical Phys.* 73: 853-877.
- Ramsden, J. J. (1995). "Optical method for measurement of number and shape of attached cells in real-time." *Cytometry* 19: 97-102.
- Ramsden, J. J. (1995). "Puzzles and paradoxes in protein adsorption." *Chem. Soc. Rev.* 74: 73-78.
- Ramsden, J. J., S.-Y. Li, J. E. Prenosil and E. Heinzle (1994). "Kinetics of adhesion and spreading of Baby Hamster Kidney and Hybridoma cells using an integrated optical method." *Biotechnol. Prog.* 10: 520-524.
- Ramsden, J. J. and D. J. Roush (1995). "Protein adsorption kinetics drastically altered repositoning a single charge." *J. Am. Chem. Soc.* 117: 8511.

Ramu, K, C.S. Perry, T. Ahmed, G. Pakenham and J.P. Kehrer (1996). "Studies on the basis for the toxicity of acrolein mercaptures", *Toxic. Appl. Pharmacol.* 140: 487-498

Rheinwald, J. G. and H. Green (1975). "Serial cultivation of strains of human epidermal keratinocytes:the formation of keratinizing colonies from single cells." *Cell* 6: 331-344.

Ridley, A. and A. Hall (1992). "The small GTP-binding protein rho regulates the assembly of focal adhesion and actin stress fibers in response to growth factors." *Cell* 70: 389-399.

Rodahl, M., F. Hook, C. Frediksson, C. A. Keller, A. Krozer, P. Brzezinski, M. Voinova and B. Kasemo (1997). "Simultaneous frequency and dissipation factor QCM measurements of biomolecular adsorption and cell adhesion." *Faraday Disc.* 107: 229-246.

Rosania, G. R. and J. Swanson (1996). "Microtubules can modulate pseudopod activity from a distance inside macrophages." *Cell Motility Cytoskel.* 34: 230-245.

Safiejko-Mrocicka, B. and P. B. Bell (1998). "Distribution of cytoskeletal proteins in neomycin-induced protrusion of human fibroblasts." *Exp. Cell. Res.* 242: 495-514.

Sandt, J. J. M. v. d., W. J. M. Maas, P. C. Doornink and A. A. J. J. L. Rutten (1995). "Release of arachidonic and linoleic acid metabolites in skin organ cultures as characteristics of in vitro skin irritancy." *Toxic. in vitro* 25: 20-28.

Sandt, J. J. M. v. d. and A. A. J. J. L. Rutten (1995). "Differential effects of chemical irritants in rabbit and human skin organ cultures." *Toxic. in vitro* 9(2): 157-168.

Schindl, M., E. Wallraff, B. Deubner, W. Witke, G. Gerisch and E. Sackmann (1995). "Cell-substrate interactions and locomotion of *Dyctyostelium* wild-type and mutants defective in three cytoskeletal proteins: a study using quantitative reflection interference microscopy." *J. Biophys.* 68: 1177-90.

Shingvi, R., G. Sthepanoloulos and e. al (1993). "Review: Effects of substratum morphology on cell physiology." *Biotech. Bioeng.* 43: 764-771.

Shipley, G. D. and R. G. Ham (1983). "Control of entry of Swiss 3T3 cells into S phase by fibroblast growth factor under serum-free medium." *Exp. Cell. Res.* 146: 261-270.

Shipley, G. D. and R. G. Ham (1983). "Multiplication of Swiss 3T3 cells in serum-free medium." *Exp. Cell. Res.* 146: 249-260.

## References

---

Simm, A., G. Bretsch, H. Frank, U. Zimmermann and J. Hoppe (1997). "Cell death of AKR-2B fibroblasts after serum removal: a process between apoptosis and necrosis." *J. Cell Biol.* 110: 819-828.

Sporn, L. A. and T. H. Foster (1992). "Photofrin and light induces microtubule depolymerization in cultured human endothelial cells." *Cancer Res.* 52: 3443-3449.

Steadman, L. B., K. C. Thompson and C. R. Middaugh (1992). "The effects of surface adsorption on the thermal stability of proteins." *Biotechnol. Bioeng.* 40: 8-15.

Takai, Y., T. Sasaki, K. Tanaka and H. Nakanishi (1995). "Rho as a regulator of the cytoskeleton." *TIBS* 20: 227-231.

Talbot, J. (1997). "Molecular thermodynamics of binary mixture adsorption: A scaled particle approach.", *J. Chem. Phys.* 106, 4696-4706

Tiefenthaler, K. (1989). "Sensitivity of grating couplers as integrated-optical chemical sensors." *J. Opt. Soc. Am. B* 6(2): 209-220.

Tiefenthaler, K. (1992). "Integrated optical couplers as chemical waveguide sensors." *Adv. Biosensors* 2: 261-289.

Tiefenthaler, K. and W. Lukosz (1989). "Sensitivity of grating couplers as integrated-optical chemical sensors." *J. Opt. Soc. Am. B.* 6: 209-220.

Tsuji, K., A. Ueno and T. Ide (1992). "Inhibitory effect of taxol, a microtubule stabilizing agent, on induction of DNA synthesis is dependent upon cell lines and growth factors." *Cell Struct. Funct.* 17: 139-144.

Vunjak-Novakovic, G., B. Obradovic, I. Martin, P. M. Bursac, R. Laner and L. E. Freed (1998). "Dynamic cell seeding of polymer scaffolds for cartilage tissue engineering." *Biotechnol. Prog.* 14: 193-202.

Ward, R. K., S. Agarwala and R. Clothier (1994). "Investigation of an in vitro cytotoxicity assay for prediction of skin irritation." *Toxic. in vitro.* 8: 659-660

Ward, S. L., T. L. Walker and S. D. Dimitrijevic (1997). "Evaluation of chemically induced toxicity using an in vitro model of human corneal epithelium." *Toxic. in vitro* 11: 121-139.

---

Wolf, B., M. Brischwein, W. Baumann, R. Ehret and M. Kraus (1998). "Monitoring of cellular signalling and metabolism with modular sensor technique: The PhysicoControl-Microsystem." *Biosensors & Bioelectronics* 13: 501-509. .

Wood, K. V. and M. G. Gruber (1996). "Transduction in microbial biosensors using multiplexed bioluminescence." *Biosensors & Bioelectronics* 11(3): 207-214.

## Appendix

**BSA-Model (Kurrat, Ramsden et al., 1998),**

Listing of the ISIM simulation program (T.Hug)

METHOD Euler

```

STARTTIME = 0
STOPTIME = 5000
DT = 1
d/dt(cs1)=(cb+cs2-2*cs1)*D/delta/delta
d/dt(cs2)=(cs1+cs3-2*cs2)*D/delta/delta
d/dt(cs3)=(cs2+cs4-2*cs3)*D/delta/delta
d/dt(cs4)=(cs3+cs5-2*cs4)*D/delta/delta
d/dt(cs5)=(cs4+cs6-2*cs5)*D/delta/delta
d/dt(cs6)=(cs5+cs7-2*cs6)*D/delta/delta
d/dt(cs7)=(cs6+cs8-2*cs7)*D/delta/delta
d/dt(cs8)=(cs7+cs9-2*cs8)*D/delta/delta
d/dt(cs9)=(cs8+cs-2*cs9)*D/delta/delta
d/dt(cs)=(cs9-cs)*D/delta/delta -((ka+ki)*cs*theta+kd*Mr/sqrt(theta))/delta
d/dt(Mr)=ka*cs*theta-kd*Mr/sqrt(theta)
d/dt(Mi)=ki*cs*theta
DM=ka*cs*theta-kd*Mr/sqrt(theta)+ki*cs*theta
M=Mr+Mi
x=M/Mjam
theta=(1-x)^3/(1-0.812*x+0.2336*x^2+0.0845*x^3)
csn=(cb*D/delta+kd*M)/((ka+ki)*theta+D/delta)
d/dt(Nr)=ka*cb*ntheta-kd*Nr/sqrt(ntheta)
d/dt(Ni)=ki*cb*ntheta
DN=ka*cb*ntheta-kd*Nr/sqrt(ntheta)+ki*cb*ntheta
N=Nr+Ni
nx=N/Mjam
ntheta=(1-nx)^3/(1-0.812*nx+0.2336*nx^2+0.0845*nx^3)
cb=if time>3000 then 0 else cbb
init cs=0
init cs1=0
init cs2=0
init cs3=0
init cs4=0
init cs5=0
init cs6=0
init cs7=0
init cs8=0
init cs9=0
init Mi =0
init Mr=0
init Ni =0
init Nr=0
cbb=100
Mjam=0.12
ka=4.1E-6
ki=2E-6
kd=1.6E-4
D=3.3E-7

```



## **Solutions for MTT, NR and BCA assays**

### **MTT-solution**

5 mg / ml Thiazolyl Blue tetrazolium bromide in PBS, pH = 7.4

### **MTT-lysis solution**

90 % (v/v) ethanol + 10 % (v/v) HEPES-NaCl with pH 8, Hepes-NaCl =1.191g HEPES +292.2 mg NaCl in 100 ml ddH<sub>2</sub>O

### **NR solution**

NR (1:60) PBS

### **NR-lysis solution**

500 ml isopropanol + 2 ml HCl

### **Karnovsky-solution**

Dissolve 4 g paraformaldehyde + 50 ml dd H<sub>2</sub>O at 60° in a water bath. Add 6-10 drops 1N NaOH to dissolve completely and cool down at room temperature. Add 10 ml 50% (w/v) Gluteraldehyde, add 40 ml PBS and adjust pH to 7.4 with 1 N HCl.

### **BCA-solution**

Freshly mix BCA Protein Assay reagent A (Pierce Nr. 23223) and 4 % (w/v) CuSO<sub>4</sub>\*5H<sub>2</sub>O

## **Assays-procedures**

### **MTT Assay**

- Warm up MTT-solution at 37°C
- Add 25 µl (96 well) MTT-solution
- Incubate the plates at 37°C for about one hour
- Remove solution inside the wells completely and then add 100 µl lysis solution to each well immediately
- Wait for 15 min at room temperature for color developing
- Measure OD value at  $\lambda = 540$  nm

---

### **Neutral Red Assay**

- Warm up NR solution at 37°C
- Add 30 µl (96 well) NR-solution
- Incubate the plates at 37°C for about one hour.
- Add 30 µl Karnovsky-solution directly into each well and wait for 5-10 min at room temperature
- Remove solution inside the wells completely and wash once immediately with 100 µl PBS per well
- Remove completely the solution and add 100 µl lysing solution to each well immediately
- Wait for 15 min at room temperature for color developing
- Fluorimetrically measure OD value at  $\lambda = 540$  nm

### **BCA Assay**

- Add 600 µl Karnovsky-solution to each well to fix the cells for 5 min
- Remove solution completely
- Wash twice with 1 ml PBS and let dry
- Add 200 µl BCA-solution and wait for 15 min at room temperature for color developing
- Prepare several BCA standards (100-3000 µg/ml)

Fluorimetrically measure OD value at  $\lambda = 540$  nm

---

## Curriculum vitae

---

### Thomas Silvan Hug

12. 6. 1973	Born in Uster, Switzerland, Swiss
1980 - 1986	Primary school, Küsnacht, Switzerland
1986 - 1992	High-school, Rämibühl, Zürich, Matura B
1992 - 1996	Studies in chemistry at the ETH Zürich
1996	Diploma in industrial chemistry at the ETH, dipl. chem. ETH
1997 - 2000	Doctoral studies at the Chemical Engineering Departement in the group of Prof. M. Morbidelli